Hydraulic functioning of permeable pile groins
Numerical simulation

Zhang, R.

DOI
10.4233/uuid:31eff784-f51f-4389-95c5-e47429c43088

Publication date
2020

Document Version
Final published version

Citation (APA)
Zhang, R. (2020). *Hydraulic functioning of permeable pile groins: Numerical simulation*. [Dissertation (TU Delft), Delft University of Technology]. https://doi.org/10.4233/uuid:31eff784-f51f-4389-95c5-e47429c43088

Hydraulic functioning of permeable pile groins

Numerical simulation

Hydraulic functioning of permeable pile groins

Numerical simulation

Proefschrift

ter verkrijging van de graad van doctor
aan de Technische Universiteit Delft,
op gezag van de Rector Magnificus prof.dr.ir. T.H.J.J. van der Hagen,
voorzitter van het College voor Promoties,
in het openbaar te verdedigen op dinsdag 14 Juli 2020 om 12:30 uur

door

Rong ZHANG

Master of Science in Hydraulic Engineering,
Dalian University of Technology, China,
geboren te Yinchuan, China.

Dit proefschrift is goedgekeurd door de promotor[en].

Samenstelling promotiecommissie bestaat uit:

Rector Magnificus,	voorzitter
Prof.dr.ir. M.J.F. Stive	Technische Universiteit Delft, promotor
Prof.dr.ir. S.G.J. Aarninkhof	Technische Universiteit Delft, promotor
Onafhankelijke leden:	
Dr.ir. J. Bosboom	Technische Universiteit Delft
Prof.dr.ir. W.S.J. Uijttewaal	Technische Universiteit Delft
Prof.dr.ir. A.J.H.M. Reniers	Technische Universiteit Delft
Prof.dr.ir. A.E. Mynett	Technische Universiteit Delft/UNESCO-IHE
Overige leden:	
Dr.ir. M. Zijlema	Technische Universiteit Delft

This research was financially supported by the China Scholarship Council (CSC), and partly supported by the Stichting Het Lamminga Fonds, Delft, the Netherlands.

Printed by: Ridderprint

ISBN 978-94-6416-000-0

An electronic version of this dissertation is available at
http://repository.tudelft.nl/.

Science is a wonderful thing
if one does not have to earn one's living at it.

Albert Einstein

Contents

Summary

Beach erosion, the loss of sand from a beach due to longshore and/or cross-shore sediment transport mechanisms, is a challenging problem. In order to stabilize the beach and to slow down the rate of beach erosion, the construction of hard hydraulic structures is a traditional option. Groins are one of the oldest man-made hydraulic structures designed to intercept the longshore sediment transport and to stimulate sediment deposition within the groin compartments. However, erosion is likely to appear at the downdrift beach stretch of a groin system, due to lack of sufficient sand feeding from the updrift groined beach reaching the downdrift beach. To alleviate sand starvation at a downdrift beach of groins, groins are suggested to be gradually shorter and more permeable approaching the downdrift terminal groin.

The primary advantage of permeable groins, compared to impermeable groins, is they do not entirely block longshore currents. The large openings of permeable groins allow littoral drift to flow through. The shoreline response to permeable groins is comparable to a straight line, other than a zig-zag shape response to impermeable groins. Nevertheless, even though the benefits of permeable groins seem obvious, the research on the subject of the hydrodynamics of permeable groins in coastal waters is limited.

In this thesis, a particular type of permeable pile groins, merely consisting of slender wooden cylinders, is investigated. In European countries, such as the Netherlands and the Germany, a long history of extensive engineering "trial-and-error" applications with permeable pile groins exists. Doubts and questions have arisen about the functioning mechanism of permeable groins and the relationship between permeable groin design and permeable groin effectiveness. This thesis explores the doubts and attempts to answer the questions by numerical simulations.

As the main purpose of groins is to retard longshore currents and to trap longshore sediment transport, groins are a theoretically wise option to control beach width on a longshore sediment transport dominated coast. To investigate groin-current interactions, a reliable model is essential to accurately predict alongshore currents induced by waves and/or tides. Although a depth-integrated radiation stress based theory of water waves could resolve the wave-induced longshore currents quite well, it still heavily relies on the calibration of free parameters, such as the bottom friction coefficient and viscosity coefficient, which are hardly known in the field. To give a good prediction, the free parameters should be carefully calibrated to guarantee that the physical processes are appropriately represented. For instance, the capture of wave breaking position dominates the initiation of wave-induced longshore currents, and the viscous mixing controls the spreading of the cross-shore

profile of longshore currents. Both these mechanisms need be represented accurately.

To simulate longshore currents, we choose to use the SWASH model, which is a phase resolving model and theoretically has no limitations on the temporal and spatial domain. Six representative data sets obtained from laboratory experiments were selected to validate the capacity of simulating longshore currents on beach slopes of the SWASH model. The range of wave conditions of the experiments includes regular waves and irregular waves, propagating on a barred slope and four plane slopes. The comparison between the simulated results and the laboratory measurements shows that the initiation of wave breaking and the cross-shore spreading of wave-induced longshore currents are accurately captured. The predicted vertical profiles of regular wave induced longshore currents on a plane slope show a strong depth-uniform distribution. Even though the SWASH simulation could not explain the inconsistency in the location of the maximal velocity of the cross-shore longshore current profile on the bar in the laboratory and in the trough in the field, the SWASH model is the only model found capable of simulating longshore currents under well-controlled laboratory conditions without special calibration of free parameters. Therefore, the SWASH model is most promising to predict wave-induced currents under varying conditions.

To investigate the hydrodynamics of permeable pile groins, the first step is to verify if the representation of permeable pile groins in the SWASH model is appropriate. The method to schematize and implement the effects of permeable pile groins in coastal waters by SWASH through Morison type forces needs to be proven valid. A good agreement is obtained between numerical simulation results and laboratory measurement data. Depending on the validated model, detailed hydrodynamics around the permeable pile groins were analysed. No eddies and circulations developed within the highly permeable groin fields. It is proven that the groins have hardly any effects on wave energy attenuation, for a groin width much smaller than the incident wave length. In contrast, the groins have significant effects on the longshore currents within groin fields. In the alongshore direction, longshore currents are effectively reduced updrift of the groins due to groin resistances, but can gradually recover their strength fed by breaking waves when flowing further downdrift of the groins. Within the groin fields, the retardation of longshore current velocities is 33% and 43% when the groin permeability is 55% and 50%, respectively. Taking into account the retarded longshore discharge, the three-long-groin-system functions better than the five-short-groin-system.

Furthermore, numerical experiments with varying layouts of permeable pile groins under different wave conditions are carried out. The configuration parameter effects of groins on nearshore flow patterns are numerically explored by comparing the reduction rate of longshore current velocities. Two design variables, namely the aspect ratio of groin spacing over groin length, and the relative groin length to wave breaker zone width, are compared under light wave and moderate wave

conditions. A bimodal cross-shore profile of longshore current velocities appears, of which the first peak is at a shoreward wave breaking position and the second peak is at a seaward groin head. The simulation results show that when the groin length is as short as about 70% of the wave breaker zone width, the maximal longshore current velocity within the wave breaker zone could not efficiently be retarded, and the cross-shore longshore current profile shifts from a bimodal shape to a unimodal shape of which the velocity peak is at the seaward groin head. The longshore current reduction rate is not sensitive to wave conditions when the aspect ratio of groin-length and groin-spacing is 1:1 and 1:1.5. In the case of the aspect ratio being 1:2, the reduction rate is larger under a light wave condition than the reduction rate under a moderate wave condition.

The findings of this thesis show that the SWASH model is a powerful tool to accurately simulate nearshore dynamics within permeable pile groin fields. Permeable pile groins are found to effectively hinder the longshore currents. If well designed, a permeable pile groin is effective to change the nearshore flow field to protect a beach from erosion. The numerical simulations, focusing only on hydrodynamics within the permeable pile groin field, provide hints to refine groin design rules and offer a good prerequisite to a more complex morphological model. However, the work of this thesis is based on a small-scale under well-controlled laboratory environments. The investigation of the similarity of numerical simulations to the natural environment requires the model to be scaled up to the field, a truly challenging task.

Samenvatting

Stranderosie, het verlies van zand als gevolg van kust-parallelle en/of kustdwarse sediment transportmechanismen, vormt een uitdagend probleem. Om het strand te stabiliseren en het proces van stranderosie af te remmen, is de bouw van harde hydraulische constructies een traditionele optie. Strandhoofden zijn een van de oudste door de mens gemaakte hydraulische constructies, ontworpen om sedimenttransport te onderscheppen en om afzetting van sedimenten tussen de strandhoofden te stimuleren. Echter, het is zeer waarschijnlijk dat benedenwaarts erosie optreedt bij gebrek aan voldoende zandtoevoer vanuit het bovenwaarts gelegen strand en onvoldoende toevoer het benedenwaartse strand bereikt. Om zandhonger op een benedenwaarts gelegen strand te voorkomen, is de suggestie om de strandhoofden geleidelijk korter en meer doorlaatbaar te maken, afhankelijk van de afstand tot het finale strandhoofd.

Het belangrijkste voordeel van doorlaatbare strandhoofden, in vergelijking met niet-doorlaatbare strandhoofden, is dat ze de kust-parallelle stroom niet volledig blokkeren. De grote openingen van doorlaatbare strandhoofden zorgen ervoor dat de kuststroming door kan stromen. De respons van de kustlijn op doorlaatbare strandhoofden is vergelijkbaar met een rechte lijn; anders dan een zigzagvormrespons bij solide strandhoofden. Ondanks het feit dat de voordelen van doorlaatbare strandhoofden voor de hand liggen, is het onderzoek naar de hydrodynamica van doorlaatbare strandhoofden in kustwateren beperkt.

In dit proefschrift wordt een specifiek type van doorlaatbare strandhoofden onderzocht, namelijk het palenstrandhoofd bestaande uit slanke houten cilindrische palen. In Europese landen, zoals Nederland en Duitsland, bestaat een lange geschiedenis van uitgebreide technische 'trial-and-error'-toepassingen met doorlaatbare palenstrandhoofden. Twijfels en vragen zijn gerezen over het werkingsmechanisme van doorlaatbare strandhoofden en het verband tussen ontwerp en effectiviteit van doorlaatbare strandhoofden. Dit proefschrift onderzoekt de twijfels en probeert de vragen te beantwoorden met behulp van numerieke simulaties.

Aangezien het belangrijkste doel van de strandhoofden is om de kust-parallelle stroming te vertragen en het parallelle sedimenttransport op te vangen, zijn strandhoofden in theorie een slimme optie om de strandbreedte van een door kust-parallelle stroming gedomineerde kust te beheersen. Om de interacties van stromingen bij strandhoofden te onderzoeken is een betrouwbaar model essentieel om de kust-parallelle stroming, geïnduceerd door golven en/of getijden, nauwkeurig te voorspellen. Hoewel een golfspanning gebaseerde, dieptegemiddelde theorie van watergolven zeer goed in staat zou zijn om de golf-geïnduceerde kust-parallelle stro-

ming vast te stellen, is deze nog steeds sterk afhankelijk van de kalibratie van vrije variabelen, zoals de wrijvingscoëfficiënt van de bodem en de viscositeits coëfficiënt, welke in het veld nauwelijks bekend zijn. Om een goede voorspelling te geven, moeten de vrije variabelen zorgvuldig worden gekalibreerd om te garanderen dat de fysieke processen correct worden weergegeven. Het vastleggen van de positie van het breken van de golf bepaalt bijvoorbeeld de initiatie van golf-geïnduceerde kust-parallelle stromingen, terwijl de visceuze menging de verspreiding van het dwarsprofiel van kust-parallelle stromingen bepaalt. Beide mechanismen moeten nauwkeurig worden weergegeven.

Om kust-parallelle stromingen te simuleren, kiezen we ervoor om het SWASH-model te gebruiken, een fase-oplossend model zonder enige beperkingen met betrekking tot het temporele en ruimtelijke domein. Zes representatieve gegevenssets, verkregen uit laboratoriumexperimenten, werden geselecteerd om de capaciteit voor het simuleren van kust-parallelle stromingen op strandhellingen van het SWASH-model te valideren. Het type golfcondities van de experimenten omvat regelmatige en onregelmatige golven, die zich verspreidden over een helling met versperringen en vier vlakke hellingen (zonder versperringen). De vergelijking tussen de gesimuleerde resultaten en de laboratoriummetingen laat zien dat de initiatie van breken van de golven en de verspreiding van golf-geïnduceerde dwars-spreiding van de parallelle stromingen nauwkeurig worden vastgelegd. De voorspelde verticale profielen van de door de regelmatige golven geïnduceerde kust-parallelle stromingen op een vlakke helling vertonen een sterke uniforme diepte- verdeling. Hoewel de SWASH-simulatie de inconsistentie in de locatie van de maximale snelheid van het dwars- en kust-parallelle profiel in het laboratorium en in de trog in het veld niet kon verklaren, is het SWASH-model het enige model dat kust-parallelle stromingen, onder goed gecontroleerde laboratoriumomstandigheden zonder speciale kalibratie van vrije variabelen, kan simuleren. Daarom is het SWASH-model het meest veelbelovend om golf-geïnduceerde stroming te voorspellen onder verschillende omstandigheden.

Om de hydrodynamica van doorlaatbare palenstrandhoofden te onderzoeken, is de eerste stap om te controleren of de weergave van doorlaatbare palenstrandhoofden in het SWASH-model geschikt is. De methode om de effecten van doorlaatbare palenstrandhoofden in kustwateren in SWASH door middel van de zgn. Morison krachten te schematiseren en te implementeren moet bewezen worden en geldig zijn. Een goede overeenkomst werd verkregen tussen numerieke simulatieresultaten en de gemeten laboratoriumgegevens. Afhankelijk van het gevalideerde model werd de gedetailleerde hydrodynamica rond de doorlaatbare palenstrandhoofden geanalyseerd. Geen wervelingen en circulaties ontstonden binnen het veld van de zeer doorlaatbare palenstrandhoofden. Het is aangetoond dat de strandhoofden nauwelijks effect hebben op de verzwakking van de golfenergie voor een lengte van een strandhoofd dat veel kleiner is dan de lengte van de golf. De strandhoofden hebben daarentegen een significant effect op de kust-parallelle stromingen binnen het strandhoofdenveld. De kust-parallelle stroming wordt effectief gere-

duceerd indien bovenwaarts van het strandhoofd vanwege de weerstand van het strandhoofd, maar kunnen echter geleidelijk hun sterkte terugkrijgen gevoed door brekende golven wanneer ze verder benedenwaarts van het strandhoofd stromen. Binnen het strandhoofdveld is de vertraging van de huidige stroomsnelheden van de kust 33% en 43% wanneer het strandhoofd een doorlaatbaarheid heeft van respectievelijk 55% en 50%. Rekening houdend met het vertraagde debiet langs de kust, functioneert het systeem met drie lange strandhoofden beter dan het systeem met vijf korte strandhoofden.

Verder werden numerieke experimenten uitgevoerd met variërende lay-outs van doorlaatbare palenstrandhoofden onder verschillende golfomstandigheden. De effecten van de configuratie van parameters van strandhoofden op stromingspatronen bij de kust worden numeriek onderzocht door de mate van vermindering van kust-parallelle stroomsnelheden te vergelijken. Twee ontwerpvariabelen, namelijk aspecten van de strandhoofd-afstand tot de strandhoofd-lengte, en van de relatieve strandhoofd-lengte tot de breedte van de strandhoofdzone, worden vergeleken onder lichte en matige golfomstandigheden. Een bimodaal dwars-profiel van kust-parallelle stroomsnelheden treedt op, waarvan de eerste piek zich in een kustwaartse en golfbrekende positie bevindt, en de tweede piek zich aan de kop van een strandhoofd, zeewaarts, bevindt. De simulatieresultaten tonen aan dat wanneer de strandhoofdlengte ongeveer zo kort is als 70% van de breedte van de strandhoofdzone, de maximale kust-parallelle stroomsnelheid binnen de strandhoofdzone niet efficiënt kon worden vertraagd en het dwarse kust-parallelle-stroomprofiel verschuift van een bi-modale vorm naar een uni-modale vorm, waarvan de snelheidspiek zich zeewaarts bij de kop van de strandhoofd bevindt. De mate van de kust-parallelle vertraging van stroming is niet gevoelig voor golfomstandigheden wanneer de verhouding van strandhoofdlengte tot strandhoofdafstand 1: 1 en 1: 1,5 is. In het geval dat de verhouding 1: 2 is, is de vertraging groter onder een conditie van lichte golven dan de vertraging onder een matige golfconditie.

De bevindingen van dit proefschrift laten zien dat het SWASH-model een krachtig hulpmiddel is om kust-dynamica binnen een veld van doorlaatbare palenstrandhoofden nauwkeurig te simuleren. Doorlaatbare palenstrandhoofden blijken de kust-parallelle stromingen effectief te belemmeren. Indien juist ontworpen, zijn doorlaatbare palenstrandhoofden zeer effectief om het stromingsveld nabij de kust te veranderen en om een strand tegen erosie te beschermen. De numerieke simulaties, beperkt tot de hydrodynamica binnen het veld van doorlaatbare palenstrandhoofden, suggereren een verfijning van het ontwerp van strandhoofden en bieden een goede voorwaarde voor een complexer morfologisch model. Dit proefschrift is echter gebaseerd op kleinschalig modelonderzoek in goed gecontroleerde laboratorium omgeving. Een vergelijkend onderzoek van numerieke simulaties in een meer natuurlijke omgeving vereist dat het model wordt opgeschaald naar het veld, een echt uitdagende taak.

1

Introduction

1

1.1. Research background

A large number of coastal defence measures have been developed to protect fragile coastlines from retreat. Among them, groins (or groynes) are one of the oldest and most popular hydraulic structures. Groins are mainly narrow structures, and are mostly perpendicular to the shoreline. Groins have been used as flow barriers to retard longshore currents and to trap the entrained longshore sediment within groin compartments to preserve coasts. From the aspect of permeability, groins could be divided into permeable groins and impermeable groins. Compared to conventional solid impermeable groins, exerting unexpected side effects on lee-side coasts by causing sand starvation downdrift, permeable groins are preferred for they permit longshore sediment to pass through their large openings, instead of being totally blocked, to feed the downdrift beach. Consequently, the shoreline response to permeable groins is more like a straight line, other than the zig-zag patterns which are frequently observed in impermeable groin fields.

Within the range of the various types of permeable groins, traditional timber groins, consisting of wooden pile cylinders, are an important category. For the application of coastal protection structures, the requirements of an easy adjustment, dynamic sustainability and the least intrusive intervention with the environment are increasing. In this aspect, timber groins have advantages over other structures, because of the ease of construction, modification and maintenance and, in addition, their smaller footprint and fewer side effects on a downdrift coast, timber groins have regained the attention in the field. Moreover, 'there is a concern that with fewer timber groins being used, knowledge and experience developed over generations may be lost'[Perdok et al., 2003]. Out of such concerns, further successive research about the hydraulic functioning of specific timber groins, viz. Permeable Pile Groins (hereinafter short as PPGs), is necessary to bridge the knowledge gap.

From the literature it can be concluded that the performance of PPG projects, whether it is positive or negative, is site specific. Since 1965 [Bakker et al., 1984], PPGs were used to protect the North Sea coast in the Netherlands from erosion. PPGs in the Netherlands are particularly abundant along the coast in the province of Zeeland, where the existence of pile groins harmonized well with the surrounding environment. Bakker et al. [1984] summarised that the effects of PPG projects in the Netherlands were controversial, because of the lack of having no statistically significant evidence. Therefore, PPGs deserve serious re-consideration and investigation as a promising type of economic and flexible coastal protection measure [Bakker et al., 1984], especially since positive performances of PPGs were observed on other sites. For instance, the permeable groins constructed in the 1950s on Naples Beach, Florida (USA), played a significant role in reducing beach material losses off the beach [Poff et al., 2004]. Four years of post-construction monitoring of an experimental permeable groin for a restoration project confirmed that the groin functioned as intended, slowing the losing rate of beach fill materials. The success of the PPG project was attributed to a benign wave climate and a low net longshore sediment transport [Poff et al., 2004]. Similarly, on a section of the

Baltic Sea coast with PPGs, a significant seaward advancement of the shoreline was found through a four-year field survey from 1993 to 1997 [Trampenau et al., 2004].

In addition to field tests, several laboratory experiments were carried out to investigate the dynamics over a PPG engineered beach. The most representative experiments are the two experiments by Hulsbergen and ter Horst [1973] and Trampenau et al. [2004]. Hulsbergen and ter Horst [1973] experiment compared the longshore current reduction rate when the PPG layout was varying. The chosen condition is a combined wave current condition, to represent the real field condition, with oblique wave induced longshore currents and strong tidal alongshore currents in the same direction, or in opposite directions, respectively. Trampenau et al. [2004] experiment mainly investigated the difference of PPG performance with varying permeability under current alone and wave alone conditions.

Despite the fact that PPGs were used more than half a century ago, there is limited research about how PPGs function. The controversial performances of PPGs on various sites complicate to summarize a universally accepted design rule. The variability of PPG applications should be carefully considered when PPGs are supposed as a way to combat the beach erosion problem.

1.2. Objective and outline

The goal of this thesis is to improve the level of understanding of the hydraulic functioning of permeable pile groins. The ability of the chosen numerical model to properly simulate wave propagation and the evolution of longshore currents induced by obliquely incident waves needs to be verified. Based on the verified numerical model, numerical experiments are the most practical route to be carried out to expand the data set of groin performance with varying geometrics and layouts under varying wave conditions. The new data set would be useful to generalise design rules of permeable pile groins and to specify the application range of a valid groin application. The numerical simulations are based on the open-source SWASH (Simulating WAves till SHore) model. As a highly robust and accurate model, the SWASH model has been successfully used to simulate, among many, wave-current interactions, infra-gravity wave hydrodynamics, and moored ship dynamics. A further evaluation of longshore current-groin interaction in the SWASH model was executed. From the numerical model results, a quantitative understanding of PPG hydrodynamics can be acquired.

The key research questions of this research are formulated as follows:
1. Is the chosen numerical model capable of simulating the processes of wave propagation and evolution of longshore currents?
2. How should permeable groin effects in the numerical model be schematised and interpreted ?
3. What the local and global hydrodynamics of a permeable groin?
4. Which configuration parameter of a permeable groin system is dominant in its

efficiency to reduce longshore current velocity?

The outline of this thesis is described as follows. First, in the present Chapter and the following Chapter 2 the research background and the motivation are elucidated. Chapter 2 provides a detailed summary of the knowledge and literature about how permeable groins function under different conditions. Then, in Chapter 3, verification of the capability of properly simulating wave induced longshore currents by the SWASH model was undertaken. Four representative and good quality data sets obtained from scaled laboratory experiments were chosen to be reproduced by the SWASH model. The experiments cover the spreading of longshore currents induced by regular and irregular waves over barred and plane sloping beaches. In Chapter 4, the PPG effects are implemented in the numerical model. The simulated results were compared with laboratory data. The simulations offer more detailed flow field information with the inference of PPGs. After that, the verified model is used to investigate the difference between varying groin layouts in the following Chapter 5. Varying wave conditions are also taken into account in this chapter.In the final Chapter 6, a summary of conclusions of each chapter is provided. Further implications of the research and outlook on wave-groin interactions and groin design are presented.

References

W. Bakker, C. Hulsbergen, P. Roelse, C. de Smit, and J. Svasek. PERMEABLE GROYNES: EXPERIMENTS AND PRACTICE IN THE NETHERLANDS. In *19th International Conference on Coastal Engineering*, pages 1983–1996, Houston, 1984.

C. Hulsbergen and W. ter Horst. Effect of permeable pile screens on coastal currents. Delft Hydraulics laboratory report M 1148, (in Dutch). Technical report, Delft Hydraulics, Delft, 1973.

U. Perdok, M. Crossman, H. J. Verhagen, S. Howard, and J. Simm. Design of timber groynes. In *Coastal Structures*, pages 1689–1699, Portland, Oregon, United States, Aug. 2003. ISBN 9788578110796. doi: 10.1017/CBO9781107415324.004.

M. T. Poff, M. F. Stephen, R. G. Dean, and S. Mulcahy. Permeable Wood Groins: Case Study on their Impact on the Coastal System. *Journal of Coastal Research*, pages 131–144, 2004. ISSN 07490208, 15515036. URL http://www.jstor.org/stable/25736250.

T. Trampenau, H. Oumeraci, and H. H. Dette. Hydraulic Functioning of Permeable Pile Groins. *Journal of Coastal Research*, pages 160–187, 2004. ISSN 07490208, 15515036. URL http://www.jstor.org/stable/25736252.

2

Longshore currents and permeable groins: literature review

2.1. Longshore currents

The mean currents flowing in an alongshore direction, generated by obliquely incident breaking waves and the resulting alongshore momentum flux thrust, are defined as longshore currents [Galvin and Eagleson, 1964, Longuet-Higgins, 1970, Basco, 1983].The reviews of previous understanding of longshore currents are undertaken by Galvin and Eagleson [1964] and Basco [1983].The longshore currents and the associated longshore sediment transportation play a significant role in beach profile evolution and shoreline variation. The theory of longshore currents has developed considerably since the radiation stress concept [Longuet-Higgins and Stewart, 1964] was introduced [Bowen, 1969, Longuet-Higgins, 1970, Thornton and Guza, 1986]. The theories, developed based on radiation stress, have a depth-averaged and wave period averaged nature. Therefore, dynamics of the instantaneous longshore current velocity within a wave period and the vertical profile of a longshore current are not resolved. In a steady-state, the current driving radiation stress force is balanced by bottom friction and lateral friction. The calculation of radiation stress needs to be solved by an additional wave model. The lack of sufficient data under varying conditions hampers the processes of uncovering new phenomena, coefficient calibration, and the verification of theories.

Basco [1983] pointed out that there is no universally accepted time interval of time-averaging field observations to obtain mean longshore currents. Consequently, the variability of field data in space and time raises concerns of how to properly use field data to verify theories and determine coefficients of analytical models. Special attention should be given to the temporal averaging resolution of field observations. In addition, when comparing laboratory measurement data of longshore currents, the uniformity of longshore currents should be checked for it is affected by unexpected recirculation in a wave basin due to wave basin geometry [Visser, 1984]. For good quality data of longshore currents, the measurement data are limited, and a reliable prediction of longshore current velocity remains challenging.

2.2. permeable groins in coastal waters

Groins have been widely used to hinder longshore currents and the associated longshore sediment transport to protect the beach from erosion. They are generally extending from the shoreline to the low water line or beyond the surf zone. For a small angle between the axial direction of groins and the wave direction, groins only affect longshore sediment transport and hardly attenuate incident wave energy. Given the permeable character of groins, groins can be divided into permeable groins and impermeable groins. The solid groins, made of pebble stone, concrete plate or other solid materials, are treated as impermeable groins. As impermeable groins block the longshore currents and the longshore sediment transport within the groin compartments, the sediment deposit updrift the groins and erosion appears downdrift the groins. Consequently, the shoreline response to impermeable groins displays

a zig-zag shape, and erosion occurs downdrift the impermeable groin system due to sand starvation. To lessen the negative effects of impermeable groins on the downdrift coast, one method is to shorten groin length, but at the expense of efficiency reduction, while another preferred method is to increase permeability of a groin, allowing water and sand to pass through. Permeable groins normally consist of wooden pile cylinders or precast concrete porous unites. With the increasing awareness of environmentally friendly applications and aesthetically agreeable solutions, the timber groins from past times are attracting reconsideration. Timber groins are generally permeable and consist of rows of pile cylinders (Figure 2.1). Easier installation, lower cost, higher flexibility of adapting to the changing beach profile, smaller damage to beach amenity and resulting in a more uniform shoreline response, permeable pile groins have been popularly used for coastal protection worldwide. While the nearshore process and the effect of impermeable groins is well understood, the hydraulic functioning of permeable pile groins has not received as much attention compared to their counterparts [Trampenau et al., 1996]. The lack of ample research has resulted in a limited understanding of the hydraulic functioning of permeable groins.

Field studies have confirmed that the coastline recession is effectively curbed by permeable pile groins [Kolp, 1970, Price et al., 1972, Trampenau et al., 1996, 2004, Abam, 1993] and the longshore current velocity is retarded to a large extent measured in laboratory experiments [Hulsbergen and ter Horst, 1973, Trampenau et al., 2004]. A five-year surveillance of a beach profile evolution at the southern coast in England, showed that a build-up in beach levels appeared after the construction of PPGs [Price et al., 1972]. Compared to a groin-less coast, the evolution of beach profiles in response to PPGs is that the beach elevation was built up and the beach slope became much gentler from the shoreline to the trough. This indicates that wave energy dissipated further seaward and a wider wave buffer zone developed, thus a reduction in wave loading per unit area occurred, alleviating the potential of beach erosion [Dette et al., 2004]. Similarly, positive effects induced by PPGs, indicated by extensive field surveys from 1993 to 1997 on the Baltic Sea coast, are: a) significant seaward advancement of shoreline; b) continuous growth of submarine terrace elevation; and c) seaward movement of the nearshore shoal [Trampenau et al., 2004]. The positive accretion appears as a result of an indirect protection mechanism of PPGs on morphological changes [Trampenau et al., 2004], as well as the direct effects on hydraulic conditions. In the case of Naples Beach, Florida, the monitored performance of an experimental groin satisfied its expectation, which successfully stabilized the beach and did not have any significant side effects on the adjacent shoreline [Poff et al., 2004].

To the author's knowledge, the earliest laboratory experiment on permeable pile groin functioning with various configurations under varying hydraulic conditions is executed by Hulsbergen and ter Horst [1973]. The different tests and their results of the extent of longshore current reduction were compared. The groin model used in the experiments were either 3.5 m long or 5 m long, consisting of single-row

Figure 2.1: Left: The single row permeable pile groins at the southern coast of the Baltic sea, German [Raudkivi and Dette, 2002] Right: The two-row permeable pile groin at Domburg coast, the Netherlands.

pile cylinders or two-row cylinders in 8.5 cm apart distance. The scales in horizontal and vertical directions are both 1:40. The permeability varied along the groin length, with the average permeability being 50% and 55% for short and long groins respectively. The main conclusions were given in the form of relative longshore current velocities, which was the ratio of longshore current velocities with groin interventions to the velocities without groins. Under the condition that a current and a wave-generated longshore current are in the same direction, the relative reduction of longshore current velocity was smaller than under the current-alone condition. The difference in longshore current reduction under the combined wave-current condition and current-alone condition attributed to the different generation mechanism of alongshore currents and wave generated longshore currents. The obliquely incident waves could penetrate into groin fields and generate longshore currents within groin fields. Therefore, once the longshore current was retarded by the groin resistance, it would however be immediately fed by the driving force from the penetrated breaking waves, leading to a smaller reduction than the current-alone condition without waves.

After the first generation of permeable pile groins in coastal engineering, about 40 years ago, the evaluation of previous projects has brought the applicability of PPGs back into the attention. The positive shoreline advancement into the sea as observed on a PPG engineered Baltic Sea coast site [Trampenau et al., 1996] encouraged a further study about optimising the PPG design. Trampenau et al. [2004] carried out a systematic laboratory experiment to investigate varying pile groin configuration parameters effects on PPG performance. The single-row groin model is spaced at a constant distance. The model test focused on PPGs with varying permeability parameters and varying groin length relative to wave breaker zone width under varying wave-alone and current-alone conditions. Similarly, the research confirmed that PPGs function differently under wave-alone and current-alone conditions. Trampenau et al. [2004] suggested a critical permeability value

when a pile groin could be seen as permeable or as impermeable. The experimental results showed that when the permeability was lower than 20%, the pile groins could be treated as impermeable groins functioning like a guiding wall for the currents. In contrast, if the groin permeability was higher than 20%, the pile groins served as a resistance to the currents. The main correlations of relative flow field features is shown in Table 2.1, the correlation of relative longshore current velocity reduction, maximal relative longshore current, and relative rip current magnitude with the permeability parameter.

Table 2.1: The correlations Trampenau et al. [2004] derived from experiments

The relative reduction of longshore currents in the vicinity of the PPGs: Re_v	$\mathrm{Re_v} = \frac{V}{V_0} = 1.03\tanh^{2.0}(2.4P)$
The relative maximum increase of the longshore currents seaward of the PPG heads: $Re_{v,max}$	$\mathrm{Re_{v,max}} = \frac{V_{\max}}{V_0} = 4.7\frac{L_g}{X_B} - \left[\left(4.7\frac{L_g}{X_B} - 0.9\right)\tanh^{2.0}(2.4P)\right]$
The relative maximum rip-current velocities in the vicinity of the PPG heads: $Re_{rip,max}$	$\mathrm{Re_{rip,\,max}} = \frac{U_{\max}}{V_0} = \frac{L_g}{X_B}(1.8 - 2.7P + 0.86P^2)$
The relative water level variations induced by the PPGs: Re_h	$\mathrm{Re_h} = \frac{\Delta h}{H} = 0.54 - 0.79\mathrm{P} + 0.25P^2$
Where the V_0 denotes the longshore current without groins, L_g is the groin length, X_B is the wave breaker zone width, P is groin permeability and Δh is the water level variation between updrift and downdrift a groin. L_g / X_B =1, the wave parameters are H= 5 cm, θ=30°.	

Other than laboratory experiments, a numerical model can be used to efficiently calculate and predict various scenarios. The numerical simulation by Mulcahy [2000] concluded that low permeability groins retarded longshore current velocities significantly, but at the expense of strong offshore currents along the updrift sides of pile groins. This is consistent with the findings in the experiments [Trampenau et al., 2004]. Briele [2014] successfully reproduced a part of experiments of Trampenau et al. [2004] through numerical modelling. Besides the confirmed effective retardation of longshore currents, the technical condition of groins has been checked. The breaches of pile groin rows brings intensive bed erosion and becomes even more harmful than non-groin engineered eroding natural beaches [Ostrowski et al., 2016].

In addition to the hydraulic functioning of permeable groins, an awareness of the ecological function has been observed throughout the field study [Sherrard et al., 2016] and the observations on site [van Lynden, 2007]. Sherrard et al. [2016]

found that porous coastal defence structures could provide internal habitat space promoting and supporting biodiversity. This finding reveals that such structures function not only as an engineering protection measure but also offer habitats for coastal species. While external surfaces are vulnerable to harsh environmental forces and human interventions from maintenance activities, internal surfaces supply more suitable habitats and have a higher species diversity. Moreover, the groin fields could be seen as a kind of natural 'sea ranch', where a seasonal abundance in wild baby mussels exists [van Lynden, 2007]. The advantage of wild mussel seeds attaching itself to groin piles is substantially beneficial to local aquaculture.

To accurately reproduce the permeable pile groin effects on nearshore waters, especially on longshore currents, wave propagation and evolution should be well simulated. Due to the lack of attention on permeable groins, in addition to few laboratory experiments and field surveys, less research has been carried out to simulate PPG effects by numerical modeling. However, numerical simulation is a powerful tool to simulate a large variety of cases under varying environmental conditions.

To have a detailed understanding of temporal variation of longshore currents, a phase resolving model is preferred. The SWASH (Simulating WAves till SHore) model is an open-source phase resolving wave flow model, considering non-hydrostatic pressure force. As a powerful alternative for various Boussinesq type models, the SWASH model not only captures the initiation and dissipation of a breaking wave correctly when the vertical resolution is fine (10-20 layers), but it is also much more computationally efficient [Smit et al., 2013]. The above-mentioned advantage of SWASH encourages us to explore its application to wave-current-groin interaction. The governing equations of the SWASH model are not given here since these are shown both in Chapter 3 and Chapter 4.

In Chapter 4, the SWASH model is tested to simulate the interaction between longshore currents and PPGs. Next, the validated model is used to further investigate the hydrodynamics of permeable pile groins under varying wave conditions. With these attempts, this research is to explore the validity of the SWASH model simulating wave-induced longshore currents on a plain slope, and to verify the representation of permeable pile groins in the SWASH model is sufficient. The simulation results are proposed to advance a better understanding of permeable pile groins.

References

T. K. S. Abam. Control of channel bank erosion using permeable groins. *Environmental Geology*, 22(1):21–25, 1993. ISSN 01775146. doi: 10.1007/BF00775280.

D. R. Basco. Surfzone currents. *Coastal Engineering*, 7(4):331–355, 1983. ISSN 03783839. doi: 10.1016/0378-3839(83)90003-0.

A. Bowen. The generation of longshore currents on a plane beach. *J. Mar. Res.*, 27 (1):206–215, jan 1969. ISSN 21699275. doi: 10.1002/2015JC011268. URL http://doi.wiley.com/10.1002/2015JC011268.

A. C. Briele. *Assessment of the appli- cation of permeable pile groins as coastal protection*. mathesis, Delft University of Technology, 2014.

H. H. Dette, A. J. Raudkivi, and H. Oumeraci. Permeable Pile Groin Fields. *Journal of Coastal Research*, pages 145–159, 2004. ISSN 07490208, 15515036. URL http://www.jstor.org/stable/25736251.

C. J. Galvin and J. P. S. Eagleson. Experimental study of longshore currents on a plane beach, Hydrodynamics laboratory report 63, Massachusetts Institute of Technology. Technical Report 1770, Massachusetts Institute of Technology, Cambridge, jul 1964. URL http://citeseerx.ist.psu.edu/viewdoc/download?doi=10.1.1.836.7507{&}rep=rep1{&}type=pdf.

C. Hulsbergen and W. ter Horst. Effect of permeable pile screens on coastal currents. Delft Hydraulics laboratory report M 1148, (in Dutch). Technical report, Delft Hydraulics, Delft, 1973.

O. Kolp. Farbsandversuche mit lumineszenten Sanden in Buhnenfeldern. Ein Beitrag zur Hydrographie der Ufernahen Meereszone. *Petermanns Geographischen Mitteilungen*, 114(2), 1970.

M. Longuet-Higgins. Longshore Currents Generated by Obliquely Incident Sea Waves, 1. *Journal of Geophysical Research*, 75(33):6778–6789, jul 1970. ISSN 15515036. doi: 10.2112/JCOASTRES-D-16-00027.1. URL http://citeseerx.ist.psu.edu/viewdoc/download?doi=10.1.1.836.7507{&}rep=rep1{&}type=pdf.

M. S. Longuet-Higgins and R. W. Stewart. Changes in the form of short gravity waves on long waves and tidal currents. *Journal of Fluid Mechanics*, 8(04):565, 1964. ISSN 0022-1120. doi: 10.1017/S0022112060000803.

S. Mulcahy. *Laboratory and numerical studies of a pile cluster groin*. mathesis, University of Florida, 2000.

R. Ostrowski, Z. Pruszak, J. Schönhofer, and M. Szmytkiewicz. Groins and submerged breakwaters – new modeling and empirical experience. *Oceanological and Hydrobiological Studies*, 45(1), 2016. ISSN 1730-413X. doi: 10.1515/ohs-2016-0003. URL http://www.degruyter.com/view/j/ohs.2016.45.issue-1/ohs-2016-0003/ohs-2016-0003.xml.

M. T. Poff, M. F. Stephen, R. G. Dean, and S. Mulcahy. Permeable Wood Groins: Case Study on their Impact on the Coastal System. *Journal of Coastal Research*, pages 131–144, 2004. ISSN 07490208, 15515036. URL http://www.jstor.org/stable/25736250.

W. Price, K. TOMLINSON, and D. Willis. Filed tests on two permeable groynes. In *13th International Conference on Coastal Engineering*, pages 1312–1325, 1972. ISBN 7731030008. doi: 10.1016/B978-0-7020-3935-5.00077-X.

A. J. Raudkivi and H. H. Dette. Reduction of sand demand for shore protection. *Coastal Engineering*, 45(3-4):239–259, 2002. ISSN 03783839. doi: 10.1016/S0378-3839(02)00036-4.

T. R. Sherrard, S. J. Hawkins, P. Barfield, M. Kitou, S. Bray, and P. E. Osborne. Hidden biodiversity in cryptic habitats provided by porous coastal defence structures. *Coastal Engineering*, 118:12–20, dec 2016. ISSN 03783839. doi: 10.1016/j.coastaleng.2016.08.005. URL http://linkinghub.elsevier.com/retrieve/pii/S0378383916301892.

P. Smit, M. Zijlema, and G. Stelling. Depth-induced wave breaking in a non-hydrostatic, near-shore wave model. *Coastal Engineering*, 76(3):1–16, jun 2013. ISSN 0378-3839. doi: 10.1016/J.COASTALENG.2013.01.008. URL https://www.sciencedirect.com/science/article/pii/S0378383913000215.

E. B. Thornton and R. T. Guza. Surf Zone Longshore Currents and Random Waves: Field Data and Models. *Journal of Physical Oceanography*, 16(7):1165–1178, jul 1986. ISSN 0022-3670. doi: 10.1175/1520-0485(1986)016<1165:SZLCAR>2.0.CO;2. URL http://journals.ametsoc.org/doi/abs/10.1175/1520-0485{%}281986{%}29016{%}3C1165{%}3ASZLCAR{%}3E2.0.CO{%}3B2.

T. Trampenau, F. Goricke, and A. J. Raudkivi. permeable pile groins. In *25th International Conference on Coastal Engineering*, pages 2142–2151, Orlando, 1996.

T. Trampenau, H. Oumeraci, and H. H. Dette. Hydraulic Functioning of Permeable Pile Groins. *Journal of Coastal Research*, pages 160–187, 2004. ISSN 07490208, 15515036. URL http://www.jstor.org/stable/25736252.

P. van Lynden. *A Resistible Force: When Man Meets the Sea*. Stichting Visual Legacy, 2007. ISBN 9789081185035. URL https://books.google.nl/books?id=nYifZwEACAAJ.

P. J. Visser. Uniform Longshore Current Measurement and Calculations. In *19th International Conference on Coastal Engineering*, pages 2192–2207, Houston, 1984. ISBN 0872624382.

3

Laboratory validation of SWASH longshore current modelling

In this paper, the ability of the numerical phase resolving model SWASH (Simulating WAves till SHore) to hindcast wave-induced longshore currents is evaluated. Using default settings for all processes modelled, highly accurate results are found for wave heights, mean water levels and longshore currents. While wave current interaction is intrinsically modelled, insights into the spatial variation of wave driven longshore currents are found. Additionally, vertical variations of modelled longshore currents have been compared. Depth uniform profiles of longshore current within surf zone are noted on plane beaches under regular waves, except for minor deviations near the shoreline. The apparent validity of a depth-uniform longshore current encourages the use of a depth-averaged moment balance equation to compute the longshore current. A simpler model is shown to also be able to predict a proper magnitude of longshore current, although the cross-shore distribution – in contrast with SWASH - needs tuning for the eddy viscosity and the bottom friction coefficient, since the distribution of the wave-induced longshore current heavily depends on lateral mixing.

This chapter have been published in Coastal Engineerng **142**, 95 (2018). Zhang et al. [2018]

3.1. Introduction

Longshore currents, generated by obliquely incident breaking waves, play an important role in driving longshore sediment transport and in changing coastal morphology. The theory of longshore currents has progressed importantly [Bowen, 1969, Longuet-Higgins, 1970a, Thornton and Guza, 1986], since the concept of radiation stress was introduced [Longuet-Higgins and Stewart, 1964, Longuet-Higgins, 1970a]. Among the proposed mathematical models, the simplest model is a 1D model based on momentum flux balance in alongshore direction on a planar beach under monochromatic wave incidence. In steady state and water depth averaged mode, the longshore current driving force is balanced by bottom friction and lateral friction. Although the average longshore current velocity across the entire surf zone could be properly predicted, the exact cross-shore distribution of the longshore current is more difficult to derive, since it highly depends on less-known lateral mixing mechanisms.

To investigate longshore current mechanisms, field investigations and laboratory experiments have been carried out. Earlier measurements are often limited to longshore maximum velocity or average velocity across the entire width of the surf zone, which does not reveal the cross-shore distribution of longshore current. The known first cross-shore distribution of longshore current was measured by Galvin and Eagleson [1964] along several shore normal profiles. These pioneering data are used widely to test longshore current theories. However, possible non-uniformity of the longshore current along the beach should be carefully considered [Visser, 1991]. To avoid non-uniformity of the longshore current, well controlled, highly representative laboratory experiments were conducted by Visser [1980, 1984b,a, 1982, 1991]. Visser found that a virtually uniform longshore current is realized when the return flow in the offshore region of the wave basin is minimal. Therefore, Visser introduced an active external recirculation system driven by pumps to minimize the circulation flow in the wave basin. Because of the well-controlled uniformity of the longshore current, this data set has been used as a benchmark set for developing longshore current theories and validating numerical models [e.g. Smith et al., 1993, Svendsen and Putrevu, 1994, Chen, 2003, Rijnsdorp et al., 2017, Hsu et al., 2017]. This experimental example setup, guaranteeing the production of an alongshore uniform longshore current in the laboratory, was also adopted by Hamilton and Ebersole [2001]. In addition, a unique, unexplored and unpublished data set produced by large-scale, outdoor laboratory experiments [Hulsbergen and ter Horst, 1973] is presented and shown to be a worthy, additional dataset for validation. Other than the previously mentioned experiments investigating wave-induced longshore currents on planar beaches, Reniers [1997] carried out experiments which focused on longshore currents over more geographically complicated, barred beaches.

The measurements of longshore currents obtained from the above-mentioned experiments provide an excellent database to validate and/or calibrate numerical simulation models. The primary aim of this paper is to validate the ability to simu-

late the spatial variation of wave-driven longshore currents by the phase resolving, non-hydrostatic numerical model SWASH (Simulating Wave till SHore). Validation is preferred over calibration, since validation relies on default parameter settings while calibration relies on adjusted parameter settings for a specific dataset. A verified (validated or calibrated) model is useful to design hard and soft coastal interventions and/or instrument deployment in experiments. Additionally, a very simplified 1D model is introduced to explore the most basic physics behind wave-induced longshore currents.

In the present work, we set up the wave-flow model SWASH with default parameters to validate its ability to simulate wave-induced longshore currents on a laboratory scale. The governing equations of the SWASH model are listed in subsection 3.2.1. Then, a separate simplified depth averaged 1D model is demonstrated in subsection 3.2.2. The configurations of the chosen laboratory experiments are described in the following subsection 3.2.3. The results of SWASH modelling longshore currents are presented and compared to the 1D model results in Section 3.3. Finally, in Section 3.4 a discussion and in Section 3.5 conclusions are given.

3.2. Method

3.2.1. Numerical model SWASH

SWASH [Zijlema et al., 2011] is a flow-wave model which can simulate unsteady, non-hydrostatic free-surface flow in the time-domain, having a wide application range in coastal waters. The governing equations are non-linear shallow water equations including non-hydrostatic effects. The local continuity equation and momentum equations in 3D configuration are given as

$$\frac{\partial u}{\partial x}+\frac{\partial v}{\partial y}+\frac{\partial w}{\partial z}=0 \tag{3.1}$$

$$\frac{\partial u}{\partial t}+\frac{\partial uu}{\partial x}+\frac{\partial uv}{\partial y}+\frac{\partial uw}{\partial z}+\frac{1}{\rho}\frac{\partial p_h+p_{nh}}{\partial x}=\frac{\partial \tau_{xx}}{\partial x}+\frac{\partial \tau_{xy}}{\partial y}+\frac{\partial \tau_{xz}}{\partial z} \tag{3.2}$$

$$\frac{\partial v}{\partial t}+\frac{\partial vu}{\partial x}+\frac{\partial vv}{\partial y}+\frac{\partial vw}{\partial z}+\frac{1}{\rho}\frac{\partial p_h+p_{nh}}{\partial y}=\frac{\partial \tau_{yx}}{\partial x}+\frac{\partial \tau_{yy}}{\partial x}+\frac{\partial \tau_{yz}}{\partial z} \tag{3.3}$$

$$\frac{\partial w}{\partial t}+\frac{\partial wu}{\partial x}+\frac{\partial wv}{\partial y}+\frac{\partial ww}{\partial z}+\frac{1}{\rho}\frac{\partial p_h+p_{nh}}{\partial z}+g=\frac{\partial \tau_{zx}}{\partial x}+\frac{\partial \tau_{zy}}{\partial y}+\frac{\partial \tau_{zz}}{\partial z} \tag{3.4}$$

The kinematic boundary conditions at the free surface and bottom are

$$w|_{z=\zeta}=\frac{\partial \zeta}{\partial t}+u\frac{\partial \zeta}{\partial x}+v\frac{\partial \zeta}{\partial y} \tag{3.5}$$

$$w|_{z=-d}=-u\frac{\partial d}{\partial x}-v\frac{\partial d}{\partial y} \tag{3.6}$$

Integrating the local continuity Equation 3.1 with substituting kinematic boundary conditions at surface and bottom Equations. 3.5-3.6, a global continuity equation

is induced

$$\frac{\partial \zeta}{\partial t} + \frac{\partial}{\partial x}\int_{-d}^{\zeta} u dz + \frac{\partial}{\partial y}\int_{-d}^{\xi} v dz = 0 \tag{3.7}$$

Where t is the time, ζ is the free surface elevation from still water level, z=-d is the bottom, d is the still water depth.

The dynamic boundary condition at the bottom is confined to bottom friction. The bottom friction stress is based on a quadratic friction law $\tau_b = C_f \frac{UU}{h}$, where $h = \zeta + d$ is the total water depth, U is the depth averaged velocity, and C_f is a dimensionless friction coefficient. At the free surface, zero non-hydrostatic pressure ($p_{nh} = 0$) is assumed and no surface stresses are considered.

The turbulent stresses are given based on eddy viscosity closure equations. The horizontal viscosity and vertical viscosity are estimated by the Smagorinsky type model [Smagorinsky, 1963] and the k- ϵ model [Launder and Spalding, 1974], respectively.

For a comprehensive description of the SWASH model and its numerical schemes, reference is made to Zijlema et al. [2011], Smit et al. [2013] and Rijnsdorp et al. [2014]. Extensive validations and applications of SWASH model can be found in the literature. For instance, Rijnsdorp et al. [2014] evaluated the ability of SWASH model to simulate infragravity wave dynamics and found a good agreement with flume observations. de Bakker et al. [2016] designed a numerical study using the SWASH model to investigate nonlinear energy transfers between waves, especially focusing on beach steepness effects on nonlinear infragravity wave interactions. Suzuki et al. [2017] validated the capability of SWASH model to estimate wave overtopping for impermeable coastal structures against physical model data.

3.2.2. 1D model

The depth averaged 1D model comprises a wave model and a current model. The wave model is based on the wave energy balance equation in the cross-shore direction including the wave roller effect, and the current model is based on the momentum balance equation in the alongshore direction. In contrast to the phase resolving SWASH model in multi-layered mode, the 1D model does not resolve the free flow surface, the vertical flow structures and the wave-current interaction. The 1D model thus is a very simplified model, expected however to include the basic physics behind the process of wave-induced currents. A comparison with the SWASH model will reveal whether including a physically more sophisticated approach is more robust.

Wave modelling

The governing equation determining the wave dynamics is the energy balance equation of wave energy:

$$\frac{d}{dx}\left(E_w c_g \cos\theta\right) = \epsilon_w \tag{3.8}$$

where x is the shore normal direction, E_w is wave energy, ϵ_w is mean organised wave energy dissipation rate due to wave breaking and bottom friction. c_g is wave group velocity. Compared to dominant wave breaking dissipation, bottom frictional dissipation is negligible, except the very shallow run-up region [Thornton and Guza, 1983]. For a monochromatic wave, using linear wave theory, the wave energy is expressed by the wave height:

$$\mathrm{E}_w = \frac{1}{8}\rho g H^2 \tag{3.9}$$

and the group velocity c_g is described by

$$c_g = c\left(\frac{1}{2} + \frac{kh}{\sinh 2kh}\right) \tag{3.10}$$

The wave energy dissipation ϵ_w serves as a source term in the roller model [Stive and De Vriend, 1994]

$$-\epsilon_w - \frac{d}{dx}\left(2E_r c \cos\theta\right) = c\tau_r \tag{3.11}$$

where τ_r is the shear stress between roller and water interface, for a steady roller it is given by [Duncan, 1981]

$$\tau_r = \rho_r g \sin\beta \frac{A}{L} \tag{3.12}$$

where A is cross-sectional area of the roller, β the slope of wave front, L wave length. ρ_r is density of the roller, generally less than undisturbed sea water for the entrainment of air at the aerated wave surface. Here, having $\rho_r \approxeq \rho$, to keep roller mass constant at a decrease in roller area A.

The second term of equation 2.9 is the gradient of roller energy flux, followed the definition by Svendsen [1984]

$$E_r = \frac{1}{2}\rho_r c^2 \frac{A}{L} \tag{3.13}$$

The wave height transformation proposed by Thornton and Guza [1983] is utilised. The wave dissipation is modelled by the classical periodic bore dissipation function as

$$\epsilon_w = \frac{f}{4}\rho g \frac{(BH)^3}{h} \tag{3.14}$$

in which B expresses the deviation of wave breaking dissipation from bore dissipation.

For the ensemble, the average wave energy dissipation rate is calculated by

$$\langle \epsilon_w \rangle = \frac{\overline{f}}{4}\rho g \frac{B^3}{h} \int_0^\infty H^3 p_b(H) dH \tag{3.15}$$

where p_b is the probability density of breaking wave distribution.

The Thornton and Guza [1983] model modified the distribution of random wave heights from a Rayleigh distribution by a weighting function, the breaking wave dissipation is related to Hrms via:

$$\langle \epsilon_w \rangle = \frac{3\sqrt{\pi}}{16} B^3 \overline{f} \rho g \frac{H_{rms}^3}{h} M \left[1 - \frac{1}{\left(1 + \left(\frac{H_{rms}}{\gamma h} \right)^2 \right)^{5/2}} \right] \tag{3.16}$$

$$M = 1 + \tanh\left[8 \left(\frac{H_{rms}}{\gamma h} - 1 \right) \right] \tag{3.17}$$

Where H_{rms} is the root mean square wave height, and γ is the wave breaker index, B denotes the intensity of wave breaking, is usually the order of 1, but should be larger cause some researchers thought the classical hydraulic jump function underestimates the wave breaking dissipation [Thornton and Guza, 1983, Stive, 1984]. According to the fitting of the model results to laboratory and field data by Thornton and Guza [1983], the range of calibrated value of B is between 0.8 and 1.7.

The wave radiation stress in the longshore direction is given by

$$S_{xy,w} = E_w \frac{c_g}{c} \cos\theta \sin\theta \tag{3.18}$$

Assuming a longshore uniform beach, the driving force of the wave-induced current is due to the cross-shore gradient of the longshore radiation shear stress, including the roller contribution:

$$F_y = -\frac{\sin\theta}{c} \frac{d}{dx} \left(E_w c_g \cos\theta + 2 E_r c \cos\theta \right) \tag{3.19}$$

Current modelling

The current in alongshore direction is determined by the alongshore momentum equation. The above current driving force (Eq 3.19) is balanced by bottom friction and lateral friction. In the present model, a depth-averaged mode is considered. The bottom friction stress is determined by the quadratic law:

$$\tau_b = \rho C_f < V|\vec{U}| > \tag{3.20}$$

where V is depth-averaged longshore current velocity, U is the instantaneous total horizontal velocity vector and C_f is a friction coefficient:

$$c_f = \frac{g}{c^2} \tag{3.21}$$

$$C = 18\log\left(\frac{12h}{k_s}\right) \tag{3.22}$$

When the current velocity is much smaller compared to the wave orbital velocity, the bottom friction stress τ_b can be linearized by the following equation [Liu and Dalrymple, 1978]

$$\tau_b = \frac{2}{\pi}\rho C_f u_m V\left(1 + \sin^2\theta\right) \tag{3.23}$$

where u_m is total velocity variance.
The parametrisation of $< V|\vec{U}| >$ for random waves adopts the formulation of Wright and Short [1984] in an empirical form is

$$< V|\vec{U}| >= \sigma_t V\left(\alpha^2 + \left(\frac{V}{\sigma_t}\right)^2\right)^{\frac{1}{2}} \tag{3.24}$$

Where α is a coefficient, the best fit for α is 1.16 by Feddersen et al. [2000].
The wave-averaged and depth-integrated longshore momentum equation governing the longshore current is

$$\tau_b = F_y + \rho\frac{dh\tau_{xy}}{dx} \tag{3.25}$$

where τ_{xy} is the horizontal turbulent stress.

$$\tau_{xy} = v_t\frac{dV}{dx} \tag{3.26}$$

where v_t is eddy viscosity.

3.2.3. Laboratory experiments

Visser (1991) experiments

Visser [1991] conducted a series of experiments to measure the spatial distribution of wave-induced longshore currents. To achieve a uniformity of the longshore current in the wave basin, Visser [1991] used a pumped recirculation in the experiments and fine-tuned the optimal recirculation discharge to minimize the return flow. The high quality control makes these experimental data one of the most popular calibration and/or validation sets for numerical models. Two cases of these experiments confined to regular waves and a 1:20 slope with a smooth concrete bottom were simulated, viz. Case 4 and Case 5 of Visser [1991] experiments (in short $V91\_C4$ and $V91\_C5$, respectively) The wave parameters are summarised in Table 3.1. The subscript "1" refers to values at the wave generators. The cross-shore profile is shown in Figure 3.1, (a).

Hamilton and Ebersole (2001) experiments

Another suitable data set of measured wave-induced longshore current for validation was produced by Hamilton and Ebersole [2001]) in the wave basin of the Large-scale Sediment Transport Facility (LSTF). The smooth concrete beach slope was 1/30 (Figure 3.1, b). Case 6N with regular waves was simulated. Similar to Visser [1991], a multiple pumping system was utilised to optimise the uniformity of longshore current.

Hulsbergen and ter Horst (1973) experiments

Although the purpose of the H73 experiments was to investigate the interaction between pile screen groins and a wave-driven longshore current, the base case without groins provides an additional valuable, validation/calibration data set. The wave only experiment was conducted in a wave basin of Delft Hydraulics. The bottom contours are straight and parallel to the shoreline. Regular waves with H=0.03 m and T=1.04 s were generated approaching the shore at an incidence angle of 15°.

Reniers et al. (1997) experiments

Reniers et al. [1997] conducted laboratory experiments for wave driven longshore currents on barred and non-barred beaches. As the above mentioned four cases are all about plane beaches, two tests with a barred beach (Figure 3.1, d), test SA243 under regular waves and test SO014 under irregular waves, were chosen to be reproduced. The height of the bar is about 10 cm, of which the inner slope is 1:8. The plane slope of the beach seaward is 1:10 while the shoreward slope is 1:20. The water depth at the wave maker is 0.55 m. The wave parameters are listed in Table 3.1.

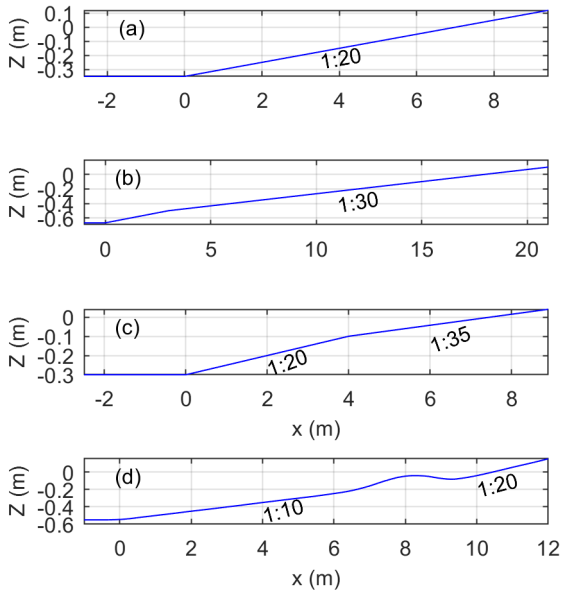

Figure 3.1: The bottom profile of each experiment: (a), Visser (1991) ; (b), Hamilton et al. (2001) ; (c), Hulsbergen et al. (1973) ; (d) Reniers and Battjes, (1997)

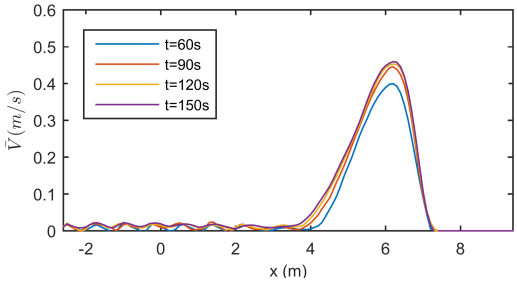

Figure 3.2: The cross-shore profile of computed longshore current at t=60 s (blue line), t=90 s (red line), t=120 s (yellow line), t=150 s (purple line). (For interpretation of the references to colour in this figure legend, the reader is referred to the web version of this article.)

Table 3.1: The parameters of the experiments

Exp.	wave	H_1 (m)	T_1 (s)	Θ_1 (°)	m	d_1 (m)	L_1 (m)	H_1/L_1	H_1/d_1	$k_1 d_1$	Beach type
V91_C4	Regular	0.078	1.02	15.4	1:20	0.35	1.46	0.053	0.22	1.51	plane
V91_C5	Regular	0.071	1.85	15.4	1:20	0.35	3.19	0.022	0.20	0.70	plane
H01_6N	Regular	0.182	2.50	10.0	1:30	0.67	5.94	0.031	0.27	0.71	plane
H73_W	Regular	0.030	1.04	15.0	1:35	0.30	1.45	0.021	0.10	1.30	plane
R97_SA243	Regular	0.08	1.00	30.0	1:20	0.55	1.53	0.052	0.15	2.26	barred
R97_SO014	Irregular	0.07	1.20	30.0	1:20	0.55	2.09	0.034	0.13	1.65	barred

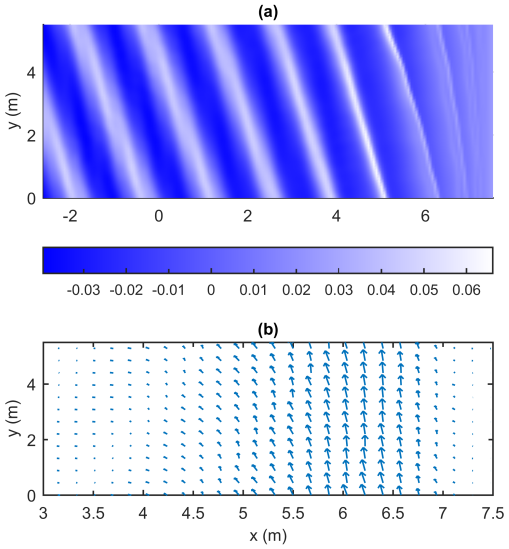

Figure 3.3: Case 4 (H=0.078 m, T=1.02 s, θ=15.4°) of V91 experiments; (a) snapshot of the computed wave field (the unit of the colour bar is m) and (b) the phase-averaged and depth-averaged current field.

3.3. Results

3.3.1. V91 experiments

To verify the ability of the SWASH model in simulating wave-induced longshore currents, a set of numerical simulations was conducted to compare to Case 4 and Case 5 of the Visser [1991] experiments. The number of vertical layers was set at 20, which is fine enough to resolve the flow vertical structure. To achieve a more efficient computation time, the so-named subgrid method [Rijnsdorp et al., 2017] was applied to derive the vertical accelerations and pressure gradients on a coarser grid of 4 layers. The remaining wave and mean flow dynamics are resolved on the fine grid. Such a two-grid system reduces computational efforts substantially by an order of magnitude. The validation of the subgrid approach showed that the predictions by subgrid simulations are comparable to that of fully resolved simulations [Rijnsdorp et al., 2017].

Case 4

For Case 4 of V91 experiments, the time step was set at δt =0.005 s, the grid resolution was set δx=0.03 m in cross-shore direction and δy=0.044 m in alongshore direction (400 × 128 grid cells in total). The obliquely incident regular waves with a period of 1.02 s, an amplitude of 0.039 m and an incident angle of 15.4°, were generated at the offshore boundary. A periodic boundary was used at the

lateral boundaries to limit the length of an unbounded beach. In the laboratory experiment, the bottom was made of smooth concrete. The roughness height value of a smooth concrete bottom is suggested as 0.001 m by Visser [1984b], 0.0005 m by Reniers [1997], and 0.0004 m by Rijnsdorp et al. [2017]. Hereinafter, the roughness height was chosen at ks= 0.0005 m for this following cases as a default setting which is qualified as validation and not calibration, since it is well within the default range.

After a computational duration of 150 s, the current field reaches a stationary state as demonstrated in Figure 3.2, indicating that the differences between the longshore current profiles at t=120 s and t=150 s are relatively small. In Figure 3.3, the computed instantaneous water level and the phase- and depth-averaged current field are shown. As waves approach the shore, waves are transforming due to shoaling effects and changing direction because of depth refraction. Then wave heights start to decrease once depth limited breaking occurs. It is clearly shown that there is a spatial lag between the location of maximal horizontal current velocity and that of the maximal wave height.

The cross-shore variations of wave height, mean water level and longshore current are shown in Figure 3.4. The blue lines denote the computed results, while the red circles are the measured V91 data. The simulation successfully captures the right location of wave breaking point. The waves start to break at x=5 m, 2 m offshore to the shoreline at x=7 m. The wave heights are slightly overpredicted within the surf zone, which suggests that the model may slightly underestimate the energy dissipation rate. This observed deviation is similar to the results of the same case simulated by Chen et al. (2003), who found the same overprediction using a phase-resolving Boussinesq type model. Nevertheless, the computed wave set up and longshore current velocity agree very well with the measured data. The slight overestimation of the wave set up is consistent with the trend of the computed wave height, and may be partly due to a minor underestimation of the longshore current velocity.

As shown in Figure 3.4 c, the model quite accurately predicts the cross-shore variation of the longshore current as well as the location and magnitude of the maximum velocity. Overall, the well-matched results reveal the validity of the wave-breaking scheme and of the transformation of momentum flux in both longshore and cross-shore directions.

Case 5

For this case, with a longer wave period of 1.85 s, the grid resolution could be increased to δx=0.05 m and δy=0.087 m (resulting in 240 × 140 grid cells in total). Other parameters are kept the same as in Case 4. The computed wave height is nearly the same as the measured data (Figure 3.5). The waves started to break at x=4.5 m, 2.5 m offshore to the shoreline at x=7 m. Although the longshore current

velocity is slightly overestimated, its cross-shore profile is well reproduced.

3.3.2. H01_6N experiment

In this simulation the time step was set at δt=0.005 s, the grid resolution was set δx=0.08 m and δy=0.16 m (275 × 225 grid cells in total). The roughness height was set at ks=0.0005 m, the same as the default value. The number of vertical layers was set at 20, which is found fine enough to resolve the vertical variation of mean flow structure from previous simulation experience, while the coarse subgrid with 4 pressure layers was turned on.

The comparable simulation results with the measurement data are shown in Figure 3.6. The simulation accurately reproduces the wave height transformation. The finer resolution of the numerical model predicts the wave breaking point at x=10.5 m, while the measured maximal wave height is at x=9.48 m and the next measurement point is beyond 10.5 m. The wave height variation cross-shore shows a good agreement with the observed values (Figure 3.6, (a)). Both the locations of the wave set-up and the maximal longshore current are accurately computed. Similarly to the V91_C4 simulation, within the surfzone, the wave set-up is slightly overestimated while the longshore current is slightly underestimated. This pattern of deviations between simulations and measurements of H01_6N and V91_C4 experiments may be due to their more similar wave steepness.

3.3.3. H73_W experiment

In addition to the above validations against the well-known V91 and H01 experiments, a unique, not well-known, but valuable data set is obtained from [Hulsbergen and ter Horst, 1973]. As part of their comprehensive measurements of the impact of groins on the longshore current, here their wave only case is used for additional validation.

To reproduce the experiments numerically, the time step was set at δt=0.005 s, the grid resolution was set δx=0.03 m and δy=0.044 m (resulting in 380 × 128 grid cells). The roughness height was set at ks=0.0005 m, again in the default range. The vertical velocity layers were chosen 20 while the coarse pressure layers were 4.

For this condition, the computed maximal alongshore velocity is 0.14 m/s at x=6.5 m (Figure 3.7c). The mean longshore current velocities show satisfactory agreement with the measured data, but the velocities are slightly underestimated. Because of the crude assumption that the vertical profiles of the longshore currents within the surf zone are uniform, the measured velocities by float points in the upper water column might need to be interpreted as depth-averaged velocities, which may partially explain the underestimation. The calculated breaker point is at about x=5.5 m (Figure 3.7a), 2 m seaward to the shoreline at x=7.5 m, consistent with the observation in the experiment [Hulsbergen and ter Horst, 1973]. Wave heights and

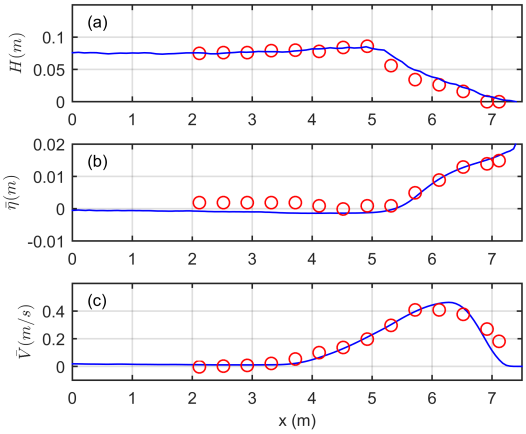

Figure 3.4: Case 4 of V91 experiments; the cross-shore distribution of wave height (a), wave set up (b) and longshore current velocity (c), (blue lines: simulations, red circles: measurements).

set-up were not measured, but as the longshore current velocities are much more sensitive to the parameters than the wave heights and mean water level, we have confidence that the simulated wave heights and mean water level are accurate. The computed maximum wave set-up reaches a value of 0.0092 m, which is approximately equal to 0.0075 m computed from linear wave theory.

3.3.4. R97 experiments

Case SA243

As the above all cases are about plane beaches, a more complex barred slope, of the experiment SA243 conducted by Reniers et al. [1997], was considered. The case Re97_SA243 was simulated and compared with experimental data. The numerical domain consists of 440 grids (δx=0.03 m) in cross-shore direction and 100 grids (δy=0.031 m) in alongshore direction. Other parameters and settings are the same as the default.

It is shown (Figure 3.8) that the locations of the wave breaking, wave set down and maximal longshore current are all accurately calculated. The waves were starting breaking on the outer bar slope when the water depth is rapidly reduced. Then the spatially lagged maximal longshore current appeared on the bar crest. The observed bimodal shape of longshore current was also reproduced, where one peak location is at the bar crest and the other peak is near the shoreline. The second peak was not measured but visually observed by dye movement in the experiment due to that the limited water depth (< 3 cm) is beyond the usage range of measurement apparatuses [Reniers, 1997].

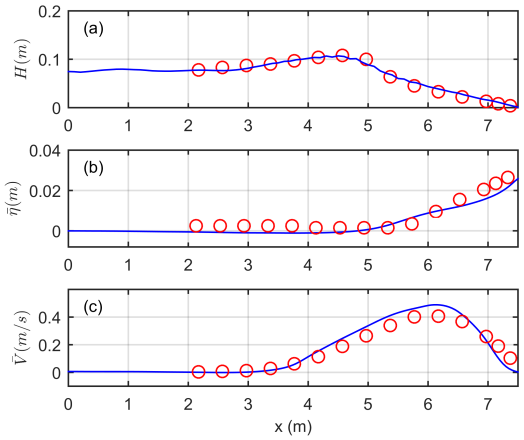

Figure 3.5: Case 5 (H=0.071 m, T=1.85 s, θ=15.4°) of V91 experiments; the cross-shore distribution of wave height (a), wave set up (b) and longshore current velocity (c), (blue lines: simulations, red circles: measurements).

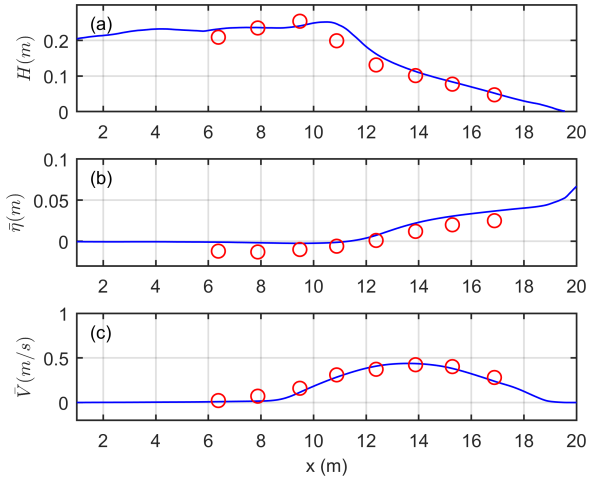

Figure 3.6: Case H01_6N (H=0.182 m, T=2.5 s, θ=10°); the cross-shore distribution of wave height (a), wave set up (b) and longshore current (c), (blue lines: simulations, red circles: measurements).

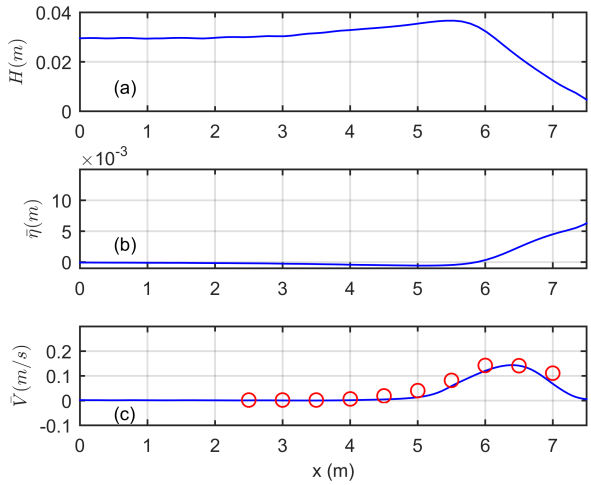

Figure 3.7: Case H73_W (H=0.03 m, T=1.04 s, θ=15°); the cross-shore distribution of wave height (a), wave set up (b) and longshore current (c), (blue lines: simulations, red circles: measurements).

3

Case SO014

Unlike the previous cases all tested under regular waves, case SO014 was tested with irregular waves. The numerical grid resolution is $\delta x = 0.041m$ in cross-shore direction and $\delta y = 0.084m$ in alongshore direction. Other parameters and settings are kept the same as previous simulations. Again, a good agreement between modelled and measured longshore current velocities was obtained (Figure 3.9).

3.4. Analysis of modelled longshore currents

To evaluate the performance of the SWASH model, three statistical parameters, i.e. root mean square error (RMSE), relative bias (the sum of errors over the sum of observed values) and correlation coefficient (R^2) are computed for all six numerical simulations. The results are listed in Table 3.2. For both wave height and longshore current computations, the root mean square errors are confined to a relatively small value. All correlation coefficients are larger than 0.97, revealing a strong correlation between the simulated results and measurements. For the specific interest in modelling longshore currents of this study, comparisons between modelled and observed values are depicted in Figure 3.10. The relative small RMSE and strong correlation coefficient validate the capacity of modelling longshore currents of SWASH with just default set parameters on both barred and non-barred beaches. However, the much larger relative bias of R97_SO014 shows that the swash model results are much worse for irregular waves than the results of other experiments under regular waves with default parameter settings.

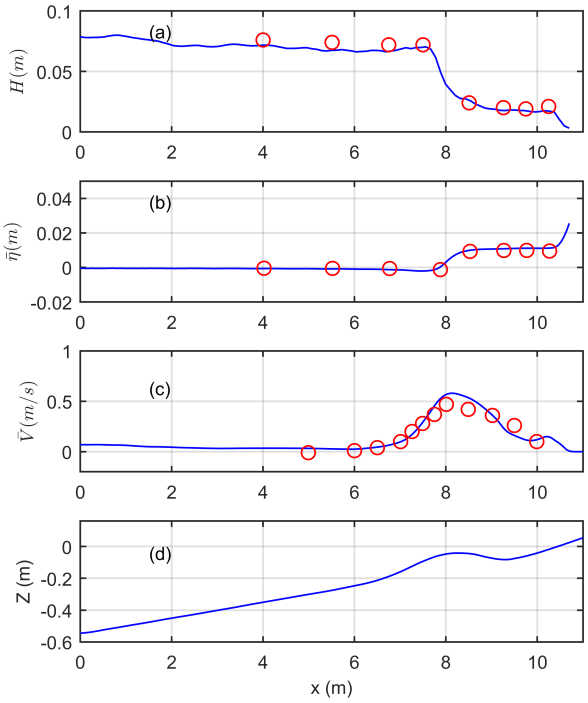

Figure 3.8: Case R97_SA243 (H=0.08 m, T=1 s, θ=30°); the cross-shore distribution of wave height (a), wave set up (b), longshore current (c) and the bottom profile (d), (blue lines: simulations, red circles: measurements).

Table 3.2: Statistics of the computed bulk parameters against the measurements

H	RMSE (m)	R^2	Relative bias (%)
V91_C4	0.0086	0.9798	9.08
V91_C5	0.0056	0.9931	1.16
H01_6N	0.0188	0.9728	5.25
R97_SA243	0.0039	0.9968	-6.34
R97_SO014	0.0085	0.9948	20.3
$\bar{v}$	RMSE (m/s)	R^2	Relative bias (%)
V91_C4	0.0415	0.9700	-9.76
V91_C5	0.0348	0.9815	-11.33
H01_6N	0.0396	0.9871	-11.13
H73	0.0195	0.9707	-25.07
R97_SA243	0.0582	0.9593	5.55
R97_SO014	0.0703	0.9523	-38.69

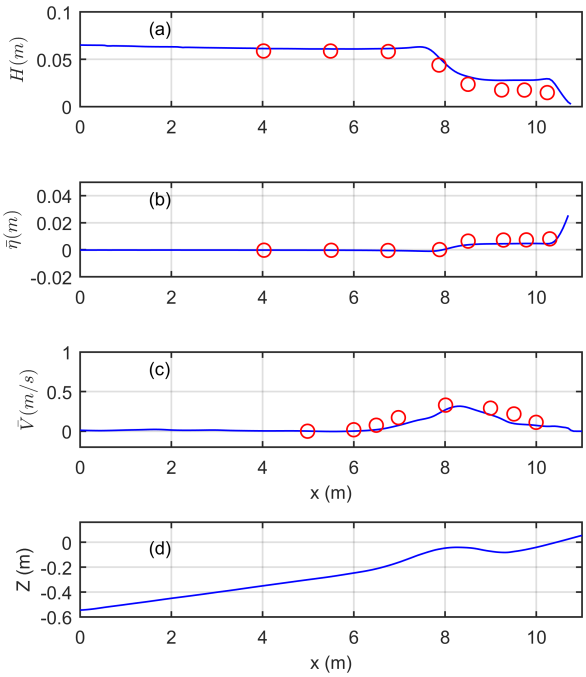

Figure 3.9: Case R97_SO014 (Hs=0.07 m, Tp=1.2 s, θ=30°); the cross-shore distribution of wave height (a), wave set up (b), longshore current (c) and the bottom profile (d),(blue lines: simulations, red circles: measurements).

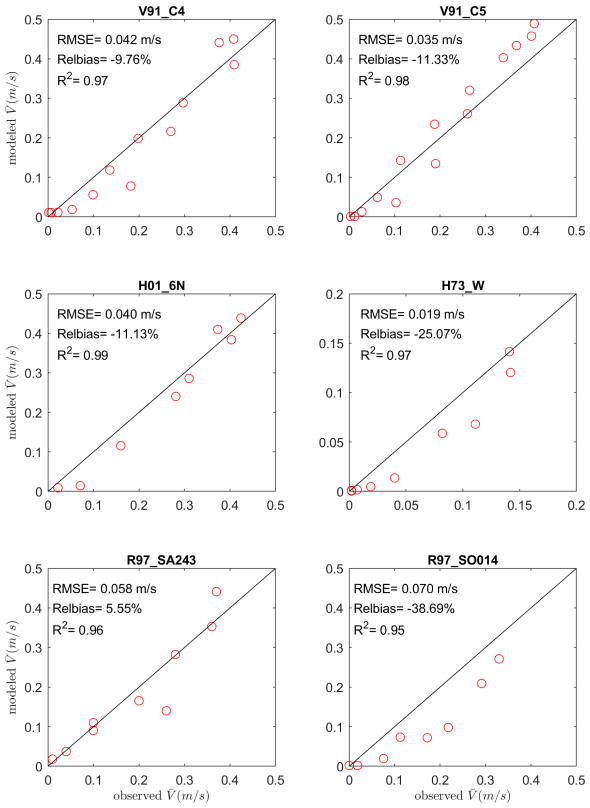

Figure 3.10: Comparison of modelled and observed longshore current velocities for each experiment showing RMSE, Bias, and R^2 values. Black solid lines represent perfect agreement.

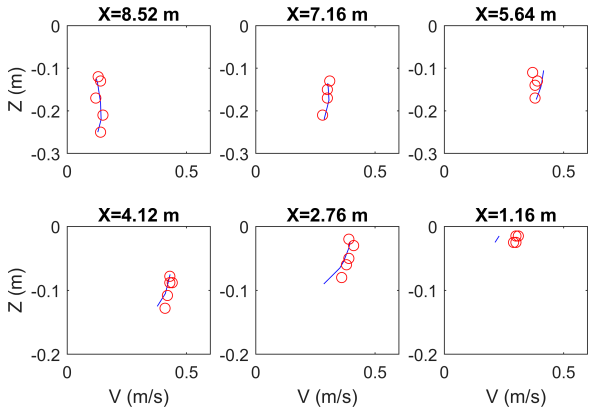

Figure 3.11: Case H01_6N, the comparison of modelled and observed vertical variations of V(z), (blue line: simulation, red circle: measurement).

3.5. Validated and predicted vertical variations of longshore currents

Given the availability of measurement data, only the vertical variations of longshore currents of experiment H01_6N could be validated (Figure 3.11). The calculated longshore current velocities V(z) matched well with observed values at five different locations, except for an underestimation at the nearest location (X=1.16 m offshore). From the furthest offshore location (X=8.52 m offshore where h=0.274 m) to the third nearest to shoreline location (X=4.12 m offshore where h=0.149 m), little vertical variations of the velocity profiles were observed (Figure 3.11). Therefore, the vertical profiles can be characterised as depth uniform. At a further inshore location (X=2.76 m), the turbulent bottom boundary layer becomes dominant, and the vertical profile changes from a rather depth uniform to a logarithmic profile.

To investigate the vertical variation of longshore current for the other five experiments, the depth variation of the predicted normalised longshore current $\bar{v}/c$ is illustrated in Figure 3.12, where c is the local shallow wave celerity. The vertical profile locations in the figure are ranging from 0.4 to 1.4 times the width of the surf zone, increasing at a 0.2 times width interval. At 1.4 times xb, the longshore current is almost zero for all cases. Similarly, the normalised longshore currents reach their largest value halfway across the breaker zone on planar beaches of the first four experiments. Because of the stronger bottom friction near the shoreline, a slight deviation from a depth uniform profile arises, where the normalised longshore current at the upper water column is slightly larger than that near bottom. Further offshore, the profiles of the longshore current are nearly vertical, verifying that the longshore current is rather depth uniform within most breaker zones under regular waves on planar beaches.

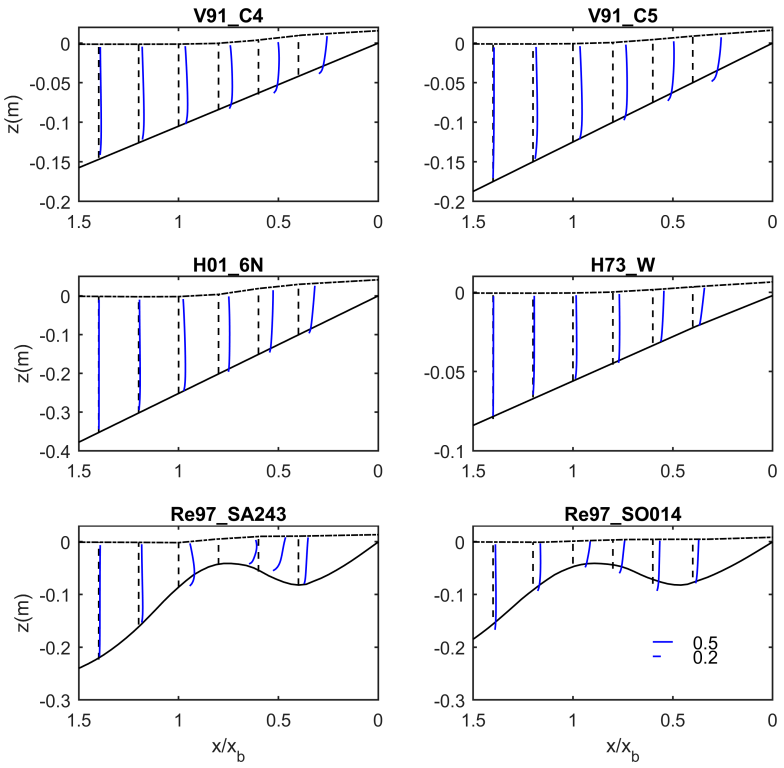

Figure 3.12: The vertical profiles of normalised longshore shore current $\bar{v}$/c, c(=$\sqrt{gd}$) is local wave celerity. The vertical black dash line denotes the vertical profile location and indicates the zero value of each vertical profile of $\bar{v}$/c (blue line). The dash dot and solid black lines represent the mean water level and slope bottom, respectively. The scale is given in Re97_SO014 figure. (For interpretation of the references to colour in this figure legend, the reader is referred to the web version of this article.)

The generally depth uniform trend is supported by similar observations in the Hamilton and Ebersole [2001] and Visser [1991] laboratory experiments, and in the Sandy Duck field experiments [Reniers et al., 2004]. One possible reason would be the breaking wave induced turbulence injected downward, smoothing the vertical current profile (for instance, Figure 1 in Svendsen and Lorenz [1989], and Figure 1 in Church and Thornton [1993]). Another possible reason would be the dispersive mixing by the interaction of mean longshore currents and cross-shore currents Putrevu and Svendsen [1992]. Due to the strong influences of dispersion and turbulence on the vertical variations of longshore current profiles, the boundary layer would not be fully developed with the existence of breaking waves. It is shown that the generally depth uniform longshore current profile is confined to regular waves on planar beaches. When the other two experiments with a barred slope were considered (Figure 3.12), it is found that the vertical profiles tend to be more uniform under random waves (Re97_SO014) than under regular waves (Re97_SA243). However, the vertical profiles of longshore currents are much more logarithmic over the bar.

3.6. SWASH model vs 1D model

If the very shallow zone is not considered and the vertical variation of the cross-shore current is not of interest, a simple 1D longshore momentum balance model is shown sufficient to compute the longshore current. This phase-averaged 1D model complemented, is used to test the H73_W experiment, Re97_SA243 and Re97_SO014 experiments, compared with the validated simulation by the SWASH model. To accurately predict the peaks in the cross-shore distribution of longshore current and wave setup and set down, the roller model developed by Dally and Brown [1995] is included. The additional roller model has been affirmed necessary to shift the computed maximum longshore current landward of the breaker point [Osiecki and Dally, 1996, Reniers, 1999], to bridge the deviation of the numerical models from the measurements [Visser, 1984b, Reniers, 1997].

The calculated results of the H73_W experiment are shown in Figure 3.13. For the 1D model, the wave set up is the most insensitive to the free parameters. In contrast, wave height is sensitive to the wave breaker index γ and the wave breaking fraction parameter B. The well calibrated γ is found to be 0.78. The value 1.75 of B is used which is the optimal value obtained by fitting to a laboratory data set [Power et al., 2013]. Besides, the variation of the wave front angle β of the roller model and the viscosity dominate the cross shore profile of the longshore current. The value of β is chosen 0.1 while the eddy viscosity is taken as 0.01 m^2/s. The bottom roughness height, which significantly affects the magnitudes of longshore current velocities, was calibrated to be 0.0015 m. The calibrated bottom roughness value used in the 1D model is three times the recommended empirical value 0.0005 m used in the SWASH model.

In Figure 3.14, the 1D model provides good results for the Re97_SA243 exper-

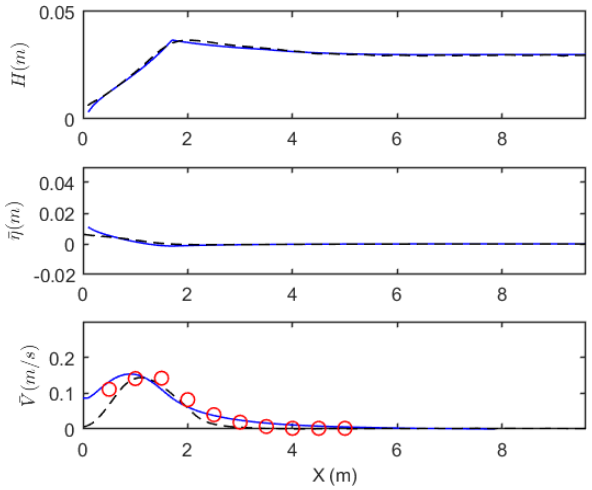

Figure 3.13: Comparison between the simulated results of the H73_W experiment by the 1D model (blue line) and the results obtained by the SWASH model (black dash line), (red circles: measurements).

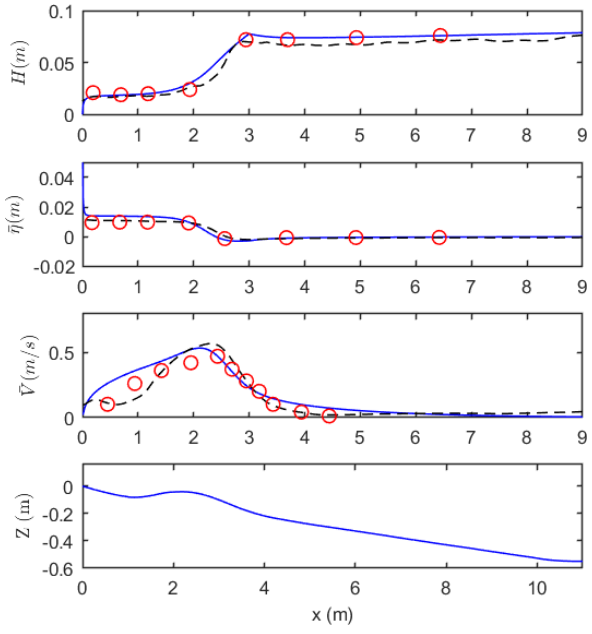

Figure 3.14: Comparison between the simulated results of the R97_SA243 experiment by the 1D model (blue line) and the results obtained by the SWASH model (black dash line), (red circles: measurements).

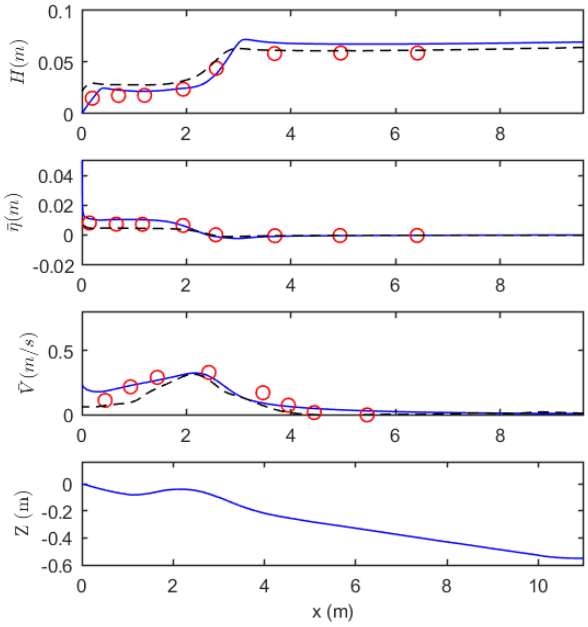

Figure 3.15: Comparison between the simulated results of the R97_SO014 experiment by the 1D model (blue line) and the results obtained by the SWASH model (black dash line), (red circles: measurements).

iment on a barred slope under regular waves, when the bottom roughness height increased to 0.01 m. For the experiment Re97_SO014 on the same slope but under irregular waves, a good agreement was obtained (shown in Figure 3.15) when the roller slope parameter was changed from 0.1 to 0.05, and the bottom roughness height 0.0005 m was used.

3.7. Disussion

The ability of the SWASH model in simulating longshore currents has been investigated and validated on barred and non-barred beaches under obliquely incident regular and irregular waves. Since the purpose of this study is to validate the SWASH model with uncalibrated default free parameters, the parameters (e.g. bottom roughness height, horizontal eddy viscosity) were set the same for all the simulation cases. Without any variation of the free parameters, the SWASH model provided promising results. It can be expected that after calibration, the accuracy of the SWASH model could even be improved. For instance, calibrating bottom friction coefficients would significantly affect modelled longshore current magnitudes, for which there is a large variability found in the literature.

The simulation results of the longshore currents on a barred slope (Re97_SA243 and Re97_SO014) are consistent with that measured in the laboratory. Confined

to a well-controlled laboratory environment, both the modelled and observed longshore currents have the same cross-shore variations. The pattern is that the maximal longshore current occurs where the wave breaking induced turbulence is the strongest. The second peak velocity appears near the shoreline. However, the field experiment DELILAH shows that the maximum longshore current velocity is on the trough but not over the bar crest. Reniers [1997] attempted to test the effects of alongshore variation and lateral mixing of their numerical model on the position of the maximum. However, neither an alongshore pressure gradient nor lateral mixing significantly affects the maximum longshore current velocity position. It was concluded that the maximal longshore current velocities observed in the trough are not attributed to the pure local wave forcing [Reniers, 1997]. The deviation of observed and predicted maximum velocity position may due to the failure to identify the alteration of the local forcing mechanism [Church and Thornton, 1993]. For complex forces (e.g. wind and tidal effects) in the field environment was not considered in the laboratory experiments and the numerical simulations by the SWASH model except for pure wave forces, the SWASH model could only reproduce the laboratory experiment results well, but could not contribute to illuminating the possible reason why the observed positions of maximal longshore currents appear in the trough.

It is shown that a simple 1D model is able to compute a longshore current distribution comparable to the SWASH model. However, the bottom roughness coefficient dominates the magnitude of computed longshore current velocity, of which the realistic value is not optimum all the time and then needs a calibration. For instance, the calibrated bottom roughness height varies a factor of twenty for the simulations on a barred slope. In addition, the cross-shore distribution of the longshore current depends on the eddy viscosity value in order to mimic the horizontal momentum flux diffusion, which is generally unknown. Different correlations between the eddy viscosity, characteristic length scale (i.e. wave height or water depth), and characteristic velocity (i.e. wave celerity or turbulent velocity) are available in the literature [e.g. Longuet-Higgins, 1970b, Battjes. J.A., 1975, Putrevu and Svendsen, 1992]. The simplest constant eddy viscosity was used in the simulations with a calibration, instead of choosing an available eddy viscosity model. While this finding illustrates the dominant mechanism for the generation of the longshore current distribution, the uncertainty of the free parameter value limits the prediction ability of the 1D model. Compared to the 1D model, the SWASH model is more accurate without having to pay attention to tuning the free parameters. When the vertical resolution is fine enough to resolve the vertical structure of mean flow, the order of O(20) in this study, and the computational domain is properly long with minor lateral boundary effects, the SWASH model reproduces the longshore current profiles in laboratory experiments fairly well, while only proper magnitude of longshore current velocity could be predicted by the 1D model. Therefore, the SWASH model with default parameter settings is suggested to predict the distribution of longshore currents accurately.

3.8. Conclusion

The SWASH model has been set up to simulate wave induced current against six laboratory experiments, four of which are confined to obliquely incident regular waves on non-barred beaches, and two experiments are on a barred beach under regular waves and irregular waves respectively. Nearly perfect agreements are found between the computed and measured wave heights, mean water levels and longshore currents. The longshore current generally spreads within 2 times the surf zone width [Longuet-Higgins, 1970a]. For simpler well-controlled experiments with regular wave incidence to alongshore uniform beaches considered in this paper, the longshore current is shown to develop mostly within 1.5 times the width of the surf zone. Along vertical direction, the longshore current is quite depth uniform on plane beaches. The exception, existing in very shallow water, is that the vertical profile of longshore current deviates from a depth uniform profile. The stronger bottom friction in shallower water enforces the vertical profile to transform into a logarithmic profile. Ignoring the very shallow zone nearshore, approximately stretching over 0.4 times surf zone width offshore, longshore currents maybe assumed depth uniform under regular waves on plane beaches. Both the numerical simulations and laboratory measurements show rather depth uniform vertical structure of mean longshore current under regular waves on plane beaches. This explains partly why the simpler 1D depth-averaged momentum balance equation can be sufficient to compute the longshore current. However, the assumption of depth uniform longshore current does not apply to a bared beach.

In conclusion, the phase-resolving SWASH model is capable to compute wave-induced longshore currents. The subgrid approach accelerates the computation without sacrificing the accuracy. The less computational effort shows that this phase-resolved model is a promising alternative to a phase-averaged model. Without tuning effort on free parameters, the SWASH model predicts wave generated longshore current fairly well on planar and barred beaches. More complex conditions such as combined wave and steady current condition, or realistic random waves in combination with tidal currents in fields would be investigated in further work.

References

Battjes. J.A. Modelling of turbulence in the surfzone. In *Proc. Symp. Model. Techniques*, pages 1050–1061, San Francisco, CA, 1975.

A. Bowen. The generation of longshore currents on a plane beach. *J. Mar. Res.*, 27 (1):206–215, jan 1969. ISSN 21699275. doi: 10.1002/2015JC011268. URL http://doi.wiley.com/10.1002/2015JC011268.

Q. Chen. Boussinesq modeling of longshore currents. *Journal of Geophysical Research*, 108(C11):3362, 2003. ISSN 0148-0227. doi: 10.1029/2002JC001308. URL http://doi.wiley.com/10.1029/2002JC001308.

J. C. Church and E. B. Thornton. Effects of Breaking Wave-Induced Turbulence Within a Longshore-Current Model. *Coastal Engineering*, 20(1-2):1–28, 1993.

W. R. Dally and C. A. Brown. A modeling investigation of the breaking wave roller with application to cross-shore currents. *Journal of Geophysical Research*, 100 (1):24873–24883, dec 1995. ISSN 0148-0227. doi: 10.1029/95JC02868. URL http://doi.wiley.com/10.1029/95JC02868.

A. T. M. de Bakker, M. F. S. Tissier, and B. G. Ruessink. Beach steepness effects on nonlinear infragravity-wave interactions: A numerical study. *Journal of Geophysical Research: Oceans*, 121(1):554–570, jan 2016. ISSN 21699275. doi: 10.1002/2015JC011268. URL http://doi.wiley.com/10.1002/2015JC011268.

J. H. Duncan. An Experimental Investigation of Breaking Waves Produced by a Towed Hydrofoil. *Proceedings of the Royal Society A: Mathematical, Physical and Engineering Sciences*, 377(1770):331–348, jul 1981. ISSN 1364-5021. doi: 10.1098/rspa.1981.0127. URL http://rspa.royalsocietypublishing.org/cgi/doi/10.1098/rspa.1981.0127.

F. Feddersen, R. Guza, S. Elgar, and T. H. Department. Velocity moments in alongshore bottom stress parameterizations. *Journal of Geophysical Research*, 105 (1770):8673–8686, jul 2000. ISSN 1364-5021. doi: 10.1098/rspa.1981.0127. URL http://rspa.royalsocietypublishing.org/cgi/doi/10.1098/rspa.1981.0127.

C. J. Galvin and J. P. S. Eagleson. Experimental study of longshore currents on a plane beach, Hydrodynamics laboratory report 63, Massachusetts Institute of Technology. Technical Report 1770, Massachusetts Institute of Technology, Cambridge, jul 1964. URL http://citeseerx.ist.psu.edu/viewdoc/download?doi=10.1.1.836.7507{&}rep=rep1{&}type=pdf.

D. G. Hamilton and B. A. Ebersole. Establishing uniform longshore currents in a large-scale sediment transport facility. *Coastal Engineering*, 42(3):199–218, 2001. ISSN 03783839. doi: 10.1016/S0378-3839(00)00059-4.

C.-E. Hsu, S.-C. Hsiao, and J.-T. Hsu. Parametric Analyses of Wave-Induced Nearshore Current System. *Journal of Coastal Research*, 33(4):795–801, 2017. ISSN 15515036. doi: 10.2112/JCOASTRES-D-16-00027.1.

C. Hulsbergen and W. ter Horst. Effect of permeable pile screens on coastal currents. Delft Hydraulics laboratory report M 1148, (in Dutch). Technical report, Delft Hydraulics, Delft, 1973.

B. Launder and D. Spalding. The numerical computation of turbulent flows. *Computer Methods in Applied Mechanics and Engineering*, 3(2): 269–289, mar 1974. ISSN 0045-7825. doi: 10.1016/0045-7825(74)90029-2. URL https://www.sciencedirect.com/science/article/pii/0045782574900292?via{%}253Dihub.

P. L.-R. Liu and R. a. Dalrymple. Bottom frictional stresses and longshore currents due to waves with large angles of incidence. *Journal of Marine Research*, 36(1):357–375, jul 1978. ISSN 15515036. doi: 10.2112/JCOASTRES-D-16-00027.1. URL http://citeseerx.ist.psu.edu/viewdoc/download?doi=10.1.1.836.7507{&}rep=rep1{&}type=pdf.

M. Longuet-Higgins. Longshore Currents Generated by Obliquely Incident Sea Waves, 1. *Journal of Geophysical Research*, 75(33):6778–6789, jul 1970a. ISSN 15515036. doi: 10.2112/JCOASTRES-D-16-00027.1. URL http://citeseerx.ist.psu.edu/viewdoc/download?doi=10.1.1.836.7507{&}rep=rep1{&}type=pdf.

M. Longuet-Higgins. Longshore Current Generated by Obliquely Incident Sea Waves, 2. *Journal of Geophysical Research*, 75(33):6790–6801, jul 1970b. ISSN 15515036. doi: 10.2112/JCOASTRES-D-16-00027.1. URL http://citeseerx.ist.psu.edu/viewdoc/download?doi=10.1.1.836.7507{&}rep=rep1{&}type=pdf.

M. S. Longuet-Higgins and R. W. Stewart. Radiation stresses in water waves; a physical discussion, with applications. *Deep Sea Research*, 11(33):529–562, jul 1964. ISSN 15515036. doi: 10.2112/JCOASTRES-D-16-00027.1. URL https://ac.els-cdn.com/0011747164900014/1-s2.0-0011747164900014-main.pdf?{_}tid=b1fd5dda-16ef-11e8-b926-00000aab0f01{&}acdnat=1519208117{_}76d80297d6d7e60b40d79dfedf8a4f54.

D. Osiecki and W. Dally. The influence of rollers on longshore currents. In *25th International Conference on Coastal Engineering*, pages 3419–3430, Orlando, 1996.

H. E. Power, T. E. Baldock, D. P. Callaghan, and P. Nielsen. Surf Zone States and Energy Dissipation Regimes — a Similarity Model. *Coastal Engineering Journal*, 55(01):1350003, 2013. ISSN 0578-5634. doi: 10.1142/S0578563413500034. URL http://www.worldscientific.com/doi/abs/10.1142/S0578563413500034.

U. Putrevu and I. a. Svendsen. A Mixing Mechanism In the Nearshore Region. In *23rd international conference on coastal engineering*, pages 2758–2771, Venice, 1992. ISBN 9780872629332. doi: 10.1061/9780872629332.210. URL http://ascelibrary.org/doi/10.1061/9780872629332.210.

A. Reniers. *Longshore current dynamics*. PhD thesis, Delft University of Technology, Venice, jul 1999. URL http://ascelibrary.org/doi/10.1061/9780872629332.210.

A. J. H. M. Reniers, J. A. Batties, and D. A. Falquês, A. Huntley. A laboratory study on the shear instability of longshore currets. *JOURNAL OF GEOPHYSICAL RESEARCH*, 102:8597–8609, Apr. 1997.

A. J. H. M. Reniers, E. B. Thornton, T. P. Stanton, and J. A. Roelvink. Vertical flow structure during Sandy Duck: Observations and modeling. *Coastal Engineering*, 51(3):237–260, 2004. ISSN 03783839. doi: 10.1016/j.coastaleng.2004.02.001.

J. A. Reniers, A. J. H. M. Batties. A laboratory study of longshore currents over barred and non-barred beaches. *Coastal Engineering*, 30(1):1–22, jul 1997. ISSN 03783839. doi: 10.1016/S0378-3839(97)00017-3. URL http://ascelibrary.org/doi/10.1061/9780872629332.210.

D. P. Rijnsdorp, P. B. Smit, and M. Zijlema. Non-hydrostatic modelling of infragravity waves under laboratory conditions. *Coastal Engineering*, 85(1):30–42, mar 2014. ISSN 0378-3839. doi: 10.1016/J.COASTALENG.2013.11.011. URL https://www.sciencedirect.com/science/article/pii/S0378383913001944?via{%}3Dihub.

D. P. Rijnsdorp, P. B. Smit, M. Zijlema, and A. J. Reniers. Efficient non-hydrostatic modelling of 3D wave-induced currents using a subgrid approach. *Ocean Modelling*, 116:118–133, 2017. ISSN 14635003. doi: 10.1016/j.ocemod.2017.06.012.

J. Smagorinsky. General circulation experiments wiht the primitive equations I. The basic experiment. *Monthly Weather Review*, 91(3):99–164, 1963. ISSN 0036-8075. doi: 10.1126/science.27.693.594.

P. Smit, M. Zijlema, and G. Stelling. Depth-induced wave breaking in a non-hydrostatic, near-shore wave model. *Coastal Engineering*, 76(3):1–16, jun 2013. ISSN 0378-3839. doi: 10.1016/J.COASTALENG.2013.01.008. URL https://www.sciencedirect.com/science/article/pii/S0378383913000215.

J. M. Smith, M. Larson, and N. C. Kraus. Longshore current on a barred beach: Field measurements and calculation. *Journal of Geophysical Research: Oceans*, 98(C12):22717–22731, 1993. ISSN 2156-2202. doi: 10.1029/93JC02116. URL http://dx.doi.org/10.1029/93JC02116.

M. J. F. Stive. Energy dissipation in waves breaking on gentle slopes. *Coastal Engineering*, 8(3):99–127, jun 1984. ISSN 2156-2202. doi: 10.1029/93JC02116. URL https://ac.els-cdn.com/0378383984900073/1-s2.0-0378383984900073-main.pdf?{_}tid=1dfb0568-f814-4c16-8a26-aa1904326026{&}acdnat=1520005962{_}ff004b4dfbbc234d273ce3df9c9f2fd4.

M. J. F. Stive and H. J. De Vriend. Shear stresses and mean flow in shoaling and breaking waves. In *24th International Conference on Coastal Engineering*, pages 594–608, Kobe, June 1994. ISBN 0872629228. doi: 10.1029/93JC02116. URL https://journals.tdl.org/icce/index.php/icce/article/viewFile/4985/4665.

T. Suzuki, C. Altomare, W. Veale, T. Verwaest, K. Trouw, P. Troch, and M. Zijlema. Efficient and robust wave overtopping estimation for impermeable coastal structures in shallow foreshores using SWASH. *Coastal Engineering*, 122: 108–123, apr 2017. ISSN 03783839. doi: 10.1016/j.coastaleng.2017.01.009. URL https://www.sciencedirect.com/science/article/pii/S0378383916302435.

I. A. Svendsen. Wave heights and set-up in a surf zone. *Coastal Engineering*, 8(3):303–329, apr 1984. ISSN 03783839. doi: 10.1016/j.coastaleng.2017.01.009. URL https://ac.els-cdn.com/0378383984900280/1-s2.0-0378383984900280-main.pdf?{_}tid=3631d9c5-e282-4226-817b-f8c2b9d8a9d7{&}acdnat=1520201537{_}ef6dbf1566507a37c357229554990597.

I. a. Svendsen and R. S. Lorenz. Velocities in combined undertow and longshore currents. *Coastal Engineering*, 13(1):55–79, 1989. ISSN 03783839. doi: 10.1016/0378-3839(89)90032-X.

I. A. Svendsen and U. Putrevu. Nearshore mixing and dispersion. *Proceedings: Mathematical and Physical Sciences*, 445(1925):561–576, 1994. ISSN 0374-5481. doi: 10.1080/037454809495909.

E. B. Thornton and R. T. Guza. Transformation of wave height distribution. *Journal of Geophysical Research*, 88(C10):5925, 1983. ISSN 0148-0227. doi: 10.1029/JC088iC10p05925. URL http://doi.wiley.com/10.1029/JC088iC10p05925.

E. B. Thornton and R. T. Guza. Surf Zone Longshore Currents and Random Waves: Field Data and Models. *Journal of Physical Oceanography*, 16(7):1165–1178, jul 1986. ISSN 0022-3670. doi: 10.1175/1520-0485(1986)016<1165:SZLCAR>2.0.CO;2. URL http://journals.ametsoc.org/doi/abs/10.1175/1520-0485{%}281986{%}29016{%}3C1165{%}3ASZLCAR{%}3E2.0.CO{%}3B2.

P. J. Visser. Longshore current flows in a wave basin. In *17th International Conference on Coastal Engineering*, pages 462–479, Sydney, 1980.

P. J. Visser. The proper longshore current in a wave basin. Technical Report 82-1, Delft University of Technology, Delft, the Netherlands, 1982.

P. J. Visser. A mathematical model of uniform longshore currents and the comparison with laboratory data. Technical Report 84-2, Delft University of Technology, Delft, the Netherlands, 1984a.

P. J. Visser. Uniform Longshore Current Measurement and Calculations. In *19th International Conference on Coastal Engineering*, pages 2192–2207, Houston, 1984b. ISBN 0872624382.

P. J. Visser. Laboratory measurements of uniform longshore currents. *Coastal Engineering*, 15(5-6):563–593, oct 1991. ISSN 03783839. doi: 10.1016/0378-3839(91)90028-F. URL http://linkinghub.elsevier.com/retrieve/pii/037838399290028S.

L. D. Wright and a. D. Short. Morphodynamic variability of surf zones and beaches: A synthesis. *Marine Geology*, 56(1–4):93–118, 1984. ISSN 0025-3227. doi: http://dx.doi.org/10.1016/0025-3227(84)90008-2. URL http://www.sciencedirect.com/science/article/pii/0025322784900082.

R. Zhang, M. Zijlema, and M. J. F. Stive. Laboratory validation of SWASH longshore current modelling. *Coastal Engineering*, 142:95–105, dec 2018. ISSN 0378-3839. doi: 10.1016/J.COASTALENG.2018.10.005. URL https://www.sciencedirect.com/science/article/pii/S0378383918301856.

M. Zijlema, G. Stelling, and P. Smit. SWASH: An operational public domain code for simulating wave fields and rapidly varied flows in coastal waters. *Coastal Engineering*, 58(10):992–1012, oct 2011. ISSN 0378-3839. doi: 10.1016/J.COASTALENG.2011.05.015. URL http://www.sciencedirect.com/science/article/pii/S0378383911000974?via{%}253Dihub.

4

Numerical Modelling of Hydrodynamics of Permeable Pile Groins

This chapter focuses on a specific form of groins, Permeable Pile Groins (PPGs), consisting of a single or double rows of wooden piles. With only few experiments and simulations available to study the hydraulic functioning of PPGs, the correlation between the effectiveness and the characteristics of the groin system has yet to be fully understood. This paper presents the application of SWASH, a non-hydrostatic wave-flow model to simulate flow fields affected by PPGs. The SWASH model was calibrated to correctly reproduce longshore current fields in the laboratory. Then, introducing PPGs in the model, the simulation results are compared with available experimental measurements to investigate current-PPG interaction. The simulation results, which generally agree well with the measurements, show that PPGs hardly attenuate wave energy but considerably retard longshore currents within the groin fields. Rip currents are predicted to develop at both flank sides of each pile groin, due to local positive water level gradients toward the pile groins.

This chapter have been published in Coastal Engineerng **153**, 95 (2019) .

4.1. Introduction

Coastal groins (or groynes), generally constructed perpendicular to the shore, are one of the most popular coastal protection structures. Groins contribute to the build-up of coasts and the widening of beaches via a) producing a sheltered area at the leeside of a groin due to wave diffraction; b) hindering wave induced longshore currents; c) deflecting strong tidal currents; d) intercepting longshore sediment transport [Bakker et al., 1970]. Considering the aspect of permeability, groins could be divided into permeable groins and impermeable groins. Impermeable groins are solid groins made of concrete, stone, wood or steel, which block the flow cells in groin fields. Permeable groins, made of wooden piles or porous stone or concrete modules, allow flow to pass through. The distinct advantage of permeable groins compared with impermeable groins is that permeable groins allow a fraction of the longshore sediment transport passing through their openings. A decrease in the blockage ratio of longshore sediment transport could alleviate the sand starvation of the coast downdrift permeable groins, where commonly large scale erosion occurs in the presence of impermeable groins. Moreover, unlike the commonly discontinuous shoreline interrupted by impermeable groins, the shoreline response to permeable groins is continuous [Bakker et al., 1984, Raudkivi, 1996, Trampenau et al., 1996]. For instance, a continous nearly stranght shoreline response to a permeable groin system is shown in Figure 4.1. In this paper, only one specific form of permeable groins, permeable pile groins (PPGs) consisting of wooden piles, was considered. Due to the appealing natural look, the ease of construction and the usage of renewable timber resources, PPGs attract more attention in coastal engineering projects especially from an environmental concern [Perdok, 2002, Crossman and Simm, 2002]. PPGs have been widely utilised to protect coasts from erosion in Europe, for instance, at the North Sea coasts in the Netherlands and the United Kingdom [Price et al., 1972, Bakker et al., 1984], and the Baltic Sea coasts in Germany and Poland [Raudkivi, 1996, Trampenau et al., 1996, Raudkivi and Dette, 2002, Dette et al., 2004, Strusiańska-Correia, 2014].

The functional mechanism of permeable pile groins, as concluded by Raudkivi [1996], is that PPGs act as hydraulic resistances to slow down longshore currents. The reduction of littoral current velocity leads to less turbulence produced by the wave-current interaction at the bed. Consequently, fewer sediment particles are mobilized. Therefore, the retarded longshore currents transport a reduced amount of sediment. As a result, the sediment is easily trapped and retained in the vicinity of the groins. The pile groins do not alter the characteristics of incident waves, which are negligible considering the wide spacing between each PPG alongshore [Raudkivi, 1996], except for a very limited wave shadow area near each PPG.

Field surveys showed that the coastline recession was effectively curbed and the nearshore accretion was promoted by massive rows of pile groins [Kolp, 1970, Price et al., 1972, Trampenau et al., 2004, Abam, 2009]. To further investigate the effects of pile groins on nearshore currents, a laboratory experiment under exquisitely controlled conditions is another effective method. When the average permeability

of a pile groin is 55%, Hulsbergen and ter Horst [1973] measured a 40% reduction of longshore current velocities within groin fields, under a combined wave and steady current condition. For the case of obliquely incident monochromatic waves in the experiment conducted by Trampenau et al. [2004], the purely wave-induced longshore current reduced to 40% of the undisturbed longshore current velocities, in the fields of groins with a 30% permeability, and to 70% in the fields of groins with a 50% permeability. Uijttewaal [2005] compared the turbulence properties near and downstream of permeable and solid groins. This author concluded that for permeable pile groins, the shear and turbulence intensity can be significantly reduced at the mixing layer between the groin fields and the main stream, and the rather unidirectional flow passing through permeable groins prevented the formation of a recirculation flow in groin fields, in contrast to solid groins.

Field studies and laboratory experiments proved that, to a large extent, PPGs slow down longshore currents and effectively curb coastline recession. In addition, timber PPGs are considered kind of appealing structures, especially at recreational coasts with a high aesthetic appreciation. The reason is that the small footprints of PPGs harm beach amenity to a small extent, and the renewable wooden construction material is environmentally friendly and economically [Perdok et al., 2003, Crossman, 2004], e.g. PPGs at a beach resort in Zeeland province, The Netherlands, Figure 4.1). However, an important consideration of beach erosion is that possible strong rip currents, incited by the existence of groins, could lead to seaward loss of beach material [Bakker et al., 1984].

Although for centuries PPGs have been applied in coastal engineering, relatively few detailed and high resolution measurements are available either from field studies or laboratory researches. To bridge the gap, numerical simulations are employed to study nearshore flow within permeable groin fields. The representative data sets obtained from the laboratory experiments [Hulsbergen and ter Horst, 1973] are selected to calibrate and validate the numerical model. The aim of the laboratory experiments was to explore the optimal layout of pile groins, mainly under a combined wave-current flow condition.

In the present work, we set up a phase resolving wave-flow model SWASH (an acronym for Simulating WAves till SHore), which includes pile groin effects on the flow. The governing equations of this model are listed in Section 4.2 and the experimental data set is described in the same section. The initial calibration of the model is presented in Section 4.3. Then the model is applied to evaluate pile groin impacts on nearshore currents, which are demonstrated in the same section. Results are discussed in Section 4.4, and conclusions are given in Section 4.5.

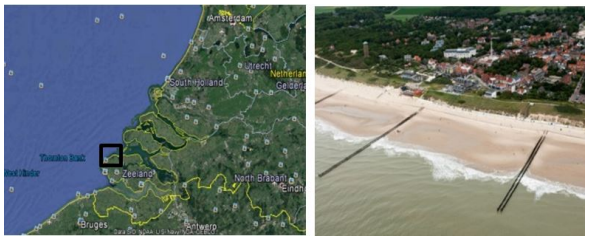

Figure 4.1: Left: The location of a pile groin engineered coast in Zeeland Province, The Netherlands (in the black rectangle, from Google earth); right: the continuous straight shoreline response to PPGs at the coast (source: https://beeldbank.rws.nl, Rijkswaterstaat).

4

4.2. Methods

4.2.1. Methods

SWASH [Zijlema et al., 2011] is an open source flow-wave model which could simulate unsteady, non-hydrostatic free-surface flow and which has been successfully applied to study various wave dynamics nearshore on a laboratory scale [Zijlema et al., 2011, Smit et al., 2013, Rijnsdorp et al., 2017]. Hereinafter A brief introduction of the SWASH model is given here. For details of the model, references are made to Zijlema and Stelling [2005, 2008], Zijlema et al. [2011] and Smit et al. [2013]. The governing equations are the RANS equations for an incompressible fluid including non-hydrostatic effects. In vertical direction, the water volume is bounded by the bottom z=-d(x,y) and the free water surface z=ζ(x,y,t),where t is the time, and x, y and z are the Cartesian coordinates. The local continuity equation and momentum equations in a three-dimensional (3D) configuration are given as

$$\frac{\partial \mathrm{u_i}}{\partial \mathrm{x_i}} + \frac{\partial \mathrm{w}}{\partial z} = 0 \tag{4.1}$$

$$\frac{\partial \mathrm{u_i}}{\partial \mathrm{t}} + \frac{\partial \mathrm{u_i u_j}}{\partial \mathrm{x_j}} + \frac{\partial \mathrm{u_i w}}{\partial z} = -\frac{1}{\rho}\frac{\partial\,(\mathrm{p_h} + \mathrm{p_{nh}})}{\partial \mathrm{x_i}} + \frac{\partial \tau_{\mathrm{ij}}}{\partial \mathrm{x_j}} + \frac{\partial \tau_{\mathrm{iz}}}{\partial z} - \mathrm{f_i} \tag{4.2}$$

$$\frac{\partial \mathrm{w}}{\partial \mathrm{t}} + \frac{\partial \mathrm{u_j w}}{\partial \mathrm{x_j}} + \frac{\partial \mathrm{w}^2}{\partial z} = -\frac{1}{\rho}\frac{\partial\,(\mathrm{p_h} + \mathrm{p_{nh}})}{\partial z} + \frac{\partial \tau_{\mathrm{zj}}}{\partial \mathrm{x_j}} + \frac{\partial \tau_{\mathrm{zz}}}{\partial z} - g \tag{4.3}$$

where i and j indicate two horizontal coordinates x/cross-shore and y/alongshore respectively, z is the vertical coordinate, u_i is the horizontal component of $\vec{u}$ in each direction, w is the vertical velocity, p_h and p_{nh} are hydrostatic and non-hydrostatic pressure components, respectively. The hydrostatic pressure p_h is explicitly expressed as $p_h = \rho g(\zeta - z)$, so $\partial_{x_i} p_h = \rho g \partial_{x_i} \zeta$ (where ∂_{x_i} stands for ∂/∂_{x_i}), and $\partial_z p_h = -\rho g$ (where g is the gravitational acceleration). τ_{ij} are turbulent stresses. Equation (4.1) is the local continuity equation, and Equations (4.2) and (4.3) are momentum equations including the effects of mixing, bottom friction and resistance of cylinders. The last sink term of Equation (4.2) is the momentum loss due to the presence of PPG cylinders. Integrating the local continuity equation in vertical direction, by substituting kinematic boundary conditions at free surface and

impenetrable bottom, a global continuity equation is induced

$$\frac{\partial \zeta}{\partial t} + \frac{\partial}{\partial x_i}\int_{-d}^{\zeta} u_i dz = \frac{\partial \zeta}{\partial t} + \frac{\partial h U_i}{\partial x_i} = 0 \tag{4.4}$$

where $h(= \zeta + d)$ is the total water depth. The bottom friction at the bottom boundary is computed according to the logarithmic law of the wall with a roughness height k_s (Launder and Spalding, 1974).The roughness height for a smooth concrete bottom used in laboratory experiment was chosen by calibration. The turbulence stresses are given based on eddy viscosity closure equations. The horizontal viscosity and vertical viscosity are estimated by the Smagorinsky type model [Smagorinsky, 1963] and the $k-\epsilon$ model [Launder and Spalding, 1974], respectively. The inclusion of vertical mixing spreads the effect of the bottom stress over the water column in vertical direction. To account for the momentum lost due to the resistance of pile cylinders, a sink term is added to the right-hand side of equation (4.2), which consists of a nonlinear quadratic drag loss term

$$\mathrm{f_i} = \frac{1}{2} N D C_D u_i |\vec{u}| \tag{4.5}$$

where C_D is the drag coefficient, N is the number of cylinder per unit bed area ($/m^2$), D is the cylinder diameter (m), f_i is the density-normalized drag force per cylinder height in x/cross-shore or y/alongshore direction.

4.2.2. Performance metrics

Three objective functions, Root Mean Square Error (RMSE), Scatter Index (SI) and correlation coefficient R^2, were applied to evaluate the performance of the model, compared to the measurement data. The interested wave height H, mean water level $\vec{\zeta}$ and mean longshore current velocity $\vec{V}$ are substituted by a variable in the flowing equations, where 'o' is short for observation and 'c' is short for calculation.

$$\mathrm{RMSE} = \sqrt{\frac{1}{N}\sum_{i=1}^{N}\left(f_c^i - f_o^i\right)^2} \tag{4.6}$$

$$\mathrm{SI} = \frac{\sqrt{\frac{1}{N}\sum_{i=1}^{N}\left(f_c^i - f_0^i\right)^2}}{\overline{f_o}} \tag{4.7}$$

$$\mathrm{R^2} = \frac{\sum_{i=1}^{\mathrm{N}}\left(f_c^i - \overline{f}_c\right)\left(f_o^i - \overline{\overline{f}}_o\right)}{\sqrt{\sum_{i=1}^{N}\left(f_c^i - \overline{f}_c\right)^2}\sqrt{\sum_{i=1}^{N}\left(f_o^i - \overline{f}_o\right)^2}} \tag{4.8}$$

4.2.3. Experimental arrangement

The data set, which was obtained by Hulsbergen and ter Horst [1973] experiments (hereafter H73 in short), is utilized to compare with the simulation results. The aim

of the scaled experiment was to examine the reduction extent of longshore currents due to the presence of PPGs with various layouts. The available experimental data are important to validate the implementation of pile groins in the numerical model and further test the interactions between pile groins and longshore currents.

A series of physical experiments were conducted in the 31.25 m long and 12.1 m wide wave basin of Delft Hydraulics in 1973, with the aim to investigate the optimal layout of a pile groin system. The bottom was made of smooth concrete and its contour is straight and parallel to the shoreline. The beach slope is 1/35 nearshore and 1:20 offshore (Figure 4.2, c). For the simulations by the SWASH model, two representative layouts are chosen to be simulated: three 5 m long PPGs at a 10 m spacing alongshore and five 3.5 m long PPGs at a 5 m spacing alongshore, respectively, both consist of two rows of wooden cylinders. The two pile rows of a PPG are at a 0.0875m alongshore interval. All the PPGs are perpendicular to the coastline. Given the geometric scaling of 1:40, the pile rows are 200 m and 140 m long respectively on a prototype scale. Each pile row of the long groin consists 373 wooden dowels, while the short row consists of 292 dowels. The permeability values are varying across shore from a low permeability at the landward end to a high permeability at the seaward head of groins. Here permeability is defined as the ratio of cross-sectional void area to the total lateral profile area of a PPG, when viewed from the side. When the pile cylinders are spaced cross-shore equidistantly, the permeability could calculated by the ratio of the cross-shore interval between each pile cylinder over the summation of the interval and the pile cylinder diameter. In this study, the average permeability is 55% of long groins and 50% of short groins.

The chosen hydraulic condition to be investigated in this paper is a combined wave-current condition, consisting of obliquely incident waves and alongshore steady currents. The pure current condition and pure wave condition are shown in Figure 4.3 to demonstrate their characteristics separately. For the pure current condition, a constant discharge 450 L/s imposed at the lateral boundary drived steady currents to flow alongshore (from left side to right side in Figure 4.3, (a1)). The magnitude of the steady current is proportional to the square root of water depth $\sqrt{h}$, decreasing gradually from deep water to shallow water on the beach slope (Figure 4.3, (a2)). When water depth h is larger than 0.05 m, the Reynolds number ($Re_c = V_0 h/\upsilon$) is beyond the threshold 2100 and the current is turbulent. The monochromatic unidirectional incident wave with H = 0.03 m and T = 1.04 s was generated approaching the shore at an incidence angle of 15° to shore normal direction (Figure 4.3, b(1)). Given the combined wave current condition, wave-generated longshore currents dominant within the breaker zone and flow in the same direction as the steady currents. Therefore, the superimposed longshore current near shore is enhanced and stronger than that under a pure wave or a pure current condition. When waves approaching the shore, waves refracted to shore normal direction, changing from a 75° intersection angle to alongshore steady current direction at offshore boundary, to a near-orthogonal angle (81.5°) when waves are breaking. The steady current

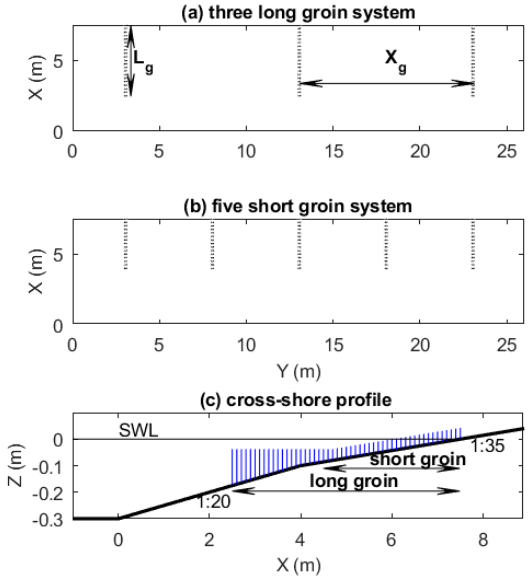

Figure 4.2: The layouts of groin systems (a: three long groin system; b: five short groin system) and the cross-shore profile of groins.

induced wave refraction was found insignificant in this case, less than 3%. A summary of the test parameters is given in Table 1. The layouts of the two groin system and the cross-shore profile are denoted in Figure 4.2.

4.2.4. Numerical implementation

To set up the model for H73 experiments, the physical domain was discretised by a structured grid. The grid resolution was constant, which was Δx=0.03 m in cross-shore direction and Δy=0.1 m in alongshore direction (resulting in 380 × 260 grid cells). Although a coarse vertical resolution (e.g. 2 layers) is sufficient to resolve wave physics (for instance wave propagation, shoaling, wave breaking and wave run-up), a very fine vertical resolution (10-20 layers) is required to well represent wave breaking dissipation in the surf zone [Smit et al., 2013]. In this study, the vertical layers were chosen to be 15 equidistant layers, which was proved to be fine enough (see the following section) to capture the proper magnitudes of longshore currents. The time step was set at Δt=0.005 s. Cyclic boundaries were used at lateral boundaries to limit the length of an unbounded coast. The obliquely incident regular waves were generated at the offshore open boundary. In addition to the waves; a constant water level gradient 3.1×10^{-5} at the lateral flow boundaries was exerted to mimic the steady longshore currents in the laboratory. The implementation of the longshore water level gradient is included in a modified version of

SWASH [de Wit et al., 2017].

To represent the PPG, we do not resolve the pile cylinders in the SWASH model. It is assumed that the cylinders are uniformly distributed within the volume between the two parallel pile rows of each PPG. We set the alongshore grid resolution approximately equal to the width of a PPG, thus pile cylinders spread uniformly within one grid cell alongshore. Given the cylinder diameter D=0.006 m and the wave length $\lambda = 1.45$ m, resulting in a ratio of D/ λ much smaller than the order of O(0.1), the pile cylinders could be seen as slender cylinders. Therefore the spatial variation of the undisturbed flow near cylinders within computational grid cells is assumed to be neglected. The projected area of the uniformly distributed PPG (udPPG) should be equal to that value of the real PPG, to guarantee the total drag forces are same. Thus, the frontal area $A_f\ (= D\sum_{i=1}^{n} h_{g,i})$ of a PPG is equal to the value $A_u d\ (= N\mathrm{W_g L_g}\overline{h}_g D)$ of a udPPG, where D is the diameter of a pile cylinder, n is the total number of pile cylinders of each PPG, L_g is the groin length, W_g is the groin width, and N is the number of cylinders per unit area, $\overline{h_g}$ is the averaged groin height. The computed $\overline{h_g}$ is 0.0525 m of short groins and 0.06 m of long groins. The drag forces by the udPPG are computed from equation (4.5). The unknown drag coefficient C_D was derived through calibration, with the aim to obtain computed longshore current velocities comparative with measured results, and having minimal root mean square errors against measurement data.

4.3. Results

In this section, the simulation results of H73 experiments are presented. The groinless base experiment is used to test the ability of predicting accurate longshore currents of SWASH model on a laboratory scale. The bottom friction coefficient was calibrated under combined wave-current flow. For the combined wave-current condition concerned in this study, the bottom roughness height was calibrated in the range of 0.0004 m to 0.001 m, and chosen to be 0.0008 m for which the minimal root mean square error was obtained. Then to calibrate the drag coefficient of udPPG, three 5 m long groins are introduced in the bottom roughness calibrated flow model. The drag coefficient is set as 1.1 calibrated in the range of 0.8 to 1.4. The calibration results of bottom roughness and drag coefficient are described in appendix A. Finally, the calibrated udPPG model was used to validate the hydrodynamics of another groin system consisting of five 3.5 m short groins.

4.3.1. Groinless bare bottom

When the groins are not involved in the numerical model, the model was calibrated to reproduce the observed wave height and longshore current variations in the experiments. Compared to measured longshore current velocities, the simulations produced good results under the pure wave condition (Figure 4.3, (a2)) and the pure current condition (Figure 4.2, (b2)). Then, the SWASH model succeeded

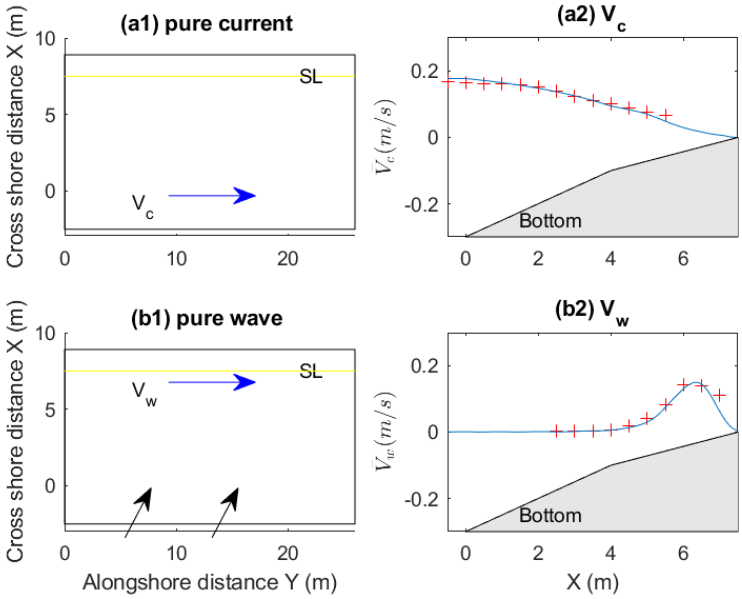

Figure 4.3: The pure current condition: (a1) steady current direction (blue arrow), (a2) steady current velocity V_c; the pure wave condition: (b1) wave direction (black arrow), and wave induced alongshore current direction (blue arrow), (b2) wave induced current velocity V_w. The red pluses denote the measured current velocity in the experiment, and the blue lines show the calculated current velocity, SL is short for shoreline.

in simulating the complex combined wave current condition (Figure 4.4,Figure 4.5,Figure 4.6). The calculated maximal wave height is 0.033 m (Figure 4.4), which is consistent with the measured breaking wave heights ranging from 0.025 to 0.035 m.

The calculated mean longshore current velocities at the first superficial layer of the water volume are shown in Figure 4.5, where the subscript 's' represents the superficial and the triangular braces '<>' denotes for longshore averaging. The thickness of each equidistant layer equals to 1/15 of the total water depth. The aim of the choice of superficial ($\overline{V_s}$) is to be consistent with the observed mean longshore current velocities measured by surface floaters in the experiment. The simulation results agree well with the measurements (Figure 4.5, a1). For instance, good agreements are observed within the inner breaker zone where the wave-induced longshore currents are dominant (X = 5.5 m to X = 7.5 m, in Figure 4.5 a1) and in the seaward zone where steady currents are dominant (X = 1.5 m to X =3 m, in Figure 4.5, a1). In the transition zone, the model underestimates the currents somewhat. The statistic indexes for the calculations, for instance, the scatter index is 0.13 and the correlation coefficient is 0.91 (Figure 4.5, a2), show a reliable reproduction of the measured longshore current velocities. The root mean square

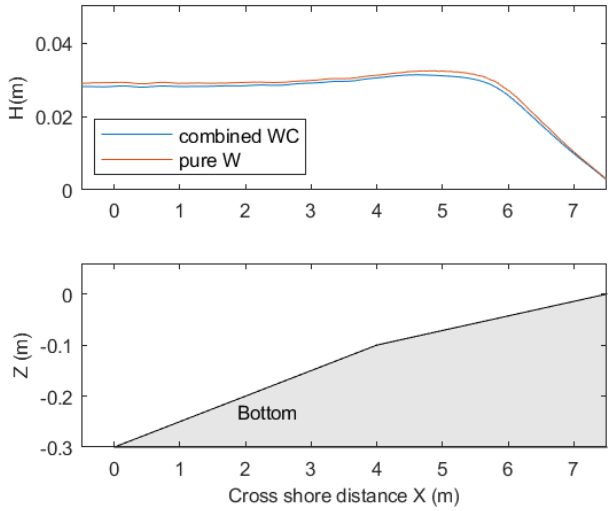

Figure 4.4: The calculated wave height evolution in cross-shore direction, (a): wave heights, blue line shows the combined wave current condition, red line shows the pure wave condition; (b): bottom slope.

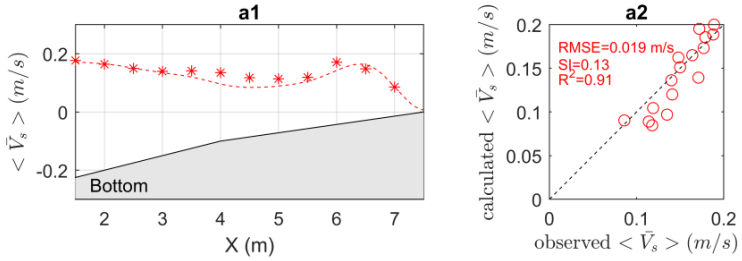

Figure 4.5: The cross-shore distribution of longshore-averaged mean longshore currents $< \overline{V_s} >$ under combined wave current condition without groin existence, (a1: longshore current velocity magnitudes, the subscript 's' represents the velocities at the superficial layer and the triangular braces '<>' denotes for longshore averaging, red line: calculations, red starts: measurements; a2: model performance statistics, the black dashed line denotes a perfect agreement

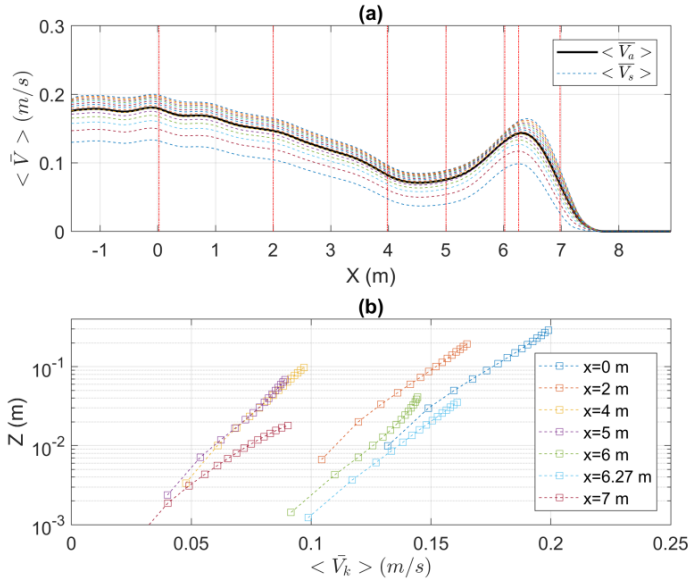

Figure 4.6: The predicted vertical structure of mean longshore currents $< \overline{V} >$, ((a): cross-shore variations of longshore current velocity magnitudes, dot lines: longshore current velocities $< \overline{V_k} >$ at each layer centre; black solid line: depth averaged longshore current velocities $< \overline{V_a} >$; red vertical lines: selected positons where the vertical variations of longshore current are shown in the bottom figure (b). (b): the vertical variations of layered longshore current velocities $< \overline{V_k} >$ at 7 selected cross-shore locations.).

error (RMSE) of the calculated longshore currents $\overline{V_s}$ is 0.019 m/s.

Within the breaker zone, the maximal combined longshore current velocity increase by 14% than that under the pure wave condition, but its location doesn't change, both are at 1.18 m seaward shoreline (X=6.32 m, in Figure 4.3, b(2), and Figure 4.5, a1). Unfortunately, there is no available information about vertical variations of longshore currents from the experiment. We present the predicted vertical structures of longshore currents at 7 selected positions cross-shore in Figure 4.6. It could be seen that the vertical longshore current profiles are nearly linear in the semi-log plot, which means they could be well described by a logarithmic profile. Considering the return current under the wave trough in cross-shore direction (Figure 4.7), its vertical structure shows two distinct kinds of profiles. Outside the breaker zone, the vertical profile of return current has less curvature. While inside, the vertical profile turns to be very curved with dominant seaward velocity near bed and a weak seaward flow or shoreward flow at the wave trough level. Such remarkably different features are consistent with observations in laboratory [e.g. Nadaoka and Kondoh, 1982], and could be well predicted by mathematical models [e.g. Putrevu and Svendsen, 1992]. Compared with the pure wave condition outside the breaker zone, the return current profile become less curved when su-

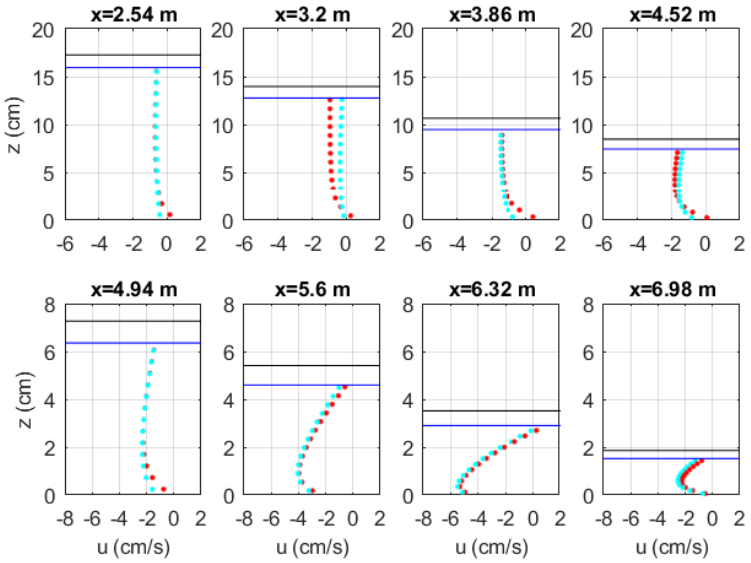

Figure 4.7: The predicted vertical structure of mean cross-shore shore return currents $< \overline{u} >$ under wave trough at 8 selected cross-shore locations, red dots display the pure wave condition and the cyan dots the combined wave current condition, the four subplots on the upper panel are locations outside the breaker zone, while the four subplots on the lower panel are inside the breaker zone, the blue lines represent the wave trough, and the black lines indicate still mean water level.

perimposed by nearly orthogonal currents (the up panel in Figure 4.7). Inside the breaker zone, the present of currents does not alter the vertical profile, only the magnitudes slightly increase but could be ignored (the down panel in Figure 4.7).

4.3.2. Three long groin system

The calculated longshore currents (averaged in longshore direction within the three-groin field from Y=3 m to Y=23 m) match well with experiment data measured by surface floaters flowing through three-groin field (Figure 4.8). The existence of groins retarded longshore currents within the three groin fields (Figure 4.9). Compared with the non-groin longshore current field (Figure 4.9, a), the groin-interfered longshore currents are less uniform within the breaker zone (Figure 4.8, b). The reason for this is that when longshore currents flow down drift the leeside of PPGs, they immediately gain energy from the breaking waves intruding into the area. However, at the seaward breaker zone, where the steady currents (representing tidal currents but seen as steady currents in the laboratory) are dominant and intercepted by PPGs, the currents recover gradually from the diffusion of mass and momentum from the main stream [Bakker et al., 1984]. The difference between the generation mechanism of steady currents and wave-induced currents explains the uniformity outside the break zone and the non-uniformity within the

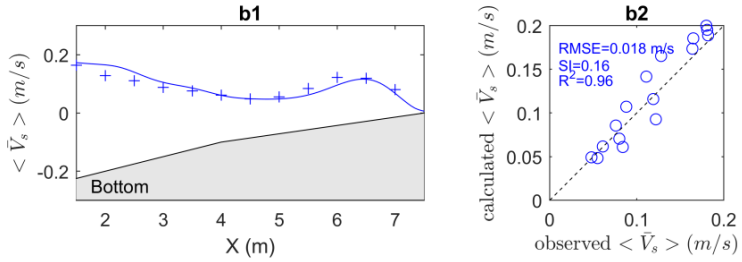

Figure 4.8: The cross-shore distribution of $< \overline{V_s} >$ (longshore averaged in three-groin fields), (b1: longshore current magnitudes, the subscript s denotes the velocities are at the superficial layer; blue line: calculations, blue pluses: measurements; b2: model performance statistics, the black dashed line denotes a perfect agreement

breaker zone respectively (Figure 4.8, c). It is clearly shown in Figure 4.8 (b) that the magnitudes of longshore currents quickly reduce when passing through a groin and only recover flowing further down drift the groin.

Although pile groins could efficiently retard wave-induced longshore currents, they appeared to hardly attenuate wave energy. This is because groin width is much smaller compared to incident wave length, for the considered case, the ratio is little more than 0.06. Figure 4.9 shows the wave height distribution near the middle groin of the three-groin system. When waves approach the groin, the wave heights increase slightly, then reduce to minimal values at the groin locations. The increase of wave height updrift the groin and the decrease of wave height downdrift at the obliquely incident wave shadow zone could be ignored given their limited affected area just around the groin location.

The longshore current velocities are more efficiently reduced within five short groin fields compared with the three-groin system, as the average resistance to the flow increased by two additional pile groins. Within the breaker zone, the maximal magnitude of longshore current velocities is 0.098 m/s (Figure 4.10), while is 0.11 m/s when the flow is hindered by three long groins (Figure 4.7), compared with 0.17 m/s without interceptions of groins (Figure 4.5). Similar to the three-groin system, the five-groin system produced a comparable pattern of longshore current fields as shown in Figure 4.11. The normalized velocities are reduced to 0.4 to 0.7 within five short groin fields (Figure 4.11, c) while such velocities are 0.6 to 0.9 within three long groin fields (Figure 4.8, c).

When groins are dense along a uniform coast, the groin interference induced the non-uniformity of the water level. For the five groin system, the water level variations are illustrated in Figure 4.12. The mean water level field is generally uniform. The contour lines are unparalleled to the shoreline, due to the increase of the water level updrift a groin and the decrease of water level downdrift a groin. The bottom

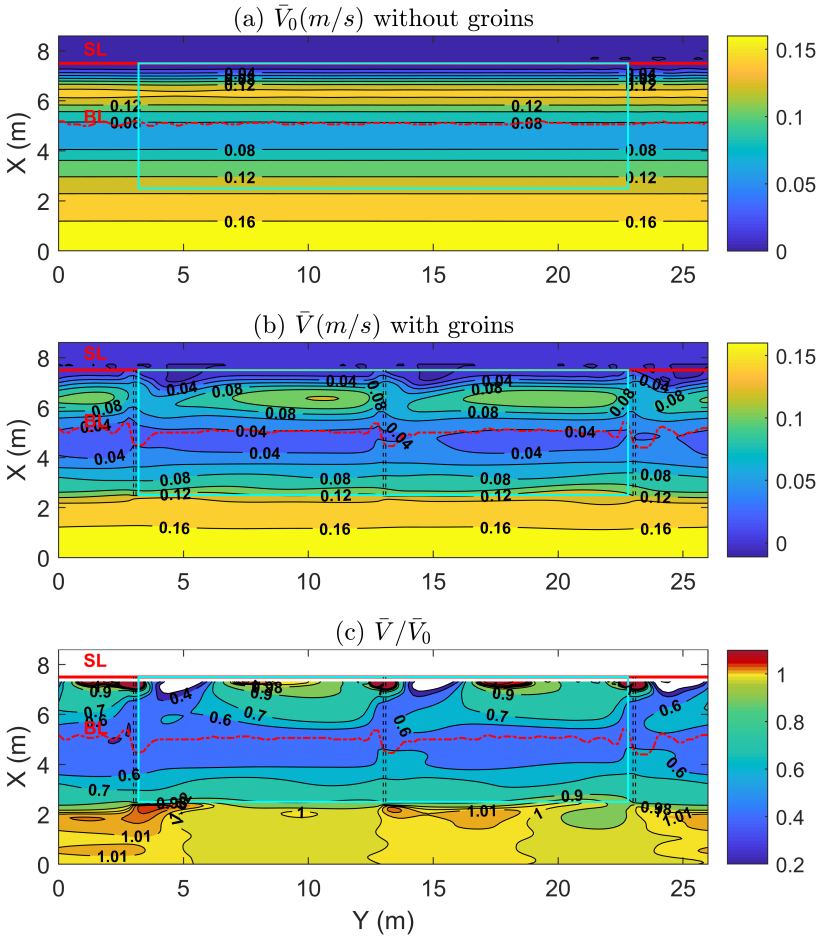

Figure 4.9: The mean depth-averaged longshore current flow fields affected by three long groins, (a: $\overline{V_0}$ without groins; b: $\overline{V}$ with three long groins; c: only positive normalised longshore current velocity magnitudes $\overline{V/V_0}$ are shown, the ratio values were excluded if V_0 is less than 1cm/s near shoreline; black dash lines denote the locations of three long groins, cyan solid rectangles show the groin fields, red solid lines denote the shoreline (SL), and red dot lines denote the wave breaker lines (BL)).

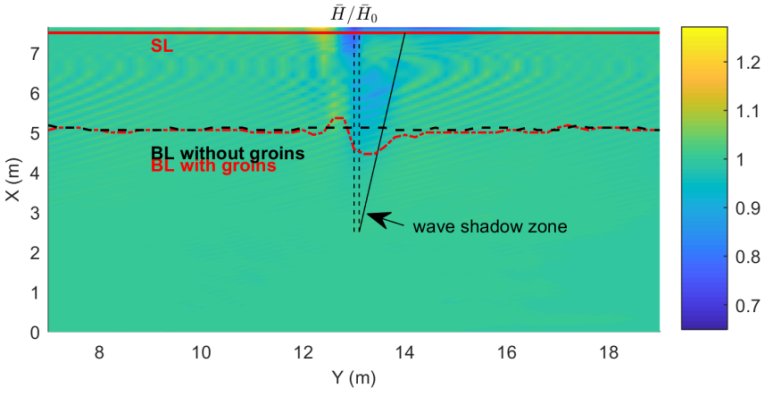

Figure 4.10: The normalized wave height $\overline{H/H_0}$ near the middle groin of a three-groin system (black line: breaker line without groins, red line: breaker line with groins.

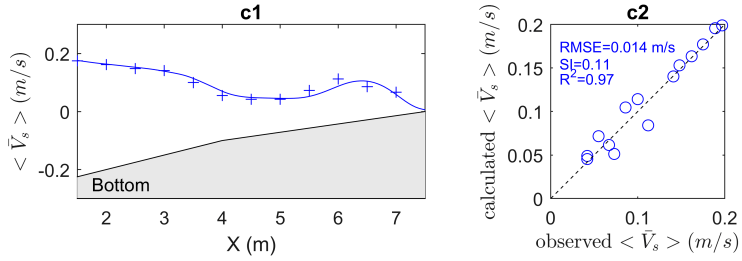

Figure 4.11: The cross-shore distribution of $< \overline{V_s} >$ (longshore averaged in five-groin fields), (c1: longshore current magnitudes, the subscript s denotes the velocities are at the superficial layer; blue line: calculations, blue pluses: measurements; c2: model performance statistics, the black dashed line denotes a perfect agreement

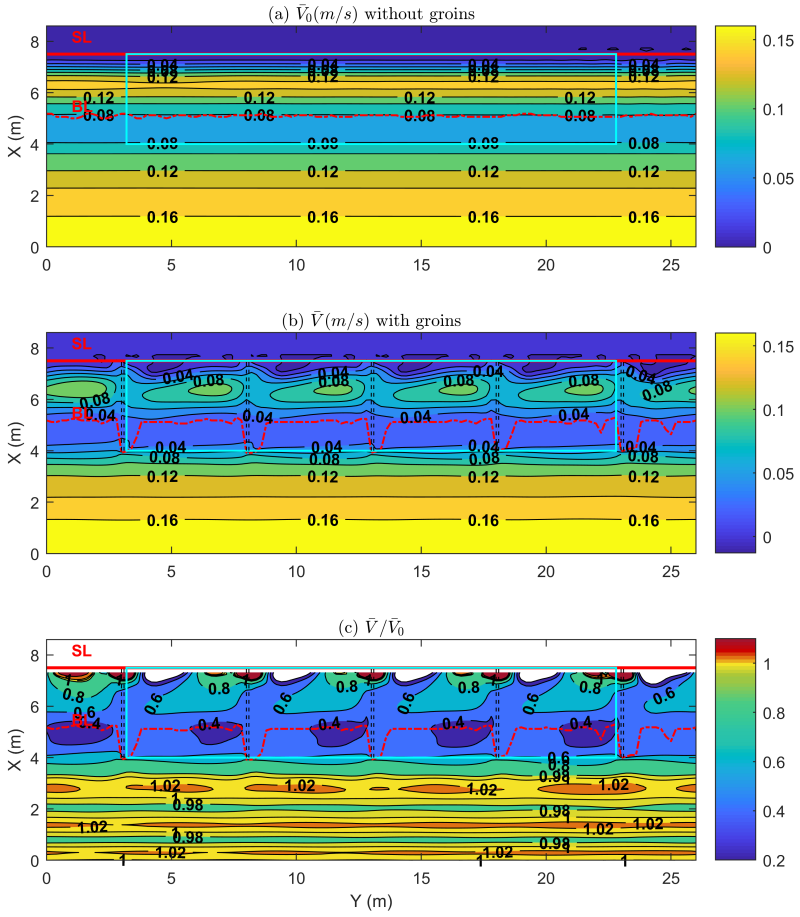

Figure 4.12: The mean depth-averaged longshore current flow fields affected by five short groins, (a: $\overline{V_0}$ without groins; b: $\overline{V}$ with five short groins; c: only positive normalised longshore current velocity magnitudes $\overline{V/V_0}$ are shown, the ratio values were excluded if V_0 is less than 1 cm/s near shoreline; black dash lines denote the locations of three long groins, cyan solid rectangles show the groin fields, red solid lines denote the shoreline (SL), and red dot lines denote the wave breaker lines (BL)).

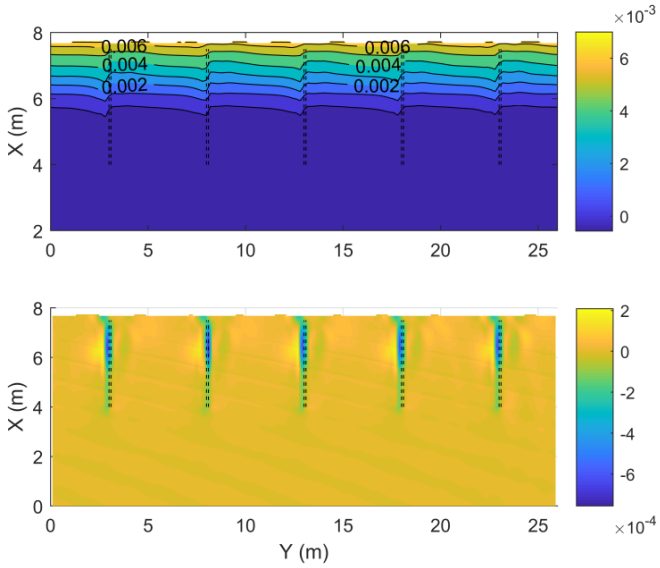

Figure 4.13: The water level filed affected by five short groins. up: time averaged water level $\overline{\eta}$ (m); bottom: alongshore gradient of water level $\partial\overline{\eta}/\partial y$ (black dash lines denote the locations of groins)

plot of Figure 4.12 demonstrates that the local alongshore water level gradients nearby groins are at the order of O(10^{-4}). The local water level gradient is larger than the global water level gradient, which is at the order of O(10^{-5}).

4.4. Discussion

4.4.1. Wave height $\overline{H}$

Theoretically, there are four kinds of wave components within groin fields: incident, diffracted, reflected and transmitted waves. Considering the small incident angle of waves, the waves could propagate into nearly the total groin fields. The diffraction of waves around groins is not obvious, because the limited interference by a very narrow width of groin piles and the littoral currents flowing through groin openings eliminate the diffraction effects. Slightly enhanced wave height is observed updrift groins (Figure 4.9), due to the water level is piled up updrift the groins and consequently wave breaking is delayed. In addition to the slightly enhanced wave height updrift the groins, the wave height reduction (20% at maximal under $15°$ incident regular waves) of transmitted waves occurs within the obliquely incident wave shadow zone. The moderate wave dissipation confined to the very limited area reveal that the effects of such pile groins on waves are of no consequence and negligible. The negligible effects of pile groins on waves are consistent with the views of Raudkivi [1996] and other researchers. Therefore, the wave height variation in pile groin fields is needless to be further discussed.

4.4.2. Water level $\overline{\eta}$

The water level field is generally uniform alongshore except in the narrow areas near both flanks of a groin. The resistance exerted to longshore flow by groins piled up the water level updrift the groins and produced a water level differential within groin fields. The water level variation $\Delta\overline{\eta}$ in alongshore direction near the groins is at the order of O(10^{-4}) m. Given the narrow width of pile groin O(10^{-1}) m, the water level gradient near groins is up to O(10^{-3}). In the simulation, the local water level gradient induced by groins is larger than the global water level gradient O(10^{-5}). The water level gradients $\partial\overline{\eta}/\partial y$ were shown in figures (Figure 4.14 and Figure 4.15). The piled up water updrift the groins induces an alongshore positive water level gradient. The positive water level gradient drive forces opposite to the currents which are flowing in the positive Y direction. It is shown that, within the breaker zone, the magnitude of $\partial\overline{\eta}/\partial y$ near the middle groin (tree long groin in Figure 4.14 and five long groin in Figure 4.15) are nearly same under wave and combined current wave conditions. Its order is O(10^{-3}), much larger than that of O(10^{-4}) under pure current condition. Therefore, the reduction effect of longshore current within the breaker zone is dominated by wave induced forces. However, outside the breaker zone, the pure waves induced $\partial\overline{\eta}/\partial y$ decrease rapidly and shift from negative to positive in a seaward direction. On the contrary, the $\partial\overline{\eta}/\partial y$ under pure current condition increases and keeps negative, and its magnitudes become smaller with that under pure wave condition. Therefore, outside the breaker zone, the effects of waves and currents on longshore current variations are opposite to wave induced forces.

4.4.3. Longshore current $\overline{V}$

In this paper, numerical simulations showed that the presence of permeable groins effectively reduces longshore currents (Figure 4.9, Figure 4.12, Figure 4.14, Figure 4.15) under different hydraulic conditions, as demonstrated by measurements in laboratory experiments [Hulsbergen and ter Horst, 1973]. The relative longshore current velocities ($\overline{V/V_0}$) are less than one within groin fields (Figure 4.9, Figure 4.12). The relative velocities $\overline{V/V_0}$ are slightly larger than one near the long groin seaward heads (Figure 4.9), while its value is less than one around the short groin seaward head (Figure 4.12). This is partly because the current (V= 0.13 m/s) at further 5 m offshore long groin head location is 1.6 times stronger than that at 3.5 m offshore short groin head location. The current streamlines deflect and contract nearby the long groin heads, which enhances the local current velocity and compensates the reduction induced by the pile groin resistance. Another reason could due to the difference of the water level gradient $\partial\overline{\eta}/\partial y$ around the groin heads. The $\partial\overline{\eta}/\partial y$ down drift the long groin heads are nearly zero (the first subplot inFigure 4.14), while the gradients are positive downdrift the short groin heads (the first subplot in Figure 4.15). The positive water level gradient induces pressure forces in opposite direction to longshore currents, therefore hinders longshore currents.

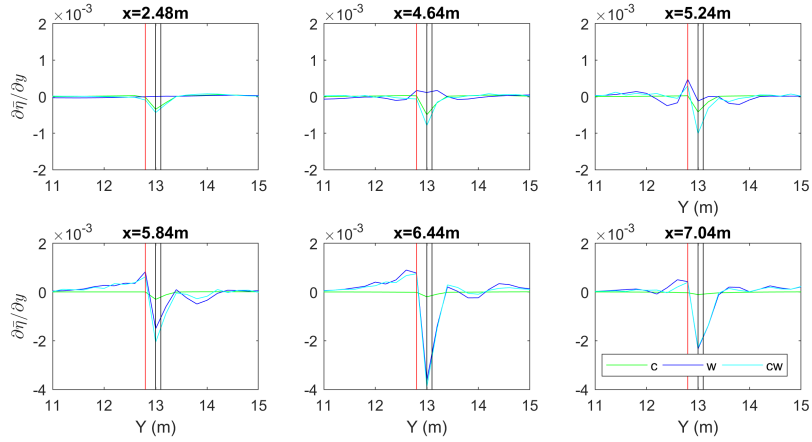

Figure 4.14: The alongshore water level gradient $\partial\overline{\eta}/\partial y$ under three conditions, at 0.2 m updrift the middle groin of the three long groin system (denoted by the red lines).The black lines represent the middle pile groin location. c is short for the pure current condition, w for pure wave condition, and cw is for combined current wave condition.

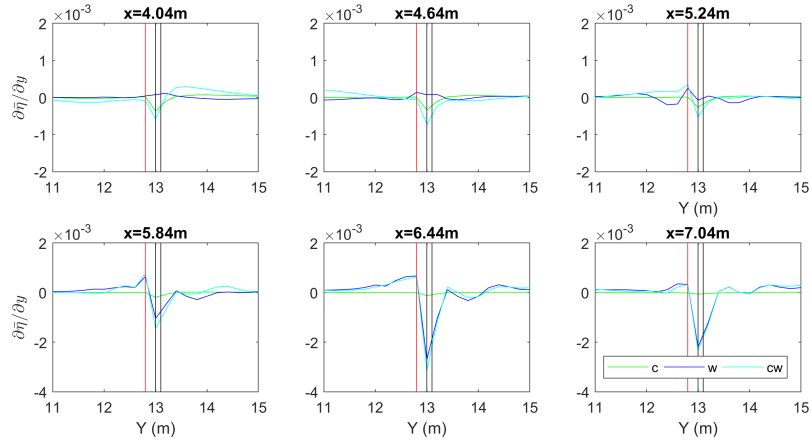

Figure 4.15: The alongshore water level gradient $\partial\overline{\eta}/\partial y$ under three conditions, at 0.2 m updrift the middle groin of the five short groin 349 system (denoted by the red lines).The black lines represent the middle pile groin location.

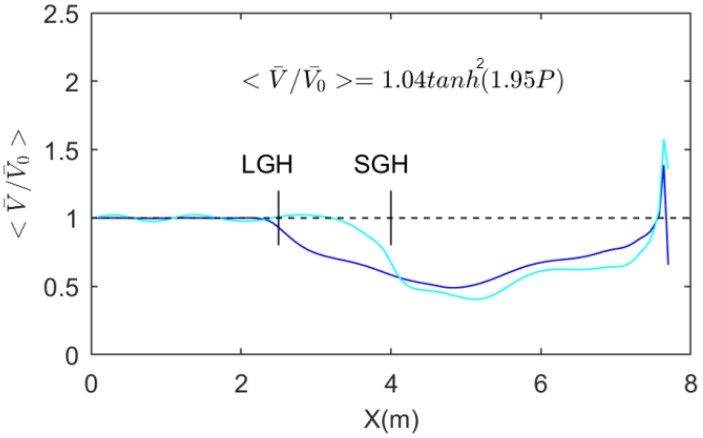

Figure 4.16: Normalized longshore current $\overline{V/V_0}$ longshore averaged in groin fields under combined wave current condition. (blue line: three-groin field, cyan line: five-groin field, black line: short groin head (SGH) location and long groin head(LGH) location, P is short for groin permeability).

On the other hand, the smaller groin gap of the short groin system limits the development of mixing layer and momentum exchange along the groin head contour.

An empirical formulation relating the groin permeability and the $\overline{V/V_0}$ averaged over the groin field was given in Figure 4.16, followed by the suggested form raised by Trampenau et al. [2004]. The relative velocity $\overline{V/V_0}$ reduced to 67% within the three long groin field of a 55% permeability and to 57% within the five short groin field of a 50% permeability. The empirical formulation shows the nonlinear relation between longshore current reduction and groin resistance (by groin permeability). However, it could be only used to give a quick prediction, since the whole groin filed averaged values disguises detailed local information.

Near the groin shoreward ends, the relative velocities $\overline{V/V_0}$ increase more than 1.5 times. At the wave set up location, the relative longshore current even increases by an order of magnitude (the 0.02 m shoreward the still water line in Figure 4.17). But such sharp change is only limited to 1 m updrift the groin, and the strength of longshore currents is quite weak due to very shallow water depth near the shoreline. Such weak currents do not harm the beach and do not need extra considerations under mild waves. However, when extreme water level surges occur, the large inundation water depth on the beach allows strong longshore currents to develop. The strong longshore current causing outflanking by groin ends to erode the beach or the shoreward dune foot if close enough could be affected. For instance, the beach slope has been eroded at shoreward ends of PPGs at Warnemünde, Germany, observed by Bakker et al. [1984]. The contracted strong longshore currents could even wash out the pile cylinders during storm surges, which is the main cause of failures of PPGs recorded in the Netherlands [Bakker et al., 1984]. Therefore, the

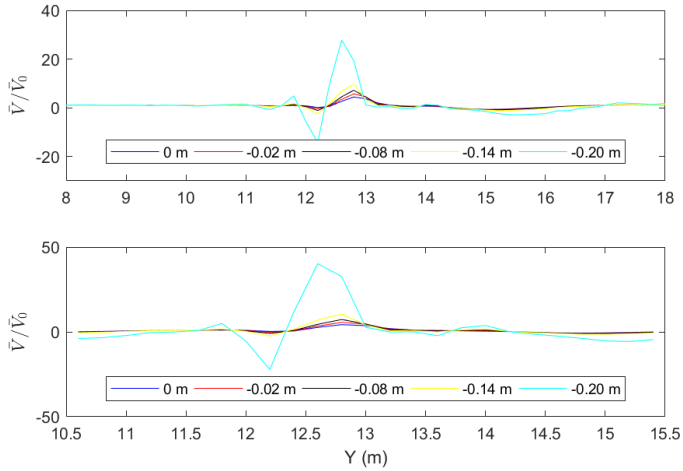

Figure 4.17: The relative longshore current $\overline{V/V_0}$ zoom in the middle groin shoreward end. (up panel: long groin system, bottom panel: short groin system.). The legend shows the shoreward distance from the still water line.

shoreward extension distance of PPGs from the shoreline deserves serious consideration, and the predictions by numerical simulations under extreme design scenarios maybe helpful to decide an appropriate shoreward length of a PPG. The extension distance should be at least shoreward beyond the wave set up line. If the dune foot erosion induced by outflanking flow should be avoided, the groin length has to extend to the dune foot location.

To isolate the waves and currents effects on longshore current reduction, we compare the cross distribution of longshore current under combined current wave condition, pure wave condition and pure current condition in Figure 4.18. The chosen cross shore profile is at 0.2 m updrift the middle groin of the three long groin system. Under combined wave current condition, with the existence of currents, the reduction of longshore current is slightly smaller than that under pure wave condition, within the breaker zone; while the reduction is nearly same as that under pure current condition, outside the breaker zone. The reason of the difference in the reduction between X=4m and X=5m is hard to assess, for the simulation underestimates the longshore current velocities in this area suggesting some uncertainty exists. The upper panel in Figure 4.18 shows that under pure current condition, $\overline{V}$ increases a little near shore (from X=6.5 m to shoreline X=7.5m). The middle panel in Figure 4.18 shows that under pure wave condition, $\overline{V}$ increases a bit near the shoreline (from X=7.5 m to shoreline X=7.7m).

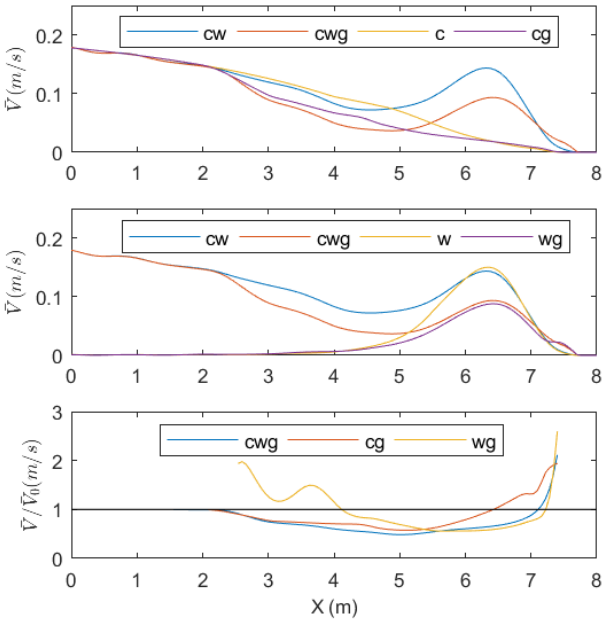

Figure 4.18: The cross shore profiles of mean longshore current $\overline{v}$ under three conditions, at 0.2 m updrift the middle groin of the three long groin system. (cw is short for the combined current wave condition without groins, c for the pure current condition, w for the pure wave condition, wg and cg for pure wave condition with groins and pure current with groins separately.)

4.4.4. Cross-shore current $\overline{U}$

In addition to the distribution of longshore currents, the cross-shore return currents under wave trough within groin fields have been predicted and investigated. The existence of groins evokes rip currents near groin flanks. The intensity of rip currents updrift the groin is the strongest within surfzone. The values could maximally reach 0.06 m/s closely updrift the groins (Figure 4.19) which is about 1.5 times the maximal return current 0.04 m/s without groin disturbance. Closely downdrift the groins, the maximal return current decreases a bit, and the locations shift to shoreward (Figure 4.21). The shoreward movement corresponds to the shoreward move of the peak of cross shore water level gradient (the subplot at y=13.4 m Figure 4.20). However, the maximal relative $\overline{U/U_0}$ is at the wave breaker line position. The lowest mean water levels appear at the locations occupied by groins (e.g.Figure 4.13). The greater water level gradients are consistent with the larger rip currents, updrift the groins and within the breaker zone (e.g. Figure 4.19, a2, b2 and Figure 4.20). Under the pure current condition, the rip current magnitude is much smaller than that under combined current wave condition (Figure 4.21). Therefore the cross-shore current $\overline{U}$ is mainly dominated by the enhanced wave induced return current besides the groins.

Another characteristic of PPGs is the induced quite unidirectional flow field in permeable groin fields , compared to the nonuniform flow field in impermeable groin fields (Figure 4.22). The high permeability of PPGs hinders the development of circulation and eddies in groin embayment and weakens the strength of rip currents updrift groins, compared to impermeable groins with the same configurations of a three long groin system.

4.4.5. Longshore volume discharge

The calculated alongshore discharge, the product of longshore current velocity and water depth, was denoted in Figure 4.23. The maximal decrease of longshore volume discharge could reach 50% by three-groin and 40% by five-groin systems, compared with a shore without groins. It has been shown that the five-groin system reduced longshore volume discharge $< q >$ is slightly higher than that by the three-groin system (Figure 4.23) within the breaker zone, while the longer groins diminish $< q >$ more efficiently at the outer seaward zone (from X=2.5 m to X=4 m). From the aspect of retardation extent of total longshore discharge integrated along groin length, the three-long groins are favorable to contribute to a larger retardation of total longshore discharge, although these two kinds of groin systems have a comparable total groin length.

4.5. Conclusion

The hydrodynamics of the flow within permeable pile groin fields on a beach slope was studied using the phase resolving wave-flow model SWASH. In this study, the

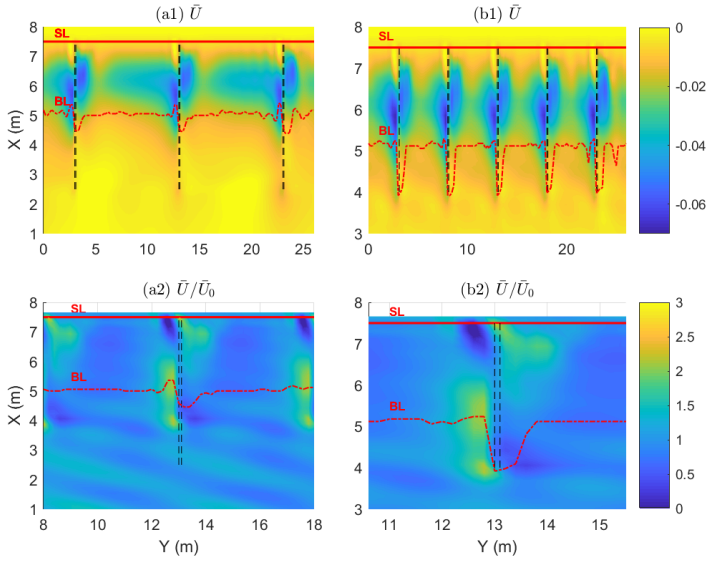

Figure 4.19: The return current $\overline{U}$ (m/s) under wave trough in the presence of three 5 m long pile groins (a1), the relative return current $\overline{U/U_0}$ (a2); the return current $\overline{U}$ in the presence of five 3.5 m short pile groins (b1), the $\overline{U/U_0}$ (b2). Black dashed lines denote the pile groins, red solid lines denote the shoreline (SL).

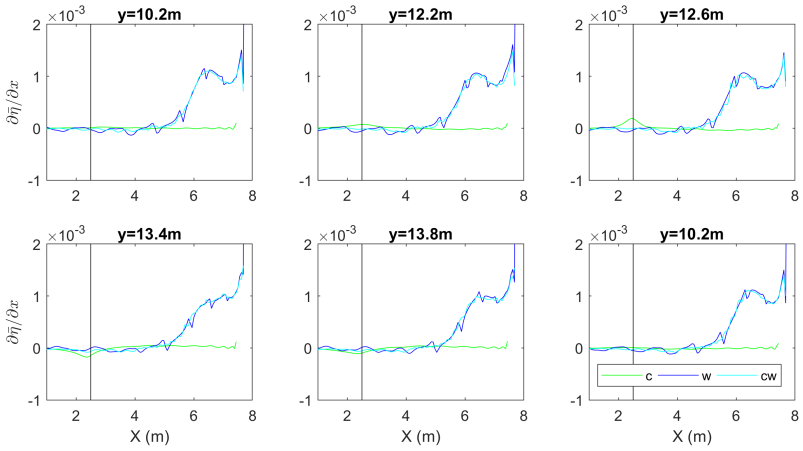

Figure 4.20: The cross shore water level gradient $\partial\overline{\eta}/\partial x$ under three conditions, at three updrift (up panel) and three downdrift (bottom panel) the middle groin of the three long groin system. The black lines represent the pile groin head location. c is short for pure current condition, w for pure wave condition, and cw is for combined current wave condition, all the conditions are interfered by the groin system.

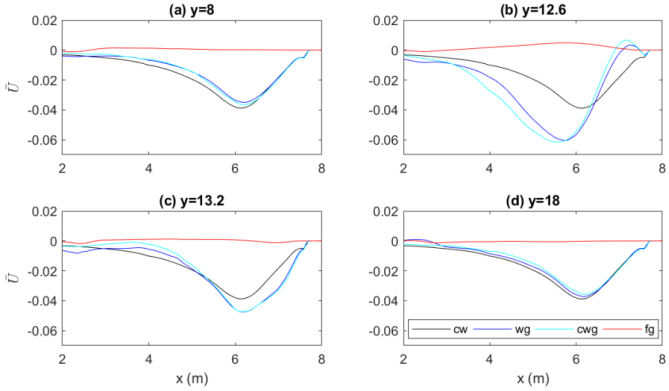

Figure 4.21: The calculated return current $\overline{U}$ at four selected cross-shore locations near the middle groin of the three long groin system, ((a): half Xg updrift, (b):0.2m updrift, (c): 0.3m down drift, (d): half Xg downdrift). cg is short for pure current condition, wg for pure wave condition, cwg is for combined current wave condition, and cw is combined current wave condition without groin interference

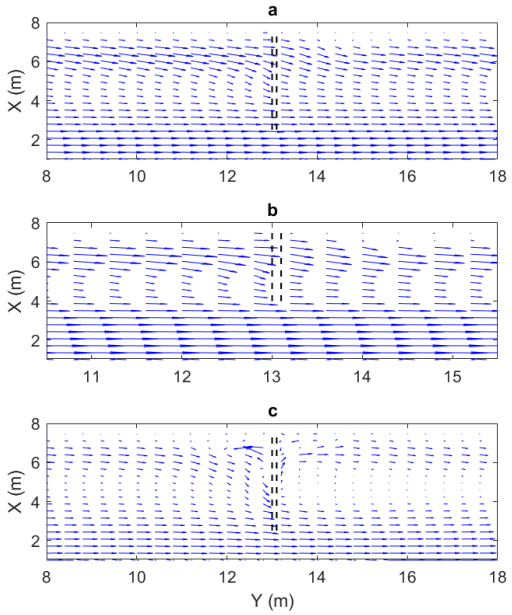

Figure 4.22: The vector flow filed near the middle groin, within three long permeable groin field (a), five short permeable groin field (b), and three long impermeable groin field (c).

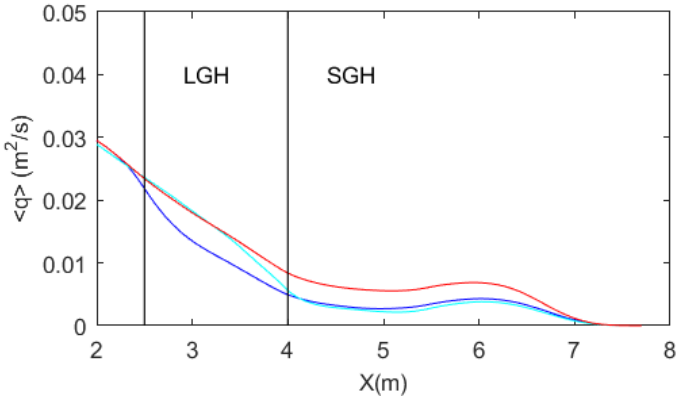

Figure 4.23: The alongshore volume discharge $< q >$ alongshore averaged in groin fields. (blue line: three-groin field, cyan line: five-groin field, red line: none-groin field, LGH: long groin head, SGH: short groin head)

multilayer mode of the SWASH model was validated to be able to predict longshore current profiles and groin-current interactions. Firstly, a uniform coast without groins was simulated to calibrate model parameters. The calculated longshore current distribution shows a good agreement with the laboratory observations [Hulsbergen and ter Horst, 1973]. To validate the interactions between permeable pile groins and combined wave current flow, the pile groins were introduced in the calibrated model. These simulations clearly show that pile groins hardly attenuate the wave energy nearshore, the small wave height reduction was found only limited to wave shadow zone downdrift a groin. However, the longshore current velocities are retarded substantially by the pile groins. The retarded flow by pile groins are expected to weaken the ability to transport sediment alongshore. Within the groin fields, the retardation of longshore currents by a three groin system with a 55% permeability is up to 33% while a larger reduction degree of 43% is obtained within the groin embayment of a five groin system with a 50% permeability. An empirical formulation between the relative longshore current velocity and the groin permeability were given, which has a second order hyperbolic tangent form similar to that summarised by Trampenau et al. [2004]. The depth integration of longshore discharge suggests that long groins function more sufficiently compared with short groins, when their total lengths are comparable.

In addition to the variations of longshore currents at a groin engineered coast, the magnitudes of cross-shore currents were investigated too. The strong cross-shore rip currents are confined to breaker zone where the gradient of wave set up/down are large beside the groins. No obvious recirculation and eddies were found in both the three groin and five groin bays, due to their high permeability.

The overall consistence of the calculated results to the experimental measurements reveals a robust capacity of the SWASH model to calculate flow fields affected by permeable pile groins. Once the hydrodynamics of permeable pile groins are clear, longshore sediment transport could be predicted with more confidence. The deeper understandings we gained about the pile groin system by the use of numerical models, will in return benefit the design process of PPGs. Our future work would focus on the optimization of configuration parameters of PPGs and layouts of pile groin system.

4.6. Appendix A

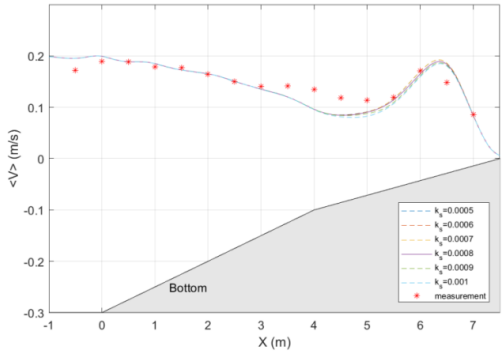

Figure 4.24: The computed mean superfical longshore current velocities < $\overline{V_s}$ > with varying k_s coefficients under the combined wave-current condition.

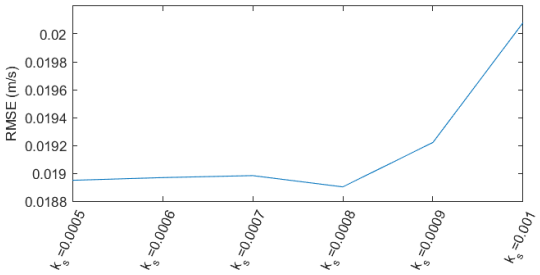

Figure 4.25: The root mean square erros (RMSE) of computed mean superfical longshore current velocities < $\overline{V_s}$ > with varying k_s coefficients against measurements.

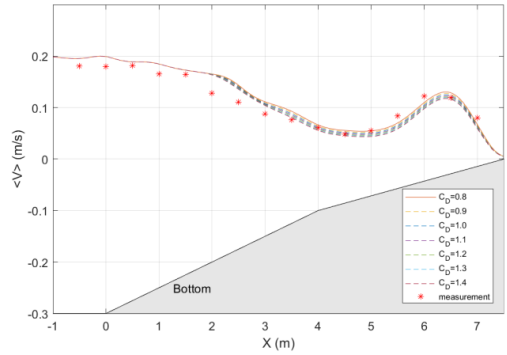

Figure 4.26: The computed mean superfical longshore current velocities $< \overline{V_s} >$ alongshore averaged within three long groin field with varying C_D coefficients under the combined wave-current condition

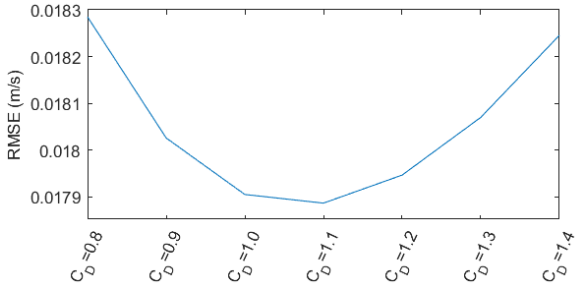

Figure 4.27: The root mean square erros (RMSE) of computed mean superfical longshore current velocities $< \overline{V_s} >$ alongshore averaged within three long groin field with varying C_D coefficients against measurements.

References

T. K. S. Abam. Bank erosion and protection in the Niger delta. *Hydrological Sciences Journal*, 38(3):231–241, 2009. ISSN 0262-6667. doi: 10.1080/02626669309492665. URL http://www.tandfonline.com/doi/abs/10.1080/02626669309492665{#}.VL{_}PwC6RZK0.

W. Bakker, C. Hulsbergen, P. Roelse, C. de Smit, and J. Svasek. PERMEABLE GROYNES: EXPERIMENTS AND PRACTICE IN THE NETHERLANDS. In *19th International Conference on Coastal Engineering*, pages 1983–1996, Houston, 1984.

W. T. Bakker, E. J. H. Klein Breteler, and A. Roos. The Dynamics of a Coast with a Groyne System. *12th Coastal Engineering Conference*, pages 1001–1020, 1970.

M. Crossman. Manual on the Use of Timber in Coastal and River Engineering. Technical report, HR Wallingford Ltd, 2004. URL http://www.icevirtuallibrary.com/content/book/100605.

M. Crossman and J. Simm. Sustainable coastal defences - The use of timber and other materials. *Proceedings of the Institution of Civil Engineers: Municipal Engineer*, 151(3):207–211, 2002. ISSN 09650903. doi: 10.1680/muen.151.3.207.38884. URL http://www.scopus.com/inward/record.url?eid=2-s2.0-0036751968{&}partnerID=40{&}md5=50f484bb9656010ea4269629474be345.

F. de Wit, M. Tissier, and A. Reniers. Including tidal currents in a wave-resolving model. *Coastal Dynamics*, pages 1638–1648, 2017. URL http://coastaldynamics2017.dk/onewebmedia/119{_}fpdewit.pdf.

H. H. Dette, A. J. Raudkivi, and H. Oumeraci. Permeable Pile Groin Fields. *Journal of Coastal Research*, pages 145–159, 2004. ISSN 07490208, 15515036. URL http://www.jstor.org/stable/25736251.

C. Hulsbergen and W. ter Horst. Effect of permeable pile screens on coastal currents. Delft Hydraulics laboratory report M 1148, (in Dutch). Technical report, Delft Hydraulics, Delft, 1973.

O. Kolp. Farbsandversuche mit lumineszenten Sanden in Buhnenfeldern. Ein Beitrag zur Hydrographie der Ufernahen Meereszone. *Petermanns Geographischen Mitteilungen*, 114(2), 1970.

B. Launder and D. Spalding. The numerical computation of turbulent flows. *Computer Methods in Applied Mechanics and Engineering*, 3(2): 269–289, mar 1974. ISSN 0045-7825. doi: 10.1016/0045-7825(74)90029-2. URL https://www.sciencedirect.com/science/article/pii/0045782574900292?via{%}253Dihub.

K. Nadaoka and T. Kondoh. Laboratory Measurements of Velocity Field Structure in the Surf Zone by LDV. *Coastal Engineering in Japan*, 25(1): 125–145, dec 1982. ISSN 0578-5634. doi: 10.1080/05785634.1982.11924341. URL https://www.tandfonline.com/doi/full/10.1080/05785634.1982.11924341.

U. Perdok, M. Crossman, H. J. Verhagen, S. Howard, and J. Simm. Design of timber groynes. In *Coastal Structures*, pages 1689–1699, Portland, Oregon, United States, Aug. 2003. ISBN 9788578110796. doi: 10.1017/CBO9781107415324.004.

U. H. Perdok. Application of timber groynes. *Technology*, 2002.

W. Price, K. TOMLINSON, and D. Willis. Filed tests on two permeable groynes. In *13th International Conference on Coastal Engineering*, pages 1312–1325, 1972. ISBN 7731030008. doi: 10.1016/B978-0-7020-3935-5.00077-X.

U. Putrevu and I. a. Svendsen. A Mixing Mechanism In the Nearshore Region. In *23rd international conference on coastal engineering*, pages 2758–2771, Venice, 1992. ISBN 9780872629332. doi: 10.1061/9780872629332.210. URL http://ascelibrary.org/doi/10.1061/9780872629332.210.

A. J. Raudkivi. Permeable Pile Groins. *Journal of Waterway, Port, Coastal, and Ocean Engineering*, 122(6):267–272, 1996. ISSN 0733-950X. doi: 10.1061/(ASCE)0733-950X(1996)122:6(267).

A. J. Raudkivi and H. H. Dette. Reduction of sand demand for shore protection. *Coastal Engineering*, 45(3-4):239–259, 2002. ISSN 03783839. doi: 10.1016/S0378-3839(02)00036-4.

D. P. Rijnsdorp, P. B. Smit, M. Zijlema, and A. J. Reniers. Efficient non-hydrostatic modelling of 3D wave-induced currents using a subgrid approach. *Ocean Modelling*, 116:118–133, 2017. ISSN 14635003. doi: 10.1016/j.ocemod.2017.06.012.

J. Smagorinsky. General circulation experiments wiht the primitive equations I. The basic experiment. *Monthly Weather Review*, 91(3):99–164, 1963. ISSN 0036-8075. doi: 10.1126/science.27.693.594.

P. Smit, M. Zijlema, and G. Stelling. Depth-induced wave breaking in a non-hydrostatic, near-shore wave model. *Coastal Engineering*, 76(3):1–16, jun 2013. ISSN 0378-3839. doi: 10.1016/J.COASTALENG.2013.01.008. URL https://www.sciencedirect.com/science/article/pii/S0378383913000215.

A. Strusiańska-Correia. Beach Stabilization at Kołobrzeg, Poland. *Journal of Coastal Research*, 71:131–142, 2014. ISSN 0749-0208. doi: 10.2112/SI71-016.1. URL http://www.bioone.org/doi/abs/10.2112/SI71-016.1.

T. Trampenau, F. Goricke, and A. J. Raudkivi. permeable pile groins. In *25th International Conference on Coastal Engineering*, pages 2142–2151, Orlando, 1996.

T. Trampenau, H. Oumeraci, and H. H. Dette. Hydraulic Functioning of Permeable Pile Groins. *Journal of Coastal Research*, pages 160–187, 2004. ISSN 07490208, 15515036. URL http://www.jstor.org/stable/25736252.

W. S. Uijttewaal. Effects of Groyne Layout on the Flow in Groyne Fields: Laboratory Experiments. *Journal of Hydraulic Engineering*, 131(9):782–791, 2005. ISSN 0733-9429. doi: 10.1061/(ASCE)0733-9429(2005)131:9(782).

M. Zijlema and G. Stelling. Efficient computation of surf zone waves using the nonlinear shallow water equations with non-hydrostatic pressure. *Coastal Engineering*, 55(10):780–790, oct 2008. ISSN 0378-3839. doi: 10.1016/J.COASTALENG.2008.02.020. URL https://www.sciencedirect.com/science/article/pii/S0378383908000380.

M. Zijlema and G. S. Stelling. Further experiences with computing non-hydrostatic free-surface flows involving water waves. *International Journal for Numerical Methods in Fluids*, 48(2):169–197, 2005. ISSN 02712091. doi: 10.1002/fld.821.

M. Zijlema, G. Stelling, and P. Smit. SWASH: An operational public domain code for simulating wave fields and rapidly varied flows in coastal waters. *Coastal Engineering*, 58(10):992–1012, oct 2011. ISSN 0378-3839. doi: 10.1016/J.COASTALENG.2011.05.015. URL http://www.sciencedirect.com/science/article/pii/S0378383911000974?via{%}253Dihub.

5

Numerical simulations of effects of layouts of permeable pile groin system on longshore currents

Coastal permeable groins have been used to protect beaches from erosion for centuries. However, the hydraulic functioning of permeable groins has not been fully understood and their design heavily depends on engineering experiences In this chapter, numerical experiments were executed to investigate the effects of layout configurations of a permeable groin system on longshore currents. The non-hydrostatic SWASH (Simulating WAve till SHore) model was employed to carry out the numerical simulations. Two data sets obtained from physical laboratory experiments with different permeable groins layouts on different slopes are used to validate the accuracy of the model. Then, the longshore current retardation by the permeable groin system with varying configuration parameters (e.g. groin spacing, groin length) was numerically investigated under different environmental conditions (e.g. a slight or a moderate wave climate). From the calculation results of numerical experiments, it is indicated that permeable groins function efficiently to retard the maximal longshore current velocity under the condition that the groin length ranging from 84% and 109% of the wave breaker zone width. The longshore current reduction rate monotonously decreases with the increase of groin spacing. When the groin spacing–groin length ratios are 1:1 and 1.5:1, the longshore current reduction is not sensitive to the wave conditions. When the spatial ratio is 2:1, the permeable pile groin system functions worse under

a moderate wave climate than under a slight wave climate, from the view of longshore current reduction.

5.1. Introduction

Coastal groins are long and narrow hydraulic structures, which are built to protect a stretch of beach from erosion. Groins are usually placed approximately perpendicular to the shoreline to hinder longshore currents and intercept longshore sediment transportation in the littoral zone. For instance in engineering practice, groins are widely used in combination with beach nourishment to sustain the recharged beach materials within groin bays, or groins serve as a terminal structure to reduce the sand loss to a sand sink (e.g. at a harbour inlet). For centuries groins have been used, but they are perhaps the least understood compared to numerous other shore-protection structures, due to the lack of research about established relationships between groin functional behaviours and environmental climates [Berg and Watts, 1965, Bakker et al., 1984, Kraus et al., 1994, Poff et al., 2004]. From the aspect of permeability, groins can be divided into two types, permeable and impermeable groins respectively. In this study, the specific traditional form of the permeable groin, consisting of wooden piles, is investigated. Compared with impermeable groins (e.g. rubble mound groins), Permeable Pile Groins (PPGs) may attract more preference given their appealing natural look, ease of construction and made of a renewable timber resource [Crossman and Simm, 2002]. In addition, because the ability of longshore sediment transport passing through large openings of PPGs, the side effects of beach erosion downdrift PPGs are much less compared to the effects associated with their impermeable counterparts. Consequently, PPGs have minor downdrift beach impacts and result in a continuous shoreline. Therefore, PPGs deserve serious consideration and investigation as a promising type of economic and flexible coastal protection measure [Bakker et al., 1984].

The primary function of PPGs is to slow down longshore currents, enable elimination of circulations within groin fields and to weaken rip currents along the groins [Raudkivi, 1996, Trampenau et al., 1996]. PPGs do not impound and block longshore sediment transport, but instead of exerting resistance on longshore currents, to retard velocity of longshore currents and weaken their capability of transporting sediment. On the other hand, the reduction of current velocity inhibits turbulence (production) at the seabed and decreases the amount of suspended sediment. As a result, the capacity of longshore currents to entrain sediment decreases [Trampenau et al., 1996]. On several sites of field surveys it was shown that coastline recession was effectively curbed and accretion nearshore was promoted by the massive rows of PPGs [Kolp, 1970, Price et al., 1972, Bakker et al., 1984, Raudkivi and Dette, 2002, Poff et al., 2004, Trampenau et al., 2004, Abam, 2009]. A five-year surveillance of beach profile evolution, at a Southern coast in England, showed that a build-up in beach levels appeared after the construction of PPGs [Price et al., 1972]. Compared to a natural coast without groins, the evolution of beach profiles in response to PPGs is that the beach elevation was built up and the beach slope became much gentler from the shoreline to the trough. This implied that wave energy dissipated further seaward and a wider wave buffer zone was developed, reducing wave loading per unit area and alleviating the potential of beach erosion [Dette et al., 2004]. Similarly, positive effects induced by PPGs,

indicated by extensive field surveys from 1993 to 1997 on the Baltic Sea coast, are: a) significant seaward advancement of shoreline; b) continuous growth of submarine terrace elevation; c) seaward movement of the nearshore shoal [Trampenau et al., 2004]. The positive accretion of morphological change appeared as a result of an indirect protection mechanism of PPGs [Trampenau et al., 2004], in addition to the direct effects on hydrodynamics. In the case of Naples Beach, Florida, USA, the monitored performance of an experimental permeable groin on-site satisfied its expectation, which successfully stabilized the beach, enabled the beach to build up and did no't have any significant side effects on the adjacent shoreline [Poff et al., 2004]. Bakker et al. [1984] reviewed the application of PPGs in the Netherlands. These authors concluded that the PPG effect was controversial due to a lack of statistically significant evidence because some PPG projects at Dutch sites did have the expected favorable effects, while other projects did have adverse effects and were abandoned.

When evaluating the effectiveness of PPGs on the morphological changes in nature, there is inevitable difficulty in isolating the effects of natural and nonnatural background noise, such as long-term morphological variations [Bakker et al., 1984] or human interventions (e.g. beach nourishment). Therefore, in this study numerical experiments were carried out merely focusing on hydrodynamics, to investigate hydraulic functioning of PPGs under varying well-controlled hydraulic conditions. Separate experiments have been carried out to isolate groin configuration effects, such as groin length and groin spacing. Our aim is to numerically quantify the relationship between layout parameters of a PPG system and the reduced longshore current reduction rate. The results may be used as a reference database to facilitate and improve PPG design.

In this chapter, the nearshore flow fields affected by different configurations of permeable pile groin systems under varying hydraulic conditions were simulated. The following section gives a brief overview of the literature about permeable groin layout design. Then, the setup of numerical experiments is given. The governing equations of the numerical tool, the SWASH model, are demonstrated in Section 5.3. The simulation results are analyzed and compared in Section 5.4. Finally, in the last section a discussion is given and the conclusions are summarized.

5.2. Methods

5.2.1. Design of permeable groins

A literature review on the design of groins is given below, listing several design concerns such as groin length, groin height (crest elevation), the spacing between neighbouring groins and the layout of the groin system. These concerns are all considered in this thesis.

Groin length

Groin length can be calculated according to the desired amount of potentially reduced longshore sediment transport. The groin is suggested to cross the average width of surf zone, to reach the low tide water line [Poff et al., 2004]. The best performance of a PPG is achieved when the groin length is in the order of the width of the surf zone [Trampenau et al., 2004]. In order to avoid outflanking at the shoreside, it is advisable for a groin to reach sufficiently landward till the high water line [Poff et al., 2004, Trampenau et al., 2004], to the foot of the dune, or an already existing revetment/seawall [Perdok et al., 2003].

Groin spacing

The groin spacing is closely related to the groin length, because groin length determines the area of groin influence. Groins are spaced at a wider interval alongshore if situated under a more perpendicular wave incident. Raudkivi [1996] summarised that the average spacing is 1.5 times the active groin length on the southern Baltic Sea coast, which is effective to prevent large-scale circulations within the groin fields. Poff et al. [2004] suggested that groin spacing should be equal to the influenced length.

5.3. Numerical experiments

5.3.1. The SWASH model

SWASH (acronym for Simulating WAves till SHore) model is an open source free surface wave flow model, considering non-hydrostatic pressure forces [Zijlema et al., 2011]. The governing equations are the RANS equations for an incompressible fluid including non-hydrostatic effects. In the vertical direction, the water volume is bounded by the bottom z=-d (x,y) and the free water surface z=ζ(x,y,t),where t is the time, and x, y and z are the Cartesian coordinates. The local continuity equation and momentum equations are given as

$$\frac{\partial \mathrm{u_i}}{\partial \mathrm{x_i}} + \frac{\partial \mathrm{w}}{\partial z} = 0 \tag{5.1}$$

$$\frac{\partial \mathrm{u_i}}{\partial \mathrm{t}} + \frac{\partial \mathrm{u_i u_j}}{\partial \mathrm{x_j}} + \frac{\partial \mathrm{u_i w}}{\partial z} = -\frac{1}{\rho}\frac{\partial \left(\mathrm{p_h} + \mathrm{p_{nh}}\right)}{\partial \mathrm{x_i}} + \frac{\partial \tau_{\mathrm{ij}}}{\partial \mathrm{x_j}} + \frac{\partial \tau_{\mathrm{iz}}}{\partial z} - \mathrm{f_i} \tag{5.2}$$

$$\frac{\partial \mathrm{w}}{\partial \mathrm{t}} + \frac{\partial \mathrm{u_j w}}{\partial \mathrm{x_j}} + \frac{\partial \mathrm{w}^2}{\partial z} = -\frac{1}{\rho}\frac{\partial \left(\mathrm{p_h} + \mathrm{p_{nh}}\right)}{\partial z} + \frac{\partial \tau_{\mathrm{zj}}}{\partial \mathrm{x_j}} + \frac{\partial \tau_{zz}}{\partial z} - g \tag{5.3}$$

where i and j indicate two horizontal coordinates x/cross-shore and y/alongshore respectively, z is the vertical coordinate, u_i is the horizontal component of $\vec{u}$ in each direction, w is the vertical velocity, p_h and p_{nh} are hydrostatic and non-hydrostatic pressure components, respectively. The hydrostatic pressure p_h is explicitly expressed as $p_h = \rho g(\zeta - z)$, so $\partial_{x_i} p_h = \rho g \partial_{x_i} \zeta$ (where ∂_{x_i} stands for ∂/∂_{x_i}), and $\partial_z p_h = -\rho g$ (where g is the gravitational acceleration). τ_{ij} are turbulent stresses.

Equation (5.1) is the local continuity equation, and Equations (5.2) and (5.3) are momentum equations including the effects of mixing, bottom friction and resistance of cylinders. The last sink term of Equation (5.2) is the momentum loss due to the presence of PPG cylinders. Integrating the local continuity equation in the vertical direction, by substituting kinematic boundary conditions at the free surface and impermeable bottom, a global continuity equation is induced

$$\frac{\partial \zeta}{\partial t} + \frac{\partial}{\partial x_i}\int_{-d}^{\zeta} u_i dz = \frac{\partial \zeta}{\partial t} + \frac{\partial h U_i}{\partial x_i} = 0 \tag{5.4}$$

where $h(= \zeta + d)$ is the total water depth. The bottom friction at the bottom boundary is computed according to the logarithmic law of the wall with a roughness height k_s [Launder and Spalding, 1974]. The turbulence stresses are given based on eddy viscosity closure equations. The horizontal viscosity and vertical viscosity are estimated by the Smagorinsky type model [Smagorinsky, 1963] and the k- ε model [Launder and Spalding, 1974], respectively. The inclusion of vertical mixing spreads the effect of the bottom stress over the water column in vertical direction. To account for the momentum lost due to the resistance of pile cylinders, a sink term is added to the right-hand side of equation (5.2),

$$\mathrm{F_i} = \frac{1}{2}\rho C_D N D u_i |\vec{u}| + \rho\,(1 + C_m)\,NA\frac{du_i}{dt} \tag{5.5}$$

where C_D is the drag coefficient, N is the number of cylinder per unit bed area ($/m^2$), D is the cylinder diameter (m), C_M is the added-mass coefficient, A ($= \pi D^2/4$) is the cross section area of a cylinder, f_i is the density-normalized drag force per cylinder height in x/cross-shore or y/alongshore direction.

5.3.2. Numerical experiments setup

In this study, 9 cases with varying parameters of wave climate and groin configuration were simulated. The waves are varying from a slight to a moderate wave state. However, the incident wave angle is invariant at 30°. The summary of wave parameters is given in Table 5.1. In addition to varying wave conditions, three groin space distances and four groin lengths were investigated. The range of relative groin spacing (X_g/L_g, where X_g is groin spacing and L_g is groin length) is from 1:1, 1:1.5 to 1:2. The groin lengths are set from 109%, 99%, 84% to 69% of the breaker zone width, and the groin height is constant and fully emergent.

5.4. validation of numerical model

In this section, the verification of the numerical model ability of simulating flow dynamics within permeable groin fields is based on a comparison with experimental measurement data. Two available data sets, obtained from physical experiments by Hulsbergen and ter Horst [1973] and Trampenau et al. [2004] respectively, are used. In Hulsbergen and ter Horst [1973] experiment, the flow field within permeable double-row pile groin fields was investigated under varying combined wave current conditions, while in Trampenau et al. [2004] experiment the focus was on

Table 5.1: The wave and PPG parameters

Wave parameters					
H (m)	T (s)	$\theta(°)$	Sea state	$H_b(m)$	$X_b(m)$
0.03	1.0	30	slight	0.0319	2.02
0.03	1.5	30	slight	0.0413	2.32
0.03	2.0	30	slight	0.0440	2.80
0.03	2.5	30	slight	0.0454	2.86
0.05	1.26	30	moderate	0.0620	3.50
PPG parameters					
L_g (m)	X_b (m)	L_g/X_b	$Y_g(m)$	Y_g/L_g	P (%)
1.4	2.02	0.69:1	2.2	1.57:1	50
1.7	2.02	0.84:1	2.2	1.29:1	50
2.0	2.02	0.99:1	2.2	1.09:1	50
2.2	2.02	1.09:1	2.2/3.3/4.4	1:1/1:1.5/1:2	50
3.5	3.5	1:1	3.5/5.3/7	1:1/1:1.5/1:2	50

permeable single-row pile groins under wave alone and under current alone conditions separately.

5.4.1. Hulsbergen and ter Horst's experiment

Hulsbergen and ter Horst [1973] did a series of experiments to investigate the optimal layout of a permeable pile groin system under combined wave-current conditions. The scale is 1:40. The obliquely waves (H=0.03 m, T=1.04 s) incident at θ=15°to shore-normal direction were superimposed on alongshore steady currents (θ=90°). The steady current velocity at 0.3 m water depth is about 0.2 m/s (Figure 5.2, a). The PPG consists of two rows of pile cylinders. The pile cylinder diameter is 0.006 m, and the row apart distance is 0.0875 m. The permeability is varying along the groin length from 50% on the shoreward to 67% on the seaward side. The average permeability is 55%. Here, the permeability is defined as the percentage of void area over the total area of the groin's cross-section. One layout of groin system, consisting of three 5 m long groins at a 10 m spacing, was selected to be reproduced. For detailed calibration and validation information reference is made to Zhang and Stive [2019]. Here, we only present the comparison between the calculated and the measured longshore current velocities averaged along the groin fields.

Generally, a good agreement between simulated and measured longshore current velocities within a PPG field is shown in Figure 5.2. The longshore current velocities retarded by PPGs are well simulated by the numerical model. The longshore current velocities are effectively reduced within a breaker zone (e.g. 2 m offshore), for PPGs are mostly emergent, while the reduction is very limited at the seaward end of the PPG (at 5 m offshore) due to the submergence of the PPG and strong mixing.

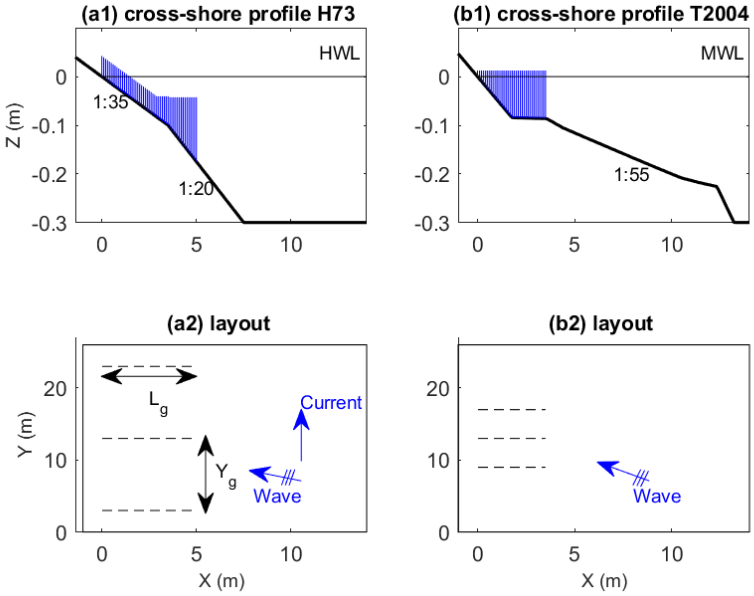

Figure 5.1: The cross-shore profiles of the physical experiments. (a): Hulsbergen and ter Horst (1973) experiment; (b): Trampenau (2004) experiment. The blue lines denotes the cross-section of permeable pile groins.

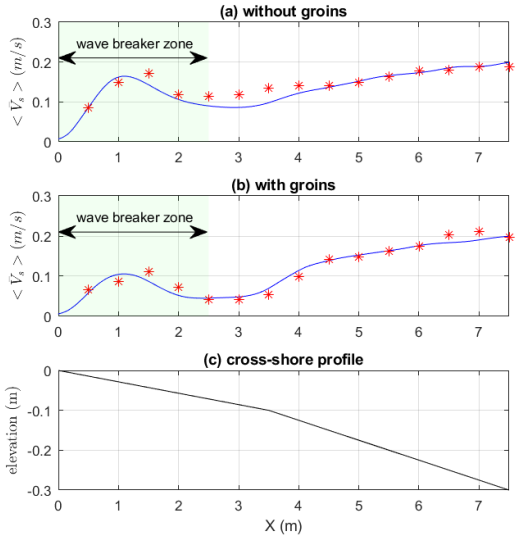

Figure 5.2: The comparison of longshore-averaged mean longshore currents $< \overline{V_s} >$ without groins (up panel) and with groin interventions (middle panel). Red stars represent measurement data, and blue lines denote calculation results.

5.4.2. Trampenau et al's experiment (2004)

Trampenau et al. [2004] performed systematic physical experiments in the Leichtweiss Institute (LWI) wave basin (26 m long and 19 m wide), focusing on the correlation between the groin configuration parameters and the current velocity and water level variations. The scale is 1:20. The beach slope near shoreline is 1/20, connecting a nearly horizontal submarine terrace with a slope of about 1:200, then a gentle slope 1:55 extending to a flat bottom (Figure 5.1, b). One of the obliquely incident regular wave conditions H=0.05 m, T=1.23 s and θ=30°was selected to validate the numerical model. The selected permeability of the single pile row groin is 50%. The diameter of cylinder dowels that were used in the experiment is 0.01 m, and the groin length (Lg) is equal to the width of breaker zone (xb).

In this simulation, the computational domain was divided into 10 layers in vertical direction, and discretized by 400 grids in x direction and 260 grids in y direction. The flow domain was 15 m long and 26 m wide. The bottom roughness coefficient was set as 0.0008 m following the validation setting of Hulsbergen and ter Horst [1973] experiment. In 5.3, the comparison of measured and calculated longshore current velocities on the bare bottom without groin effects is shown . The calculated longshore current velocities agree well with the measured values, showing the maximal current velocities V=0.23 m/s appearing at about 2 m seaward of the shoreline. When the groin intervention was considered, the drag coefficient C_D was set 1.1. The reason of omitting the calibration of C_D was the lack of available

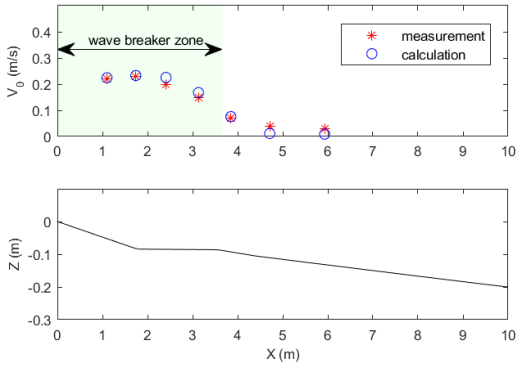

Figure 5.3: The comparison of longshore current velocities without groin intervention (the up panel), and the bottom topography (the bottom panel).

measurement data. The deduction of measured longshore current velocities from available dimensionless, relative longshore current velocities would introduce uncertainties. Therefore, the simulations will have a higher confidence in a qualitative analysis. When the permeability is 50%, the cylinder density is N=5000 stems/m2. The simulated relative longshore current velocities are similar to the measured values within the breaker zone (Figure 5.4). The relative longshore current velocities are the percentage of velocities at 0.5 m downdrift of the first upstream groin over the uninterrupted values updrift the groins. The derived longshore current velocities are given as a reference in Figure 5.4, (b). The values are obtained from the product of the dimensionless relative velocity values and the calculated unimpeded longshore current velocities updrift of the groins. Shoreward from the PPGs' head to the shoreline, the relative longshore current velocities are successfully reproduced (Figure 5.4, a), except for an underestimation at the seaward groin head (at X =3.5 m). Such a large underestimation is due to a further deflection of the stronger longshore currents near the groin head, as observed in Figure 5.4, b. The stronger deflection of the longshore current is partly due to the imperfect implementation of a PPG in the SWASH model. There are no real cylinders blocking some part of water volume and allowing water to pass through their openings. Instead, the drag forces exerted by a PPG on the water volume are calculated . Although the representation of a PPG in SWASH is simplified, it reproduces the principal effects of PPGs on longshore currents. The bulk reduction of longshore current velocities within a groin field by PPGs was appropriately simulated.

It was observed that in laboratory experiments the lower permeability of PPG induced a higher velocity reduction within a groin field. The experimental data show that the reduction ratio 0.5 m downdrift the first groin is 62% of undisturbed longshore current velocity when the permeability is 30%, compared to a 27% reduction when the permeability is 50%. Suzuki et al. [2017] found that when the permeability of a vegetation patch, is low, the porosity effect was validated as very important

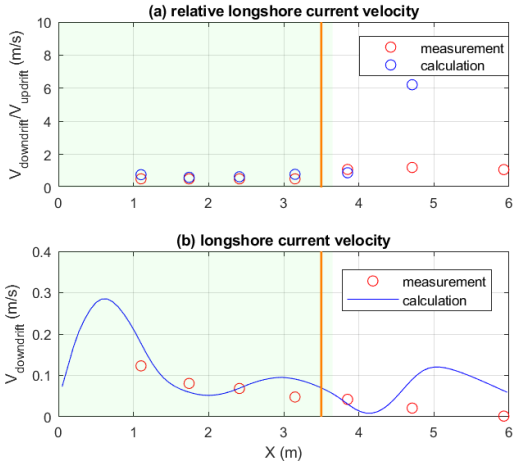

Figure 5.4: The relative longshore current velocity at 0.5 m downdrift the groin over that at 2 m updrift the first groin (a), and the calculated (blue line) and derived measured (red stars) longshore current velocities at 0.5 m downdrift the groin (b). The groins have a permeability of 50% and a length of 3.5 m. The orange lines represent the location of groin seaward heads and the green shadow denotes the wave breaker zone width

to wave propagation over the patch. The rigid vegetation is represented in the same way as a PPG in the SWASH model, namely by rigid cylinders. Similarly, the porosity effects of a low permeability PPG on longshore currents in the SWASH model were tested. Figure 5.5 (b) demonstrates that when the porosity effect was considered, the SWASH model calculates a more accurate longshore current velocity downdrift of the groin than without porosity effect. However, when the inertial coefficient Cm=1 is applied, no notable changes are found (Figure 5.5). In general, the longshore current profiles downdrift of the groin, calculated by the SWASH model, agree with the experimental results. However, the longshore current reduction ratio downdrift of the groin is underestimated. This would be partly due to the fact that the PPG cylinders are not resolved, instead the PPG cylinder induced forces (e.g. drag force, inertial force) are resolved within a computational grid cell. In this case, the grid resolution is 0.04 m of PPG implementation, which is four times the true pile cylinder diameter 0.01 m. For the model, the groin consists of a one-pile cylinder row, where the groin width is equal to the cylinder diameter. Therefore, the total PPG forces averaged over a coarser grid cell actually lead to a weaker force per unit area. On the other hand, the porosity (n=1-N*π*D2/4, where N is the density of cylinders) has to be changed with the varying density, to keep the frontal area of a groin constant, namely N*Widthgroin=N*Widthgrid. In addition, more significant deviations of longshore current velocities are observed both near groin shoreward root and groin seaward head. This illustrates that the measured sharper velocity gradients of longshore currents at these locations are underestimated., which implies that the local momentum mixing there needs a more sophisticated viscosity model.

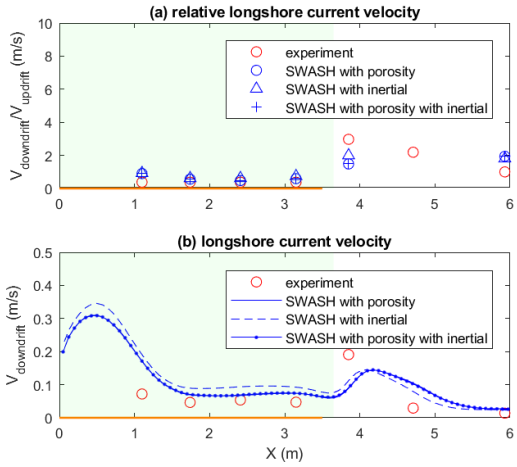

Figure 5.5: The relative ration of longshore current velocity at 0.5 m downdrift of the groin over the undisturbed velocity updrift the first groin (a), and the calculated (blue lines) and derived measured (red circles) longshore current velocities at 0.5 m downdrift of the groin (b). The groins have a permeability of 30% and a length of 3.5 m. The orange lines denote the groin length in cross-shore direction.

5.5. Comparison of different groin layouts

In this section, the simulation results of different groin layouts under varying wave conditions are compared. The beach bottom and the two-pile-row configuration of the PPG from Hulsbergen and ter Horst [1973] experiment were adopted, because the width of the two-pile-row groin is similar to the computational efficient grid resolution than was the case for the one-pile-row groin. Consequently, when keeping the vertical frontal area of a groin constant, the porosity and unit groin reduced forces are closer to that of a real groin.

5.5.1. Groin spacing

To investigate the groin spacing effect on the longshore current reduction rate, three spatial ratios of groin spacing over groin length (i.e. 1:1, 1: 1.5 and 1:2) were set up. The groin lengths are 2.2 m under slight waves and 3.5 m under moderate waves, which are both slightly larger than the breaker zone widths. The permeability of the PPG is 50%. Under a slight wave state (H=0.03 m), as shown in Figure 5.6, the longshore current reduction of a maximal longshore current is 65%, when the spatial ratio is 1:1. Along with the groin spacing increasing to 1.5 times and 2 times the groin length, the longshore current reduction capacity of PPGs decreases to 57% and 51%, respectively. Under a moderate wave climate (H=0.05 m), the results are similar. The longshore current reduction ratios are 65%, 57% and 41%, when the spatial ratio is 1:1, 1:1.5 and 1:2, respectively. The maximal

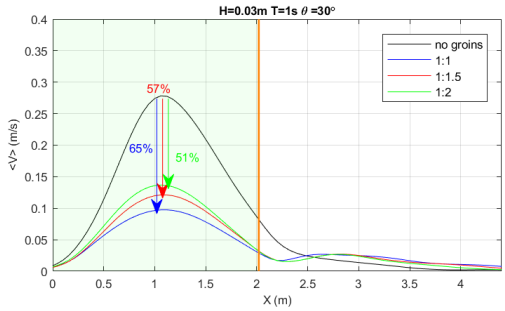

Figure 5.6: The comparison of longshore current velocities averaged along groin fields <v> with and without groin intervention under waves (H=0.03 m). The groin spacing-distance varies from 1, 1.5 and 2 times the groin length. The groin permeability is 50%. The orange lines represent the location of groin seaward heads and the green shadow denotes the wave breaker zone width.

enhancement of a longshore current by a groin's seaward head is found to be about 20% of a groin's length seaward further under slight waves and is about 30% of a groin's length under moderate waves.

5.5.2. Groin length

In addition to the groin's spatial ratio factor, groin length is a crucial configuration parameter. To quantify the difference of a groin's longshore current reduction capacity with varying groin length, four different groin lengths were simulated. The wave condition was light (H=0.3 m, T=1 s). The width of the breaker zone is 2.02 m. The groin lengths are 2.2, 2.02,1.7 and 1.4 m respectively, and the ratios of groin length to the width of the breaker zone are 109%, 99%, 84% and 69%, respectively. In Figure 5.8, the results show that when the groin length is slightly longer (Lg/Xb=109%), or nearly the same (Lg/Xb=99%), the longshore current velocities are efficiently reduced. When the groin length is 16% shorter than the width of wave breaker zone, the maximal/um longshore current at the middle of the breaker zone is likewise quite obstructed, but the longshore currents are hardly reduced by the seaward heads of a groin and significantly enhanced at the seaward breaker line (i.e. from 2 m seaward to 4 m seaward, Figure 5.8, left lower panel). For the shortest groin length (Lg =1.4 m, Lg/Xb=69%), the reduction ratio of maximal longshore current velocity increases from about 35% to 40%. From the groin head to the wave breaker line, the interrupted longshore current increases. When the offshore distance reaches 19% of the groin length, or 82% of the breaker zone width, the interfered longshore current is the strongest. These quantities verify the design rule that the groin length should cross most part of the wave breaker zone to guarantee an efficient longshore current reduction. From the simulations, we suggest the groin length should not be 85% shorter than the wave breaker zone width.

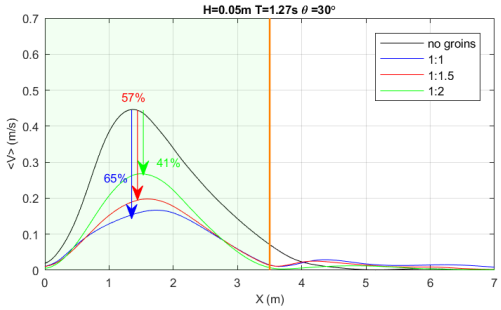

Figure 5.7: The comparison of longshore current velocities averaged along groin fields <v> with and without groin intervention under waves (H=0.05 m). The groin spacing-distance varies from 1, 1.5 and 2 times the groin length. The groin permeability is 50%.

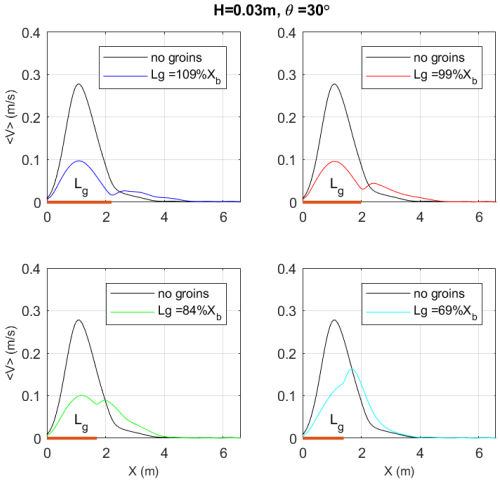

Figure 5.8: The comparison of longshore current velocities averaged along groin fields <v> with and without groin intervention under waves (H=0.03 m, T=1 s,, X_b= 2.02 m). The groin length varies from 1.09, 0.99 ,0.84 to 0.69 times the wave breaker zone. The orange lines denote the groin length in cross-shore direction. The groin permeability is 50%.

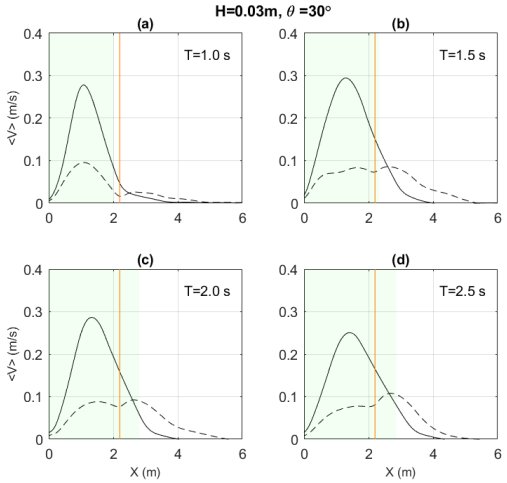

Figure 5.9: The comparison of longshore current velocities averaged with groin fields <v> with and without groin intervention under waves with different periods (i.e. T= 1.0s, 1.5s, 2s, 2.5s). The solid lines denote the situation without groins, and the dashed line show that with groins. The orange lines represent the location of groin seaward heads and the green shadow denotes the wave breaker zone width.

5.5.3. Wave periods

In Figure 5.9, the simulated longshore currents over the non-groin engineered bottom and over the groin engineered bottom under regular wave conditions with different wave periods are shown. The wave periods vary in the range of 1.0 s and 2.5 s. The wave height was set constant as 0.03 m. The groin spacing equals the groin length, which is set as 2.2 m. The wave direction is 30°. Without groin intervention, the longshore currents are longshore uniform. In cross-direction, the longshore currents spread mostly within the breaker zone. For a given wave height, when the wave period is longer, the wave breaker locations shift further seaward from 2.02 m when T= 1 s to 2.86 m when T= 2.5 s (Table 5.1). Consequently, the longshore currents spread further seaward till 4 m offshore (Figure 5.9). The maximal longshore current velocity increases slightly with a wave period increase. However, when the waves are longer, the waves refracted faster to shore-normal direction than shorter waves, according to the Snell's law. The surf zone average longshore current velocity is positively correlated to the sinusoidal of twice the breaker angle. The smaller wave breaker angle induced by longer waves leads to a reduction of the maximal longshore current velocity, which ccompensates the enhancement effect of the longer wave period.

When groin effects on longshore currents are involved in the calculations, the longshore currents are efficiently reduced within the groin fields. For all wave conditions, the longshore current increases by the groin seaward head. However, there appears a second peak of longshore current velocity seaward of the groin's head

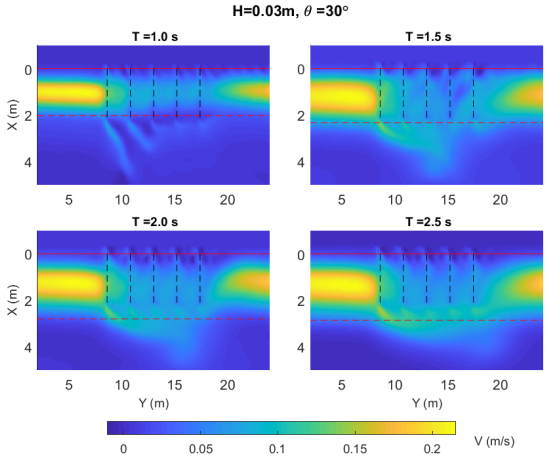

Figure 5.10: The comparison of longshore current velocities V with groin intervention under waves with different periods (i.e. T= 1.0s, 1.5s, 2s, 2.5s). The groin length keeps constant (L_g=2.2 m). The dashed lines show the locations of groins. The red lines represent the location of shore line and the red dashed lines illustrate the wave breaker lines.

when a wave period is longer than 1.5 s. When a wave period is as long as 2.5 s, the seaward longshore current peak is even larger than that within the breaker zone (Figure 5.10, d). The strong second longshore current peak could be explained by the further initial wave breaking locations of longer waves. As shown in Figure 5.10, the increased longshore currents by the groin heads are directed seaward. When the waves are shorter, the increased currents are directed into a shoreline-oblique direction. Further downdrift the groin, the enhancement of longshore currents by the groin heads become less distinct. Therefore, when averaging longshore current velocities over a groin field in alongshore direction, the increase of longshore current velocities is smeared. While, when waves are longer, the longshore currents by the groin heads are redirected into shoreline-parallel direction and even forms a uniform second peak longshore current band (Figure 5.10, d). When the groin length is not longer than the breaker zone width, the second seaward longshore current peak magnitude could be similar to the first peak value, or even larger than the first peak.

5.6. Discussion and conclusions

The aim of this study was to introduce the numerical model to assist permeable pile groin design. The phase resolving, non-hydrostatic SWASH model was used to solve the wave induced longshore current pattern within the permeable groin field. The implementation of PPGs in the SWASH model and the robust capability of simulating wave-current-groin interactions have been validated by Zhang and Stive [2019]. An numerical reproduction of relative longshore current velocities mea-

sured in Trampenau et al. [2004] experiment was included in this paper. A good match was found between the numerical calculations and the physical observations on a small laboratory scale. The validated model was further used to investigate varying PPG configurations under different wave conditions.

In this study, the different layouts of permeable groins are compared based on their capability of retarding longshore currents. Two design variables, the aspect ratio of groin spacing over groin length and the relative groin length to wave breaker zone width, are compared under different wave conditions (e.g. different wave heights, wave periods).

Under a light wave condition, the longshore current reduction rate decreases with the increase of the distance between the groins. The reduction rate decreases by 8% when the groin spacing is 1.5 times the groin length compared to the distance equal to the groin length. With groin space increasing to 2 times the groin length, the reduction rate decreases by 6% from 57% to 51%. In the case of a moderate wave climate, the reduction rate is nearly the same as under the slight wave condition when the groin spacing and length ratio is 1:1 and 1.5:1. The reduction rate decreases significantly by 16% from 57% to 41% when the groin spacing is as large as two times the groin length. The results suggest that if the groin space-length ratio is not larger than 2:1, the permeable pile groin functions similarly under light and moderate wave conditions. If the groin spacing is as large as 2 times the groin length, the permeable pile groin system performs worse under a moderate wave climate than under a light wave climate, from the aspect of longshore current reduction rate.

For the varying groin length simulations, it is shown that when a groin length is about 70% of the wave breaker width, the maximal longshore current velocity within the breaker zone could not be efficiently hindered. In case of increasing wave periods with a constant wave height, the wave length increases leading to a wider wave breaker zone and a consequent smaller groin length-breaker zone width ratio. Within the breaker zone, the longshore current reduction decreases slightly with the decreasing relative groin length to the breaker zone width. However, outside the breaker zone, the longshore current increases significantly and even transfers the retarded longshore current velocity peak from inside the breaker zone to the wave breaker location. Moreover, the expanding seaward distance of enhanced longshore current velocity is much further when the wave period is longer. In a plan view, the enhanced longshore current area by the groin heads is a band-like shape, when the wave period is the largest 2.5 s among the four simulation cases (T= 1 s, 1.5 s, 2 s, 2.5 s).

The validated SWASH model offers a practical opportunity to compare the different layouts of pile groin system. However, the simulations are carried out under well-controlled conditions. Therefore, the model results are able to provide a quick prediction of groin performance in a preliminary design phase. Furthermore, the

validated numerical model could be used to investigate different alternatives of pile groins under more complex environmental conditions. The results obtained from the schematized numerical experiments may expand the database for permeable pile groin systems, which then are a valuable tool to assist the design and evaluation process in coastal engineering planning and management.

References

T. K. S. Abam. Bank erosion and protection in the Niger delta. *Hydrological Sciences Journal*, 38(3):231–241, 2009. ISSN 0262-6667. doi: 10.1080/02626669309492665. URL http://www.tandfonline.com/doi/abs/10.1080/02626669309492665{#}.VL{_}PwC6RZK0.

W. Bakker, C. Hulsbergen, P. Roelse, C. de Smit, and J. Svasek. PERMEABLE GROYNES: EXPERIMENTS AND PRACTICE IN THE NETHERLANDS. In *19th International Conference on Coastal Engineering*, pages 1983–1996, Houston, 1984.

D. W. Berg and G. M. Watts. VARIATIONS IN GROIN DESIGN l. In *Proceedings Santa Barbara specialty conference*, 1965.

M. Crossman and J. Simm. Sustainable coastal defences - The use of timber and other materials. *Proceedings of the Institution of Civil Engineers: Municipal Engineer*, 151(3):207–211, 2002. ISSN 09650903. doi: 10.1680/muen.151.3.207.38884. URL http://www.scopus.com/inward/record.url?eid=2-s2.0-0036751968{&}partnerID=40{&}md5=50f484bb9656010ea4269629474be345.

H. H. Dette, A. J. Raudkivi, and H. Oumeraci. Permeable Pile Groin Fields. *Journal of Coastal Research*, pages 145–159, 2004. ISSN 07490208, 15515036. URL http://www.jstor.org/stable/25736251.

C. Hulsbergen and W. ter Horst. Effect of permeable pile screens on coastal currents. Delft Hydraulics laboratory report M 1148, (in Dutch). Technical report, Delft Hydraulics, Delft, 1973.

O. Kolp. Farbsandversuche mit lumineszenten Sanden in Buhnenfeldern. Ein Beitrag zur Hydrographie der Ufernahen Meereszone. *Petermanns Geographischen Mitteilungen*, 114(2), 1970.

N. C. Kraus, H. Hanson, and S. H. Blomgren. Modern functional design of groin systems. *Icce 1994*, pages 1327–1342, 1994. ISSN 08938717.

B. Launder and D. Spalding. The numerical computation of turbulent flows. *Computer Methods in Applied Mechanics and Engineering*, 3(2): 269–289, mar 1974. ISSN 0045-7825. doi: 10.1016/0045-7825(74)90029-2. URL https://www.sciencedirect.com/science/article/pii/0045782574900292?via{%}253Dihub.

U. Perdok, M. Crossman, H. J. Verhagen, S. Howard, and J. Simm. Design of timber groynes. In *Coastal Structures*, pages 1689–1699, Portland, Oregon, United States, Aug. 2003. ISBN 9788578110796. doi: 10.1017/CBO9781107415324.004.

M. T. Poff, M. F. Stephen, R. G. Dean, and S. Mulcahy. Permeable Wood Groins: Case Study on their Impact on the Coastal System. *Journal of Coastal Research*,

pages 131–144, 2004. ISSN 07490208, 15515036. URL http://www.jstor.org/stable/25736250.

W. Price, K. TOMLINSON, and D. Willis. Filed tests on two permeable groynes. In *13th International Conference on Coastal Engineering*, pages 1312–1325, 1972. ISBN 7731030008. doi: 10.1016/B978-0-7020-3935-5.00077-X.

A. J. Raudkivi. Permeable Pile Groins. *Journal of Waterway, Port, Coastal, and Ocean Engineering*, 122(6):267–272, 1996. ISSN 0733-950X. doi: 10.1061/(ASCE)0733-950X(1996)122:6(267).

A. J. Raudkivi and H. H. Dette. Reduction of sand demand for shore protection. *Coastal Engineering*, 45(3-4):239–259, 2002. ISSN 03783839. doi: 10.1016/S0378-3839(02)00036-4.

J. Smagorinsky. General circulation experiments wiht the primitive equations I. The basic experiment. *Monthly Weather Review*, 91(3):99–164, 1963. ISSN 0036-8075. doi: 10.1126/science.27.693.594.

5

T. Suzuki, C. Altomare, W. Veale, T. Verwaest, K. Trouw, P. Troch, and M. Zijlema. Efficient and robust wave overtopping estimation for impermeable coastal structures in shallow foreshores using SWASH. *Coastal Engineering*, 122: 108–123, apr 2017. ISSN 03783839. doi: 10.1016/j.coastaleng.2017.01.009. URL https://www.sciencedirect.com/science/article/pii/S0378383916302435.

T. Trampenau, F. Goricke, and A. J. Raudkivi. permeable pile groins. In *25th International Conference on Coastal Engineering*, pages 2142–2151, Orlando, 1996.

T. Trampenau, H. Oumeraci, and H. H. Dette. Hydraulic Functioning of Permeable Pile Groins. *Journal of Coastal Research*, pages 160–187, 2004. ISSN 07490208, 15515036. URL http://www.jstor.org/stable/25736252.

R. Zhang and M. J. F. Stive. Numerical modelling of hydrodynamics of permeable pile groins using SWASH. *Coastal Engineering*, 153:103558, nov 2019. ISSN 03783839. doi: 10.1016/j.coastaleng.2019.103558. URL https://linkinghub.elsevier.com/retrieve/pii/S0378383918303910.

M. Zijlema, G. Stelling, and P. Smit. SWASH: An operational public domain code for simulating wave fields and rapidly varied flows in coastal waters. *Coastal Engineering*, 58(10):992–1012, oct 2011. ISSN 0378-3839. doi: 10.1016/J.COASTALENG.2011.05.015. URL http://www.sciencedirect.com/science/article/pii/S0378383911000974?via{%}253Dihub.

6

Conclusions and Outlook

6.1. Conclusions

This thesis makes efforts to predict interactions between permeable pile groins, waves and currents by numerical simulations. The response of permeable pile groins in coastal waters is dominated by longshore currents. The key precondition of numerically predicting the longshore current field is that the wave evolution especially concerning the wave breaking position should be accurately captured. To answer the first research question, the comparison of longshore currents between numerical simulations and laboratory observations is made (Chapter 3).

Among the available wave-flow models, there are two main types, phase-averaged (or stochastic) models and phase-resolving (or deterministic) models [Smit et al., 2014]. The SWASH model, which is a phase-resolving model, is superior to phase-averaged models from the aspect of resolving instantaneous variables within a wave period. In addition, in SWASH it is easier to improve frequency dispersion via increasing the number of vertical layers than in a Boussinesq type phase-resolving model via increasing the derivatives orders of dependent variables. Therefore, the non-hydrostatic wave-flow model SWASH was adopted in this work as the numerical methodology.

The potential of the SWASH model to resolve wave-induced longshore currents was evaluated. Four wave basin experiments [Visser, 1991, Hamilton and Ebersole, 2001, Reniers et al., 1997] consisting of six cases were reproduced. The simulated longshore currents over the alongshore uniform barred and non-barred beaches, induced by regular and irregular waves, have been extensively compared with laboratory measurements. General good results are obtained for all the test cases, under the circumstance that the vertical layer number and the bottom roughness coefficient of the SWASH model are set as constant values without any specific calibration. The good agreement found between the simulation results and the measurement data reveals that the SWASH model is sufficiently validated. The validity of the SWASH modelled longshore currents proves that the SWASH model is a robust tool to predict longshore currents over an alongshore uniform beach on a small laboratory scale. In contrast, an analytic longshore current model based on the radiation stress theory only provides good simulation results in the case the coefficients are properly calibrated. For instance, the maximal longshore current velocity magnitude relies on the bottom roughness coefficient value, and the shape of the longshore current cross-shore profile depends on the viscous mixing parameter. Moreover, the analytical model needs an additional calculation of wave propagation. For the wave calculation, a roller model is necessarily included to delay wave breaking and to accurately capture the initiation of longshore currents. The roller model introduces extra ad hoc coefficients such as the roller dissipation coefficient, which likewise have to be calibrated.

Considering the longshore currents over a barred slope, both the depth-averaged analytical model and the multi-layered SWASH model results show that the maximal longshore current velocity is over the bar crest. This is consistent with the labora-

tory measurements, but it is in contrast to the observed maximal longshore current over the trough in the DELILAH field experiment. Reniers et al. [1997] tried to interpret the maximum location shift in their numerical model by testing the effects of the alongshore pressure gradient and the lateral mixing. Nonetheless, the two factors that were tested do not affect the location of the maximal longshore current velocity. In the laboratory experiment and in the numerical simulation pure wave forcing is applied, while in the field, other complex forces resulting from winds and tides could coexist with waves. The local forcing alteration and alongshore bathymetric variation would be possible causes for the maximal longshore current location transfer. The measurement data are not sufficient to uncover the mechanisms behind this phenomenon.

The multi-layered SWASH model enables a prediction of the vertical structure of longshore currents. It is shown that under a pure wave condition, the vertical profile of longshore currents near the wave breaking position is rather uniform over depth on a planar beach. This implies that the strong turbulence induced by wave breaking contributes to a vertical momentum mixing, smearing out a large depth variation of the vertical profile of the longshore current velocity. When approaching the shoreline, the vertical profile deviates from depth uniform to a more logarithmic profile. However, the very depth-uniform vertical profile of longshore currents does not apply to a barred slope.

With default settings and without a specific calibration of the coefficients, the SWASH model reproduces the small-scale experimental results fairly well. On the contrary, the coefficients of the analytical model need to be measured in a laboratory or calibrated in simulations. The fine-tuning of the coefficients of the analytical model limits the model to provide a reliable prediction.

Next, the implementation of permeable pile groins of the SWASH model is tested responding to the second research question. It is found that the schematized way of using the Morison-type model to exert PPG forces to the water column in the calculations is sufficient to represent the PPG resistance felt by the longshore currents. The representative laboratory data set [Hulsbergen and ter Horst, 1973] is chosen to calibrate the coefficients and verify the simulation results. The calibrated model is capable to reproduce the flow field within the groin fields. Instead of only measuring the alongshore averaged longshore current velocities by floats within groin fields in the laboratory, the numerical simulation reveals the flow characteristics in the entire groin field in answer to the third research question. It has been found that in the experiment by [Hulsbergen and ter Horst, 1973] the three long groins function better than the five short groins when considering the averaged relative longshore current velocity reduction in the entire groin field. The relative longshore current velocity is 67% averaged along the field with three long groins with a 55% permeability and is 57% averaged along the field with five short groins with a 50% permeability. Given the far more smaller groin width than the incident wave length and the small angle between incident wave direction and the groin axis direction,

the wave attenuation is, by the existence of a PPG, confined to a limited area and to a very limited extent, which could be ignored. The large permeability of groins hinders the development of eddies and recirculation in groin compartments.

Lastly, to reply to the fourth research question, the performance of varying layouts and configurations of permeable pile groins are compared through numerical experiments. The correlation between the configuration parameters of groins and longshore current reduction ratio is investigated. The groin lengths range between 69% and 109% of the width of wave breaker zone. The simulation results suggested that a groin length should be comparable to the wave breaker zone width. For instance, if the groin length is within the range of 99% and 109% of the width of wave breaker zone, the maximal longshore current velocity can be sufficiently reduced. In the case of the groin length equals to 84% of the width of wave breaker length, the maximal longshore current velocity can be efficiently retarded, but the longshore current velocity by the groin seaward head is hardly being slowed down. While the groin length is as short as 69% of the width of wave breaker zone, both the maximal longshore current velocity is less reduced compared to that with longer groin lengths and the longshore current velocity around the groin seaward head is significantly enhanced. In addition to the relative groin length, the spatial ratio of the groin apart distance in alongshore direction and the groin length is examined. If the spatial ratio is small (e.g. 1:1 and 1.5:1), the longshore current retardation is not sensitive to wave conditions (e.g. slight or moderate). The correlation of the reduction ratio of longshore current velocity and the groin spatial ratio is linear. If the spatial ratio is 2:1, the permeable pile groin system hinders longshore currents to a larger extent under a slight wave climate than that under a moderate wave climate (H=0.05 m, T=1.27 s).

6.2. Outlook

This thesis work demonstrates the ability of the SWASH model to reproduce wave-induced longshore currents on a small scale. The SWASH model is supposed to have the potential to be used on a large scale, for instance, on a field scale. However, given a barred beach, the maximal longshore current velocity of its cross-shore profile is over the bar through calculation. Such a finding is different from the field measurements. The reason behind the shift of location of the maximal longshore current is likely due to the bathymetric variation and local forcing alteration in the field, more data is needed to support further investigation. Moreover, as the SWASH model resolves the vertical structure of longshore currents, the insight about fitting the vertical structure of longshore currents would be promoted by numerical simulations. Among the literature, a logarithmic profile, a power-law profile and a depth-uniform have been suggested to fit a measured vertical profile of longshore currents. The application range for the different fitting profiles may be further refined by a robust numerical simulation.

Permeable pile groins have been proven to be effective to reduce longshore currents

to a large extent. The verified model would have a great potential to predict hydrodynamics around permeable pile groins with varying configurations under more complex hydraulic conditions. The reliable prediction would promote considerations during the design procedure of permeable pile groins and is very practical to optimize their layouts and configurations.

The schematized way to include PPG exerted forces to the water column by the Morison type drag forces and inertial forces is proven to be sufficient when the permeability is as large as about 50%. When the permeability is smaller, for instance 30%, the simulated reduction ratio of longshore current velocity is underestimated. In the case of a greater pile groin density, the porous effects are shown as important to improve the simulation results. The wooden pile usually has a diameter of 25 cm on a field scale, which is much smaller than the incident wavelength. In the numerical model, a sufficiently long domain is necessary to allow the longshore currents to fully develop. The large computational grid resolution compared with the small pile cylinder diameter makes it is easier to calculate the averaged forces of a PPG, instead of resolving a PPG itself. Such schematization of PPG representation would be further compared by the direct way to resolve a PPG in the flow domain. The trade-off between the computational efficiency and the accurate representation of a PPG should be carefully taken into account.

For the permeable pile groins that have been utilized for over half a century, the condition of the present PPG should be checked and compared for strength. For instance, the groin heads are easily washed away. Due to the lack of sufficient data, the applicability of a permeable pile groin under extreme wave conditions is unknown. The main concern under extreme conditions is, that when a storm surge accompanies waves, whether the permeable pile groin is still serving to offer sufficient protection, since the evoked rip current strongly enhances the seaward transport of sediment.

In addition, one of the main advantages of permeable pile groins is the low cost of construction and maintenance. The average life span of a timber groin is about 25 years. The whole life cost of a permeable pile groin project, compared to other methods, such as the recently developed mega beach nourishment project, is worthy of analysing. The performance of permeable pile groins, alone or a hybrid system, such as permeable pile groins in combination with beach nourishment, needs further investigation and comparison.

The SWASH model is reliable to predict hydrodynamics within groin fields. The accurately simulated flow field is the precondition to properly simulate the morphological changes after construction of permeable pile groins. The integrated evaluation of the performance of permeable pile groins includes morphological changes in addition to hydrodynamic changes. The simulation of ultimate morphological change would lead to an efficient outcome-oriented procedure of permeable pile groin design.

References

D. G. Hamilton and B. A. Ebersole. Establishing uniform longshore currents in a large-scale sediment transport facility. *Coastal Engineering*, 42(3):199–218, 2001. ISSN 03783839. doi: 10.1016/S0378-3839(00)00059-4.

C. Hulsbergen and W. ter Horst. Effect of permeable pile screens on coastal currents. Delft Hydraulics laboratory report M 1148, (in Dutch). Technical report, Delft Hydraulics, Delft, 1973.

A. J. H. M. Reniers, J. A. Batties, and D. A. Falquês, A. Huntley. A laboratory study on the shear instability of longshore currets. *JOURNAL OF GEOPHYSICAL RESEARCH*, 102:8597–8609, Apr. 1997.

P. Smit, T. Janssen, L. Holthuijsen, and J. Smith. Non-hydrostatic modeling of surf zone wave dynamics. *Coastal Engineering*, 83:36–48, jan 2014. ISSN 03783839. doi: 10.1016/j.coastaleng.2013.09.005.

P. J. Visser. Laboratory measurements of uniform longshore currents. *Coastal Engineering*, 15(5-6):563–593, oct 1991. ISSN 03783839. doi: 10.1016/0378-3839(91)90028-F. URL http://linkinghub.elsevier.com/retrieve/pii/037838399290028S.

Acknowledgements

How time flies. I cannot imagine that one day I could make my PhD to an end. In the beginning, I heard that PhD means permanent head damage. That makes me worried about my brain, and I even dare not to have an apple every day. Because there is a saying that 'an apple a day keeps the doctor away'. But it finally proves that it is not the case. I am convinced that what I obtained from my PhD study is a kind of permanent head development. Therefore, I reach the stage to manage my defense.

I am very grateful to the people I met at Delft. Firstly. I want to thank the most important person, my promotor Prof. Stive. The start of my PhD is attributed to his willingness to accept me five years ago. I was so lucky to have such a great chance to study at Tu Delft. Without his guidance and unconditional trust, I would lose my direction. Thanks for his great patience with me and his strong support. Whenever I lost my confidence, he is always there giving me encouragement. I also want to thank my promotor Prof. Aarninkhof. After Marcel's retirement, he offered his hand to be one of my promoters and helped me to apply for the Stichting Het Lamminga Fonds. Especially when I am waiting for my defense and being stuck in the Netherlands due to the coronavirus pandemic, Stefan and Marcel agreed to offer me one-month allowance to support my living during such a hard time. In addition, I would like to express my sincere admiration for the rigorous attitude of Prof. Uijttewaal. He is always very nice to students but only be critical to research questions. From him, I learned a lot about doing research. Then, I sincerely thank Marcel Zilijma. Your course of computational hydrodynamics opened the world of numerical models for me. It is amazing to use a numerical model to simulate and reproduce nature. But you have to be careful to use numerical models unless you understand the background numerics and the natural process. Otherwise, the numerical model's results cannot be explained. Next, I want to thank Dirk. With his experienced guidance, I could obtain a reasonable simulation from SWASH.

Qinghua, thank you for your guidance making me familiar with the Delft 3D software, and learn how to set a good model. Kees Hulsbergen, thank you for providing information about the unpublished experimental data that I used to validate my model. Henk Jan Verhagen, thank you for helping me find the very old scientific report. Pauline Van Lynden, thank you for your amazing photo book that makes me know more about the history of permeable pile groins in the Netherlands. Mariette van Tilburg, thank you for polishing my papers and translating my summary. Besides, thank you for organizing our non-Dutch group meeting to help us to quickly adjust to academic life at Tu Delft. Martijn Henriquez, thank you for sharing your ideas with me and talking with me about cultural differences.

Caroline, thanks for your pioneering work on simulating permeable pile groins. Your great work inspires me to continue research on this specific hydraulic structure. I am very grateful you shared your experience with me. Panagiotis, thank you for testing the SWASH model. Your work further convinced me that SWASH is a powerful tool to be applied to my research. Azimi, thank you for exploring wave induced current interaction with mangroves. I am very happy to be one of your thesis committee members and followed up with the knowledge about mangroves from you.

Thank every friend with whom I share my happiness and sorrow. Yang, you have a so strong will. Before I know you, I could not imagine how a woman could be that strong to face difficulties in life. Sien, from you, I learned how to be a friend. Chunyan, I am happy to share with you my ideas, and especially thank you for providing our group your home as our party room. Jianliang, you are not only a good researcher, but also a great chef. Thank you for your delicious dishes. Yuning, you are a lovely and energetic girl. I like your vlog and photos. Min, Peng, Lixia, Runxiang, Jianliang, Zaiyang, Yuning, Yu, Yujian, Jianwei, Jinshan, the party time spent with you are also unforgettable. Nan, you are so close to me and could understand most of my feelings, thanks for your patience. Xiang, you are so into your research. Your passion inspires me to keep trying into my research. Fei, Anqi, I am glad to be your roommate for two years. You are so nice and responsible. Shi, Lei, thank you for helping me with relocating. Pengling, Lei, Jian, Xin, Xing, Meixia, and so on, the leisure time spent with you makes me relaxed and happy. Lei, Wenwan, thank you all for chatting with me whenever I need you. I am so lucky to have such good friends like you. Zhan, thank you for introducing job opportunity to me and inviting me to visit SYSU. Zhongbo, I enjoyed discussing modelling with you.

Thuha, you are a strong woman. I am very happy to share the same office with you. I admire your iron will to fight with illness and continue to do research. I wish you happy and healthy all your life. Anh do, thank you for taking care with Ha. Inge, thank you for your administrative work to support us.

I appreciate the accompany of my friends with me traveling in Europe. The wonderful traveling experiences with you are the sparking stars in my life. Thank you all again.

Last but not least, thank my parents. They teach me how to be a good person. Whenever I met with difficulties, I know I always have a backup from them. Their love and care are the sources of my courage. Although they don't know my research work, they always support me unconditionally. Love you all my life.

Rong
at Delft
June, 2020

Curriculum Vitæ

Rong ZHANG

13-07-1991 Born in Yinchuan, China.

Education

2008–2012 BS. Port, Waterway and Coastal Engineering
Dalian University of Technology
Dalian, China

2012–2014 MS. Hydraulic Engineering
Dalian University of Technology
Dalian, China

2014–2020 PhD. Hydraulic Engineering
Thesis: Hydraulic Functioning of permeable pile groins
Promotor: Prof. dr. ir. Marcel J. F. Stive
Promotor: Prof. dr. ir. Stefan G. J. Aarninkhof

List of Publications

3. **R. Zhang**, M. J. Stive, *modelling of hydrodynamics of permeable pile groins using SWASH*, Coatal Engineering **153**,103558,(2019).

2. **R. Zhang**, M. Zijlema, M. J. Stive, *Laboratory validation of SWASH longshore current modelling*, Coatal Engineering **142**,95,(2018).

1. **R. Zhang**, M. J. Stive, *REVISITED HYDRAULIC FUNCTIONING OF PERMEABLE PILE GROINS.*, Coatal Engineering Proceedings**1**(36), structures.13. (2018).